Final Progress Report

NIOSH Small Research Grant R03OH010699

Project Title: Evaluating and controlling airborne emissions from desktop 3D printers

Principal Investigator:
Brent Stephens, Ph.D.
Department of Civil, Architectural, and Environmental Engineering
Built Environment Research Group
Illinois Institute of Technology
Alumni Hall Room 228
3201 S Dearborn Street
Chicago, IL 60616
Phone: 312-567-3356
Email: brent@iit.edu
Web: http://built-envi.com

Awardee:
Illinois Institute of Technology
Contact: Domenica G Pappas, CRA, Director, Sponsored Research and Programs
10 West 35th Street
IIT Tower 7th Floor (STE 7D7-1)
Chicago, IL 60616-3717

Grant Number: 5R03OH010699-02

Project Starting and Ending Date: September 1, 2014 – August 31, 2016

Date of Completion of Final Report: November 14, 2016

Table of Contents

Abstract

Project Title: Evaluating and controlling airborne emissions from desktop 3D printers

Principal Investigator:
Brent Stephens, Ph.D.
Department of Civil, Architectural, and Environmental Engineering
Built Environment Research Group
Illinois Institute of Technology
Alumni Hall Room 228
3201 S Dearborn Street
Chicago, IL 60616
Phone: 312-567-3356
Email: brent@iit.edu
Web: http://built-envi.com

Abstract:
Desktop three-dimensional (3D) printers are rapidly increasing in popularity. The majority of desktop 3D printers designed for the consumer market utilize an additive manufacturing technology called fused filament fabrication, in which a solid thermoplastic filament is forced through a heated extrusion nozzle, melted, and deposited in thin layers onto a moving bed. A three-dimensional solid shape is formed layer-by-layer as the filament material cools and hardens. A wide variety of polymeric filament materials are now being used at a variety of extruder nozzle temperatures and bed temperatures. Previous research has shown that desktop 3D printers utilizing this process can emit large numbers of ultrafine particles (UFPs: particles less than 100 nm in size) and some hazardous volatile organic compounds (VOCs) during printing, although very few filament and 3D printer combinations had been tested prior to this project. Moreover, we are not aware of any studies that had explored in detail the likely human exposures to both VOCs and UFPs emitted from desktop 3D printers and filaments in realistic indoor environments.

In this work, we quantified emission rates of UFPs and speciated VOCs from 5 commercially available filament extrusion desktop 3D printers utilizing up to 9 different filaments using controlled experiments in a test chamber. We also provided preliminary data on the impact of print object geometry and the use of partial and whole printer enclosures with and without a filtration system to mitigate printer emissions. Subsequently, we used computer simulations to predict the magnitudes of human exposures to these same pollutants that would be expected in three spatial locations within a typical small office environment. Last, we also used the worst case UFP and VOC emission scenarios to model the likely impacts of several potential control strategies for reducing exposures.

Median estimates of time-varying UFP emission rates ranged from ~10^8 to ~10^{11} #/min across all tested printer and filament combinations, varying primarily by filament material and, to a lesser extent, printer bed temperature. The individual VOCs emitted in the largest quantities included caprolactam from nylon-based and imitation wood and brick filaments (ranging ~2 to ~180 μg/min), styrene from acrylonitrile butadiene styrene (ABS) and high-impact polystyrene (HIPS)

filaments (ranging ~10 to ~110 μg/min), and lactide from polylactic acid (PLA) filaments (ranging ~4 to ~5 μg/min). Predicted concentrations in the modeled indoor environment demonstrate that UFP and VOC concentrations within close or moderate proximity to some operating desktop 3D printers can exceed recommended exposure levels and may be cause for concern for both acute and chronic health effects. The results also suggest that the most effective control strategies for reducing both UFP and VOC concentrations in all zones from high emitters used in the modeled environment, in descending order of impact, include: (1) installing a high-flow spot ventilation system, (2) operating the printer in a sealed enclosure with high efficiency gas and particle filtration, (3) installing a moderate-flow spot ventilation system, and (4) operating a high-efficacy stand-alone air cleaner with both gas and particle filtration within immediate proximity to the operating 3D printer. Results also demonstrate that some 3D printer and filament combinations with lower emissions (e.g., PLA filaments, which have both low UFP and VOC emissions) should be prioritized over higher emitting filaments to limit human exposures.

Section 1

Significant or Key Findings

Key findings of this work include:

1. Ultrafine particle (UFP) and speciated volatile organic compound (VOC) emissions vary widely by filament material and to a lesser extent, printer characteristics. Median estimates of time-varying UFP emission rates ranged from ~10^8 to ~10^{11} #/min across all tested combinations. The individual VOCs emitted in the largest quantities included caprolactam from nylon-based and imitation wood and brick filaments (ranging ~2 to ~180 µg/min), styrene from acrylonitrile butadiene styrene (ABS) and high-impact polystyrene (HIPS) filaments (ranging ~10 to ~110 µg/min), and lactide from polylactic acid (PLA) filaments (ranging ~4 to ~5 µg/min). Some of these VOCs present potential public and workplace health hazards, as styrene is classified as a *possible human carcinogen* by the International Agency for Research on Cancer (IARC Classification Group 2B) and acute exposure to high concentrations of caprolactam is known to be "irritating to the eyes and the respiratory tract" and "may cause effects on the central nervous system" according to the Centers for Disease Control and Prevention.
2. Occupying a space in a typical indoor office environment within close or moderate proximity to some operating desktop 3D printer and filament combinations can result in concentrations of UFPs and some VOCs that either exceed known recommended exposure levels (RELs) (e.g., from the California Office of Environmental Health Hazard Assessment) and/or may generally be cause for concern for both acute and chronic health effects based on other evidence in the health effects literature.
3. The most effective control strategies for reducing both UFP and VOC concentrations from high-emitting 3D printers in a typical workplace environment, in descending order of impact, include: (1) installing a high-flow spot ventilation system, (2) operating the printer in a sealed enclosure with high efficiency gas and particle filtration, (3) installing a moderate-flow spot ventilation system, and (4) operating a high-CADR stand-alone air cleaner with both gas and particle filtration within immediate proximity to the operating 3D printer.
4. Combined, the applied results from this work lead us to make the following recommendations to improve occupational safety and respiratory health in workplaces in various sectors including manufacturing and retail: (1) additional measurements should be conducted to more accurately quantify personal exposures to both UFPs and speciated VOCs that account for proximity effects presented by typical 3D printer use patterns in a wide variety of realistic settings; (2) manufacturers should work towards designing low-emitting filament materials and/or printing technologies; (3) in the absence of new low-emitting filaments, manufacturers should work to evaluate the effectiveness of sealed enclosures on both UFP and VOC emissions and/or to introduce combined gas and particle filtration systems. Until these recommendations are accomplished, we continue to suggest that caution should be used when operating many printer and filament combinations in enclosed or poorly ventilated spaces or without the aid of gas and particle filtration systems. This is particularly true for both styrene- and nylon-based filaments based on data from the relatively large sample of printers and filament combinations evaluated here.

Translation of Findings

The significant findings herein can be used to prevent workplace diseases and injuries and improve safety practices or programs in the following ways:

1. We now have greater knowledge of the types and magnitudes of pollutants emitted from desktop 3D printers and the effectiveness of viable control strategies, which allows for more informed decision-making by a variety of stakeholders. For example, we have had personal communication with several environmental health and safety (EHS) staff members from universities, K-12 schools, and private industry across the country regarding our findings, which has helped them to either select lower-emitting filaments for their installations or design control strategies to mitigate 3D printer emissions in their facilities.
2. These same stakeholders and many others, including the broader academic community as well as the general public, now have greater awareness of the hazards presented by emissions from desktop 3D printers. We have presented our work at academic conferences including the American Association for Aerosol Research (AAAR), the International Society of Exposure Science (ISES), and Healthy Buildings conferences. We have also published our scientific findings in high impact journals (including in *Environmental Science and Technology*, with an impact factor of 5.4 in 2015) under open access licenses so that anyone in the world can read the findings for free. This has also led to significant media attention for the work, including articles in the Chicago Tribune, Fox News, Yahoo News, FastCo.Design, and dezeen, as well as a television interview with CBS Chicago, all of which has helped to translate research findings to the general public.
3. Our study has also gained the attention of leaders in the 3D printing industry, including a number of printer and filament manufacturers and distributors, who have used our results to inform their customers of the emissions from their existing products and to inform designs for new filaments, printers, enclosures, and gas and particle filtration systems. Our work has provided the foundation for innovation in these areas, which is expected to lead to more research and development of products to mitigate emissions from 3D printers, and ultimately, to widespread adoption of these technologies in workplace environments and many other indoor environments in which 3D printers are used.

Research Outcomes/Impact

Findings from this project have a high potential for improving occupational safety and health, and it is clear that some progress is already being made via intermediate outcomes. Results have informed occupational safety and health by informing stakeholders of the types and magnitudes of emissions from popular desktop 3D printers and filaments, their impact on pollutant concentrations and exposures in typical workplace environments, and recommendations for how to mitigate emissions, all of which establish the framework for ***potential positive outcomes*** as this work is further disseminated. ***Intermediate outcomes*** have already included influencing industry practices, product design, and safety management programs, as stakeholders with whom we have engaged have used our work to inform their printer and filament manufacturing and sales, their product designs (particularly for gas and particle filtration systems and printer enclosures), and safety management programs at universities, businesses, and K-12 schools.

Section 2

Scientific Report

Background Information

Desktop three-dimensional (3D) printers are rapidly increasing in popularity. The majority of commercially available desktop 3D printers designed for the consumer market utilize an additive manufacturing technology called fused filament fabrication (FFF), also known as fused deposition modeling (FDM) or molten polymer deposition (MPD). In the FFF process, a solid thermoplastic filament is forced through a heated extrusion nozzle, melted, and deposited in thin layers onto a moving bed (Gross et al., 2014). A three-dimensional solid shape is formed layer-by-layer as the filament material cools and hardens. A wide variety of filament materials are now being used in desktop FFF 3D printers, including acrylonitrile butadiene styrene (ABS), polylactic acid (PLA), polyvinyl alcohol (PVA), polycarbonate (PC), high-density polyethylene (HDPE), high-impact polystyrene (HIPS), nylon, and many other polymers, metals, ceramics, and other materials (MatterHackers, 2015). Filaments are melted at a variety of extruder nozzle temperatures and bed temperatures, and manufacturers typically recommend ranges of optimal temperatures for each filament material and thickness. ABS and PLA are currently the most commonly used filaments in desktop 3D printers, although others are also gaining popularity (Ragan, 2013).

It is well known that both gases and particles are emitted during thermal processing of many thermoplastic materials (Contos et al., 1995; Unwin et al., 2013). However, little is known about the types and magnitudes of emissions from desktop FFF 3D printers and how they vary according to filament material or printer characteristics. In 2013, we published the first known measurements of emissions of ultrafine particles (UFPs: particles less than 100 nm in diameter) resulting from the operation of a single make and model of a commercially available desktop FFF 3D printer using both ABS and PLA filaments (Stephens et al., 2013). These findings were crucial, as exposure to emissions from thermal decomposition of thermoplastics has been shown to have toxic effects in animals (Zitting and Savolainen, 1980; Schaper et al., 1994; Oberdorster et al., 2005) and exposure to UFPs from other sources have been linked to a variety of adverse human health effects (Oberdörster et al., 1995, 2004; Delfino et al., 2005; Stölzel et al., 2007; Weichenthal et al., 2007; Andersen et al., 2010; HEI, 2013). As of 2015, we were aware of only one other published study that had investigated emissions from extrusion-based desktop 3D printers, although a few others have since been published, including our own work from this report. Kim et al. (2015) measured emissions of particles, total volatile organic compounds (TVOCs), several aldehydes and phthalates, and benzene, toluene, ethylbenzene, and m-,p-xylene (BTEX) from two different FFF printers operating in a small chamber, again using both ABS and PLA filaments (Kim et al., 2015). They confirmed that particle emissions were higher for printers utilizing ABS filaments compared to PLA filaments, and also demonstrated higher VOC emissions from the printers using ABS filaments compared to PLA.

Despite these prior studies, important gaps in our knowledge of emissions from 3D printers still remain. As of 2015, only a very limited number of makes and models of printers had been tested to date, and even fewer filament materials had been characterized for gas and/or particle

emissions (i.e., only ABS and PLA). Further, we hypothesize that previous studies such as Kim et al. (2015) may have missed some individual VOCs that are emitted when using some filaments because they were not specifically targeted or identified using a mass spectral library compound search. Also at the time, we had no information on how the design or shape of printed materials, or how printer characteristics such as the presence of enclosures, may influence gas and/or particle emissions. Moreover, we are not aware of any studies to date that have explored in detail the likely human exposures to both gas and particle emissions from desktop FFF 3D printers and filaments in more realistic indoor environments.

Specific Aims

Therefore, there are three specific aims of this work, which are consistent with those originally outlined in the project proposal:

1. Perform laboratory chamber testing to characterize emission rates of particles and VOCs from some of the most popular commercially available FFF desktop 3D printers operating with multiple filaments;
2. Perform chamber testing to evaluate the efficacy of a custom built gas and particle filtration add-on device in preventing emissions from the highest emitting desktop 3D printer; and
3. Model the impact of emission rates of particles and VOCs and viable control strategies on concentrations in workplace environments.

Methodology

The specific aims of this work were met with the following activities. First, we advanced prior studies by quantifying emission rates of UFPs and a broad range of speciated VOCs from 5 popular commercially available desktop FFF 3D printers utilizing as many as 9 different filaments to print standardized test objects in a medium-sized test chamber. We used the results to explore differences in particle and VOC emissions based on filament material and printer characteristics. We also provided preliminary data on the impact of print object geometry and the use of partial and whole printer enclosures to mitigate printer emissions. Second, we performed pilot testing to evaluate the effectiveness of a prototype sealed enclosure with a recirculating gas and particle filtration system for reducing UFP and TVOC emissions from high-emitting combinations of desktop 3D printers and filaments. Third, we used our published measurements of emission rates of both UFPs and speciated VOCs from a wide variety of desktop FFF 3D printers and filaments to predict the magnitudes of human exposures to these same pollutants that would be expected in multiple spatial locations within a typical small office environment. We also used the worst case UFP and VOC emission scenarios to model the likely impacts of several potential control strategies for reducing exposures.

Emissions testing procedures

All measurements were conducted inside a 3.6 m^3 stainless steel chamber (dimensions of 1.2×1.2×2.4 m) located in the Built Environment Research Group Laboratory at the Illinois Institute of Technology (Figure 1). The exterior walls of the chamber were made of 1.1 cm plywood sheets and the interior walls, floor, and ceiling were covered with 0.25 cm stainless steel sheets cut to the same size as the walls, floors, and ceiling. Gaps and edges inside the

chamber were sealed with adhesive PTFE film tape (3M 5490). Each printer was tested while operating on a 0.6×0.9×0.9 m stainless steel table at the center of the chamber. A small stainless steel mixing fan was operated to achieve well-mixed conditions in the chamber, which were confirmed prior to the experiments with CO_2 concentration measurements in four locations throughout the chamber. Each printer was connected to a desktop computer located outside the chamber so that it could be operated without opening the chamber door during the test period.

Filtered room air was supplied to the chamber using a 10 cm 12 VDC diameter blower connected to a fibrous activated carbon filter to remove both gases and particulate matter. A DC power supply was used to control the speed of the blower to keep the ventilation rate of the chamber constant near 1 hr^{-1} throughout each test. The ventilation rate was also measured during each test using CO_2 injection and decay. The chamber exhaust port was connected to a 20 cm diameter sheet metal duct that vented directly to a powered fume hood. The interior walls of the chamber were cleaned with distilled water after each experiment and the entire chamber was cleaned with isopropyl alcohol on a weekly basis. The chamber was left unused for at least 2 days after each alcohol cleaning to avoid contamination of VOC samples.

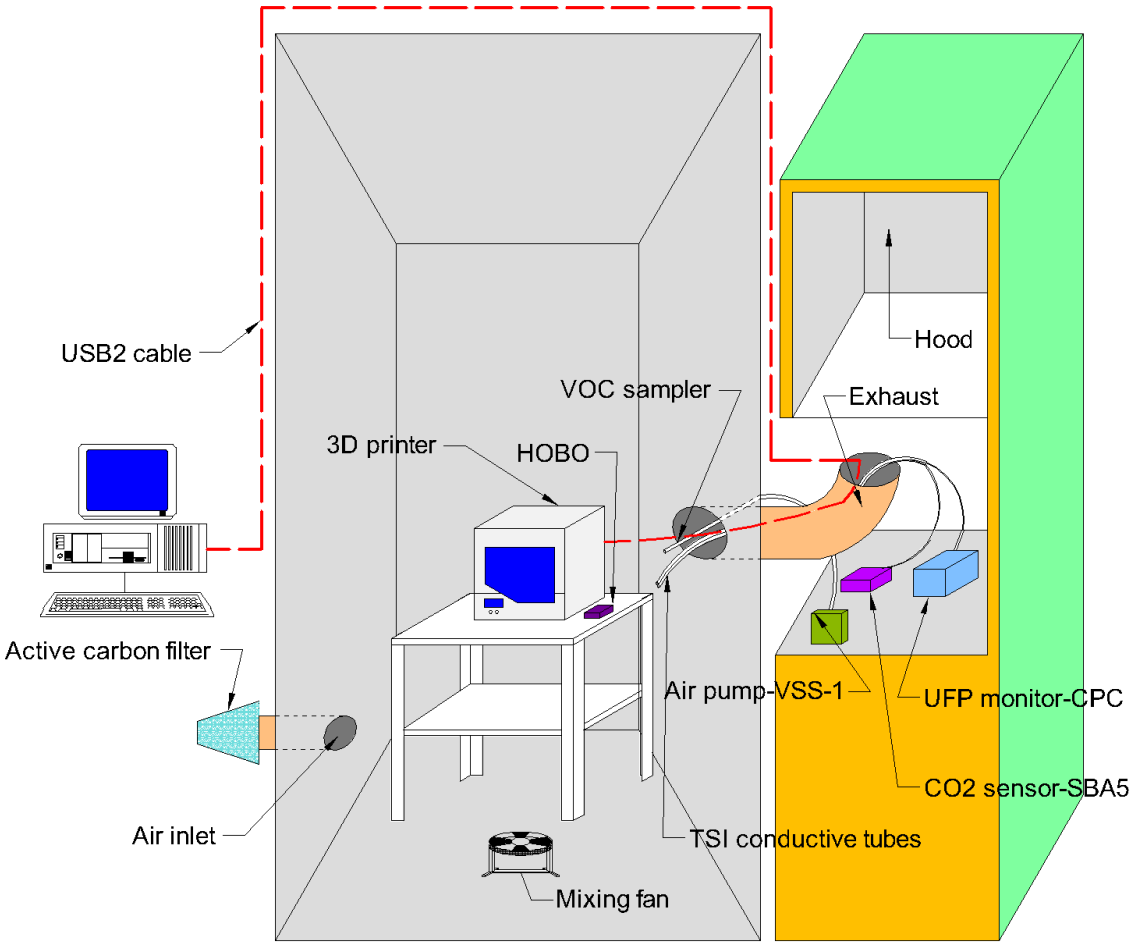

Figure 1. Schematic of the experimental test chamber

Each printer was connected to a desktop computer located outside the chamber. Before each experiment began, filtered supply air was delivered to the chamber at a constant ventilation rate of approximately 1 hr^{-1} for a period of at least 8 hours to achieve initial steady-state background conditions. The 3D printer beds were prepared for printing before sealing the chamber by wiping with isopropyl alcohol, or, in some cases, depending on the printer and filament combination, by applying small amounts of adhesive from glue sticks following manufacturer recommendations. The printer was then powered on and began printing a small object.

For all tests but one, we printed a 10×10×1 cm standardized sample from the National Institute of Standards and Technology (NIST), as shown in Figure 1 (Moylan and Slotwinski, 2012). The sample was chosen because it was developed as a standardized test part to evaluate the performance of additive manufacturing technologies and it has a range of features that were thought to potentially influence dynamic printer emissions, including a combination of solid volumes, thin protrusions, holes, and indentations. We also repeated one test with a single printer and filament combination printing a ~195 cm^3 cube of approximately the same printing duration as the NIST sample, allowing for an evaluation of the impact of print object shape on emissions. Nozzle and bed warm-up periods typically lasted between 5 and 10 minutes depending on the printer and filament and the printing time varied from 2.5 to 4 hours depending on the combination of printer, filament, and object shape.

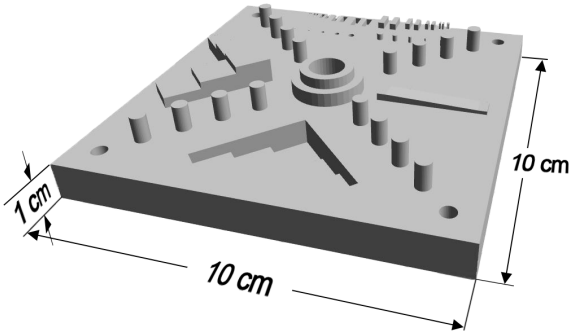

Figure 2. Shape file image of the NIST 3D printer test part used for emissions testing

Air sampling and analysis

Particle concentrations were continuously measured in the exhaust port of the chamber using a TSI Model 3007 Condensation Particle Counter (CPC) logging at 1-minute intervals. The CPC was located inside an external exhaust hood and connected to the chamber exhaust port by a 0.9 m long piece of conductive tubing 0.6 cm in diameter. The CPC measures the total number concentrations of particles between 10 nm and 1 μm with a reported maximum concentration of 10^5 #/cm^3 and a sample flow rate of 0.7 L/min. Particle concentrations were measured during all phases of the experiment, beginning with the last 45-60 minutes of background measurements, spanning the 2.5-4 hour print period (which includes the 5-10 minute warm-up phase), and ending with a final ~3-hour decay period during which particle concentrations were allowed to decrease towards background concentrations with the printer off.

We should note that although the measurement range of the CPC is 10 nm to 1 μm, the vast majority of particles emitted from most FFF printers were assumed to be in the UFP size range, which was consistent with our previous study and most other recent studies (Stephens et al.,

2013; Kim et al., 2015). Thus, we consider these measurements largely representative of UFPs and use this nomenclature from here on. We also periodically calibrated the CPC used for the chamber measurements using co-location measurements with a TSI Model 3910 NanoScan Scanning Mobility Particle Sizer (SMPS) that had been recently calibrated by the manufacturer. We considered the SMPS to be the most accurate for UFP measurements, but it was not available for use during all of the tests. Thus, we calibrated the CPC to the SMPS using a polynomial regression from these periodic co-location experiments. The calibration between CPC particle counts and total UFP counts from the SMPS (Figure 3) was nearly linear throughout the manufacturer-reported measurement range of the CPC (up to 10^5 #/cm^3) but increased exponentially beyond this range, as is typical for this instrument (Westerdahl et al., 2005). This was important to account for because several of the highest UFP emitters yielded raw CPC concentrations greater than 10^5 #/cm^3 in the experimental chamber.

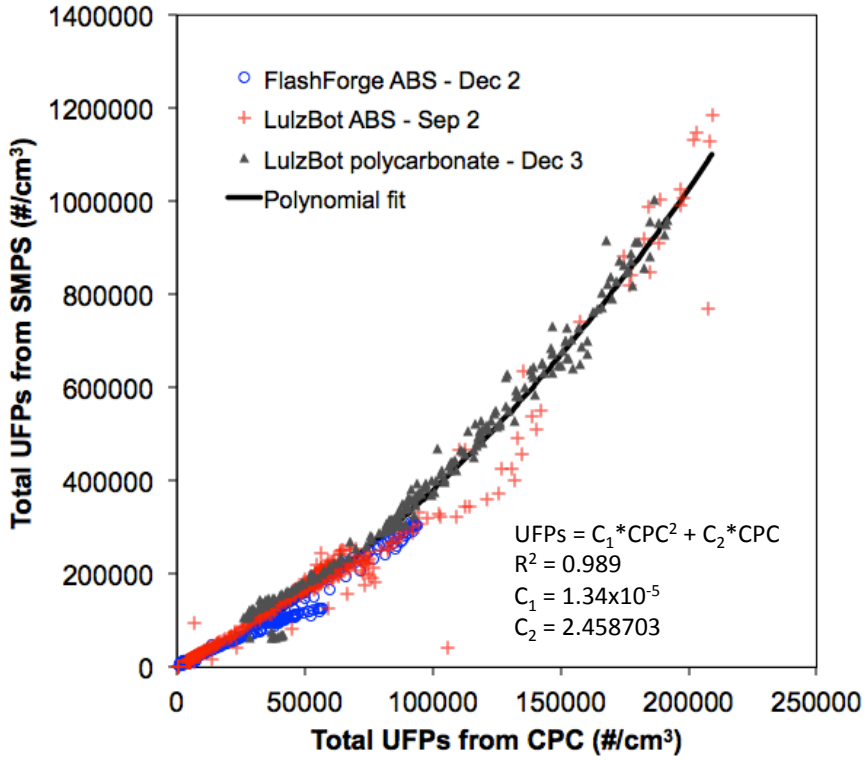

Figure 3. Measured UFP concentration inside the chamber using CPC and SMPS

Chamber air was also sampled during the tests for VOC analysis using Tenax-GR sorbent tubes during two periods: once during the last ~45 minutes prior to printing (with a printer in the chamber but not powered on or operating), and again during the last ~45 minutes of printing after VOC concentrations reached approximately steady state. We used the differences in concentrations between the two samples to estimate emission rates for both speciated VOCs and for the sum of the 10 highest detectable VOCs (i.e., ΣVOC). Total VOC (TVOC) concentrations inside the chamber were also continuously measured during a subset of experiments using a TSI Q-Trak Model 7575 Indoor Air Quality Monitor with a Model 982 photo-ionization detection (PID) probe to verify that TVOC concentrations achieved approximately steady state by the time

air sampling for VOC analysis was conducted. These measurements were used to verify that approximately steady state conditions were typically achieved within 2 hours from the beginning of printing and that TVOC emissions followed a characteristic constant emission rate profile. Thus we consider air sampling for VOC analysis during the final 45 minutes of printing each object reasonably representative of steady-state concentrations.

The procedure for sampling and analyzing the sorbent tubes was based on a modified version of U.S. EPA Method TO-17 (U.S. EPA, 1999). Sorbent tubes were inserted into a small hole in the exhaust port of the chamber and connected to a Buck VSS-1 low-flow air sampling pump located outside of the chamber operating at ~20 mL/min. Airflow rates of the sampling pumps and tubes were measured after each test using a Gilian Gilibrator 2 and combined with the recorded sampling duration to estimate the total air volume passed through the tubes during sampling. All sorbent tubes were shipped in a freezer pack overnight to the University of Texas at Austin and analyzed using thermal desorption followed by gas chromatograph and electron ionization mass spectrometry (TD/GC/MS). An internal standard, 4-Bromoflourobenzene (BFB), was used for all analysis. Individual VOCs were statistically identified and quantified using a NIST Library Compound Search (LCS). The mass of the identified compounds was estimated using the response of the internal standard and a relative response factor of one. The majority of the uncertainty associated with these calculations is related to the assumption that the relative response factor is one. Relative response factors for this method have been shown to commonly range from approximately 0.75 to 1.25 for most VOCs (Allgood et al., 1990), thus we use 25% as an approximate estimate of the uncertainty in our VOC quantification method. Individual VOCs may not have the same response factors, but this provides a reasonable base estimate of the uncertainty in the reported concentrations.

We also sampled for VOCs outside of the chamber during several tests. These sorbent samples were taken during the entire printing period to ensure that there were no unexpected external sources of VOCs transported into the chamber. Blank sorbent tubes were also collected outside the chamber without connecting them to the air pumps during each test to characterize adsorption of any unexpected compounds during shipping and storage. Finally, temperature and relative humidity (RH) were measured during each test using an Onset HOBO U12 data logger recording at 1-minute intervals, and ventilation rates were measured during each test using CO_2 as a tracer gas. CO_2 was injected from a small tank into the chamber at the beginning of each test and the subsequent decay of chamber CO_2 concentrations was measured using a PP Systems SBA-5 CO_2 monitor connected to an Onset HOBO U12 data logger, also recording at 1-minute intervals.

Ventilation rate estimations

We estimated the air exchange rate (AER) of the chamber during each experiment using a CO_2 injection and decay method, which involved increasing the CO_2 concentration inside the chamber by injection from a filtered compressed CO_2 cylinder and measuring the subsequent decay. We applied a dynamic mass balance equation for change in CO_2 concentration inside the chamber as shown in Equation 1.

$$\frac{dC_{co2,in}(t)}{dt} = \lambda C_{CO2,out} - \lambda C_{CO2,in}(t) \quad (1)$$

Where $C_{co2,in}(t)$ is the concentration of CO_2 inside the chamber during an experiment (ppm); t is time (min); λ is the air exchange rate of the chamber during an experiment (1/min); and $C_{CO2,out}$ is the concentration of CO_2 outside the chamber during an experiment (ppm). We also measured the background chamber CO_2 concentrations when it achieved steady state levels prior to the printing experiment and used this value for the concentration outside the chamber. Thus, Equation 1 can be re-written for background period as Equation 2.

$$C_{CO2,out} = \bar{C}_{CO2,in,bg} \tag{2}$$

Where $\bar{C}_{CO2,in,bg}$ is the average background CO_2 concentration during an experiment (ppm). We estimated the AER of the chamber by re-arranging and integrating Equation 1, as shown in Equation 3.

$$-ln\frac{C_{CO2,in}(\mathrm{t}) - \bar{C}_{CO2,in,bg}}{C_{CO2,in}(\mathrm{t}=0) - \bar{C}_{CO2,in,bg}} = \lambda t \tag{3}$$

We plotted the left hand side of Equation 3 versus time for the first 60 minutes of the decay periods and considered the slope of linear regression line through the data points as the air exchange rate of the chamber during the entire experiment.

UFP emission rate estimations

We applied a dynamic well-mixed number balance on the total particle number concentrations measured inside the chamber (Equation 4) to estimate time-varying particle emission rates, which we considered largely representative of UFPs.

$$\frac{dC_{UFP,in}(t)}{dt} = P_{UFP}\lambda C_{UFP,out} - L_{UFP}C_{UFP,in}(\mathrm{t}) + \frac{E_{UFP}(t)}{V} \tag{4}$$

Where $C_{UFP,in}(t)$ is the UFP concentration inside the chamber at time t (#/m^3), P_{UFP} is the UFP penetration factor of the chamber (-), λ is the air exchange rate of the chamber (1/min), $C_{UFP,out}$ is the UFP concentration outside of the chamber (#/m^3), L_{UFP} is the total UFP loss rate constant inside the chamber (1/min), $E_{UFP}(t)$ is the time-varying UFP emission rate from a single 3D printer at time t (#/min), and V is the chamber volume (m^3).

The UFP concentration inside the chamber prior to testing (i.e., during the background period) reached steady state conditions prior to all experiments. Therefore, the average measured background concentration $\bar{C}_{UFP,bg}$ was used in place of $P_{UFP}\lambda C_{UFP,out}$ using Equation 5.

$$P_{UFP}\lambda C_{UFP,out} = \bar{C}_{UFP,bg}L_{UFP} \tag{5}$$

The total UFP loss rate (L_{UFP}) was estimated using a log-linear regression with data from the final decay period after printing finished, as shown in Equation 6. We plotted the left hand side of Equation 6 versus time for the first 60 minutes of the decay period and used the slope of the linear regression as the total UFP loss rate during the entire experiment.

$$-ln\frac{C_{UFP,in}(\mathrm{t})-\bar{C}_{UFP,bg}}{C_{UFP,in}(\mathrm{t}=0)-\bar{C}_{UFP,bg}}=L_{UFP}t \quad (6)$$

Because there was a large amount of scatter in the resulting UFP concentration data, we first applied a smoothing function to the UFP data using the '*smooth*' function in MATLAB R2015a. These smoothed concentration data were then used to estimate the time-varying UFP emission rate for each printer and filament combination using a discrete solution to a dynamic well-mixed number balance applied on the total particle number concentrations measured inside the chamber, as shown in Equation 7.

$$\frac{E_{UFP}(t_{n+1})}{V}=\frac{\left[C_{UFP,in}(\mathrm{t_{n+1}})-C_{UFP,in}(\mathrm{t_n})\right]}{\Delta t}-L_{UFP}\bar{C}_{UFP,bg}+L_{UFP}C_{UFP,in}(t_n) \quad (7)$$

Where $E_{UFP}(t)$ is the time-varying UFP emission rate from a single 3D printer at time t (#/min), V is the chamber volume (m^3), $C_{UFP,in}(t)$ is the UFP concentration inside the chamber at time t (#/m^3), Δt is the time step for UFP measurements (1 min), L_{UFP} is the total UFP loss rate constant (1/min), and $\bar{C}_{UFP,bg}$ is the average background UFP concentration inside the chamber prior to emissions testing. We should note that Equation 7 makes several important assumptions that may lead to inaccuracies in estimates of UFP emission rates such as ignoring size-resolved particle dynamics, ignoring coagulation, and assuming constant particle loss rates, but that these limitations do not drastically affect the overall results.

The time-varying UFP emission rate estimates were also used to quantify the total number of UFPs emitted during printing, normalized by the mass of filament used, as shown in Equation 8.

$$\dot{E}_{UFP}=\frac{\sum_{k=1}^{N}E_{UFP}(t_k)\times\Delta t}{m_{object}} \quad (8)$$

Where $\dot{E}_{UFP}$ is the total number of UFPs emitted during printing per mass of filament used (#/g), N is the total number of time intervals during printing (min), and m_{object} is the mass of filament used (i.e., the mass of the final printed object) (g).

VOC emission rate estimation

The TD/GC/MS library compound searches (LCS) identified and quantified approximately 50 speciated VOCs inside the chamber during the initial background periods and the last ~45 minutes of the printing periods. The emission rate of each identified VOC was estimated using Equation 9, which assumes that ventilation was the only removal mechanism in the chamber, that the concentrations of top 10 measured emitted VOCs from 3D printers were negligible outside the chamber (verified by measurements), and that VOC concentrations achieved steady state during the final sampling period.

$$E_{VOC,i}=\left(C_{VOC,i,print}-C_{VOC,i,bg}\right)\lambda V \quad (9)$$

Where $E_{VOC,i}$ is the estimated constant emission rate of an individual VOC (µg/min), $C_{VOC,i,print}$ is the steady state concentration of an individual VOC inside the chamber during the last ~45 minutes of printing (µg/m^3), and $C_{VOC,i,bg}$ is the background concentration of an individual VOC inside the chamber prior to printing (µg/m^3). The emission rate of each printer for the sum of the 10 highest detectable VOCs (i.e., ΣVOC) was estimated by adding all positive individual VOC emission rates of the top 10 compounds with the highest concentrations inside the chamber during the last 45 minutes of the printing period. We limited to the top 10 highest concentration compounds because compounds below the top 10 added negligible amounts to the overall detectable ΣVOC_i mass. We also normalized ΣVOC emission rates by the mass of filament consumed using Equation 10.

$$\dot{E}_{\Sigma VOC} = \frac{\sum_{k=1}^{N} E_{\Sigma VOC}(t_k) \times \Delta t}{m_{object}} \quad (10)$$

Where $E_{\Sigma VOC}$ is the total VOC emission rate of a printer for the top 10 identified compounds and $\dot{E}_{\Sigma VOC}$ is the total VOC emission rate per mass of filament used (µg/g).

Time to reach steady-state

TVOC concentrations inside the chamber were continuously measured during a limited subset of experiments using a TSI Q-Trak Indoor Air Quality Monitor Model 7575 with a Model 982 PID-based TVOC probe to verify that TVOC concentrations achieved approximately steady state by the time air sampling for VOC analysis was conducted. As an example, Figure 4 shows time-resolved TVOC concentrations measured during printing the standard NIST sample from using just one printer and filament combination (FlashForge with ABS filament).

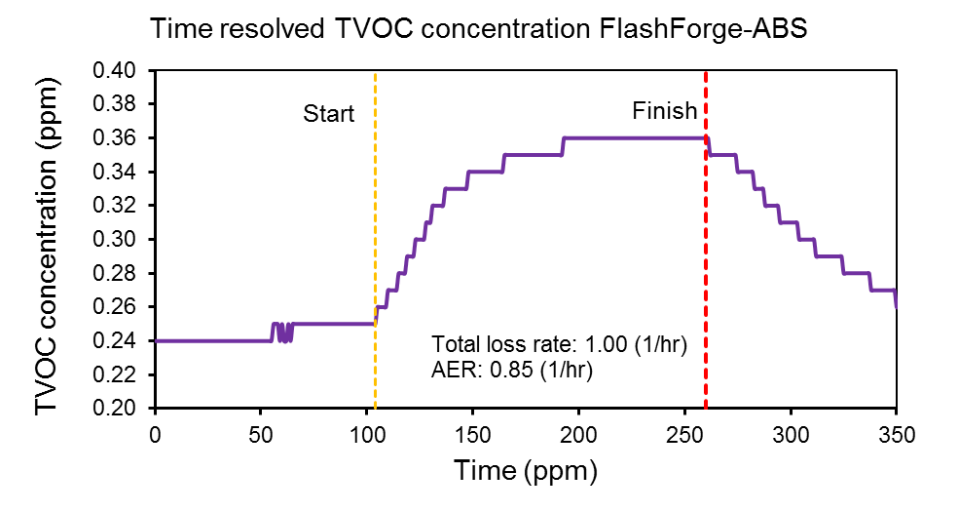

Figure 4. Time resolved TVOC concentration inside the test chamber

Figure 4 shows that the TVOC concentration reached to approximately steady state conditions ~100 minutes after printing started. Two other similar experiments with different printers/filaments were also similar. These measurements verified that approximately steady state conditions were typically achieved within 2 hours from the beginning of printing. Thus we consider air sampling for VOC analysis during the final 45 minutes of printing each object (the printing durations were at least 2 hr 26 min for all experiments) a reasonable assessment of

steady state concentrations and can use the difference between the two samples to make reasonable estimates of speciated VOC emission rates.

Additionally, we also used these data to investigate the potential for sorption effects to the stainless steel chamber walls by estimating the total TVOC loss rate from the final decay period in Figure 4 (i.e., after printing stopped, around 260 mins). The total TVOC loss rate was approximately 1.0 hr^{-1} using these data while the measured air exchange rate was 0.85 hr^{-1}. Thus, it appears that in this case, other removal mechanisms such as sorption on the chamber walls may have contributed an additional 0.15 hr^{-1}. However, when we applied the same method to two other experiments the results varied. The total TVOC loss rates were 1.12 and 1.22 hr^{-1}, with corresponding AERs of 1.04 and 1.24 hr^{-1}, respectively. These corresponded with the total loss rate being 7% higher and 2% lower than the chamber air exchange rate. Thus, we consider it reasonable to assume that sorption effects were negligible herein and that ventilation is indeed the major loss mechanism.

Uncertainty analysis

We estimated the uncertainty in our UFP and VOC emission rate estimates using a variety of approaches. First, we calculated the uncertainty in each smoothed concentration of UFP data, the average background concentration of UFPs, the chamber air exchange rate (AER), and the total UFP loss rate by adding standard errors of regression coefficients from related equations and the accuracy of each monitoring device in quadrature. The uncertainty associated with the smoothed concentration of UFP is a function of the reported accuracy of the TSI CPC model 3007 (±20%) and the standard error due to both calibration (R^2_{calib} = 0.981) and smoothing (R^2_{smooth} > 0.9, varied depend on the experiment), which was calculated using Equation 11.

$$\Delta C_{UFP,smooth} = \sqrt{(AC_{CPC})^2 + \left(\frac{SE_{UFP,calib}}{\bar{C}_{UFP,calib}}\%\right)^2 + \left(\frac{SE_{UFP,smooth}}{\bar{C}_{UFP,smooth}}\%\right)^2} \quad (11)$$

Where $\Delta C_{UFP,smooth}$ is the uncertainty associated with smoothed UFP concentration inside the chamber for each combination of 3D printer, filament and printing object shape (%); AC_{CPC} is the average accuracy of TSI CPC model 3007 (±20%); $SE_{UFP,calib}$ is the standard error of the calibration (± 933 #/cm^3); $\bar{C}_{UFP,calib}$ is the average concentration of UFP inside the chamber during the calibration measured by SMPS (± 183444 #/cm^3); $SE_{UFP,smooth}$ is the standard error of the smoothing procedure for each studied combination (#/cm^3); and $\bar{C}_{UFP,smooth}$ is the average smoothed concentration of UFP inside the chamber during the printing period for each studied combination (#/cm^3). The uncertainty associated with the background concentration of UFPs is a function of the average accuracy of the CPC, the standard error of the mean, and the standard error due to calibration, which was calculated using Equation 12.

$$\Delta C_{UFP,bg} = \sqrt{(AC_{CPC})^2 + \left(\frac{SE_{UFP,calib}}{\bar{C}_{UFP,calib}}\%\right)^2 + \left(\frac{SE_{UFP,bg}}{\bar{C}_{UFP,bg}}\%\right)^2} \quad (12)$$

Where $\Delta C_{UFP,bg}$ is the uncertainty associated with average background UFP concentration inside the chamber for each combination of 3D printer, filament and printing object shape (%);

$SE_{UFP,bg}$ is the standard error of the mean background UFP concentration inside the chamber for each studied combination (#/cm^3); and $\bar{C}_{UFP,smooth}$ is the average background concentration of UFP inside the chamber during the printing period for each studied combination (#/cm^3).

The uncertainty associated with the AER of chamber is a function of the average accuracy of SBA-5 CO_2 analyzer, the standard error of the mean CO_2 background, and the standard error due to fitting a linear regression line to the left hand side (LHS) of Equation 3, which was calculated using Equation 13.

$$\Delta AER = \sqrt{\left(\frac{AC_{SBA5}}{\bar{C}_{CO2,decay}}\%\right)^2 + \left(\frac{AC_{SBA5}}{\bar{C}_{CO2,bg}}\%\right)^2 + \left(\frac{SE_{CO2,bg}}{\bar{C}_{CO2,bg}}\%\right)^2 + \left(\frac{SE_{CO2,LHS}}{\overline{LHS}_{CO2}}\%\right)^2} \quad (13)$$

Where ΔAER is the uncertainty associated with AER of the chamber for various experiments (%); AC_{SBA5} is the average accuracy of SBA5 CO_2 monitor (±20 ppm); $\bar{C}_{CO2,decay}$ is the average concentration of CO_2 during the decay period for each experiment (ppm); $\bar{C}_{CO2,bg}$ is the average concentration of background CO_2 for each experiment (ppm); $SE_{CO2,bg}$ is the standard error of the mean CO_2 background concentration for each experiment (ppm); $SE_{CO2,LHS}$ is the standard error of linear regression line fitted to left hand side values of Equation 3 to estimate AER for each experiment (-); and $\overline{LHS}_{CO2}$ is the left hand side values average in Equation 3 to estimate AER for each experiment (-).

We also estimated the uncertainty associated with the total loss rate for each combination of printer, filament, and printing object shape based on the regression coefficients from curve fits to the exponential decay data. The total loss rate uncertainty is a function of the background and smoothed UFP concentrations and the standard error of the linear regression between to the left hand side (LHS) of Equation 6 versus time, which was calculated using Equation 13.

$$\Delta L_{UFP} = \sqrt{\left(\Delta C_{UFP,smooth}\right)^2 + \left(\Delta C_{UFP,bg}\right)^2 + \left(\frac{SE_{UFP,LHS}}{\overline{LHS}_{UFP}}\%\right)^2} \quad (14)$$

Where ΔL_{UFP} is the uncertainty associated with the UFP loss rate for various experiments (%); $SE_{UFP,LHS}$ is the standard error of linear regression line fitted to left hand side values of Equation 6 to estimate UFP total loss rate for various experiments (-); and $\overline{LHS}_{UFP}$ is the average of left hand side values in Equation 6 to estimate UFP total loss rate for various experiments (-).

Next, we used the previous uncertainty estimations to calculate uncertainty associated with time varying UFP emission rate, VOC concentration in background and printing periods, and VOC emission rate from each printer. We calculated the uncertainty of time-varying UFP emission rates based on Equation 7, as shown in Equation 15.

$$\Delta E_{UFP}(t_{n+1}) = \sqrt{\left(\Delta C_{UFP,in}(t_{n+1})\right)^2 + \left(\Delta C_{UFP,in}(t_n)\right)^2 + (\Delta L_{UFP})^2 + \left(\Delta \bar{C}_{UFP,bg}\right)^2} \quad (15)$$

Where $\Delta E_{UFP}(t_{n+1})$ is the uncertainty associated with UFP emission rate (%).

Next, we estimated the uncertainty associated with the speciated VOC emission rate estimates. For each VOC sampling tube and pump combination, we measured the air flow rate through the tube five times, and calculated the uncertainty in this airflow rate as a function of the average accuracy of the air flow meter and the standard error of the mean measured air flow rate, as shown in Equation 16.

$$\Delta Q_{pump} = \sqrt{\left(\frac{AC_{flowmeter}}{\bar{Q}_{pump}}\%\right)^2 + \left(\frac{SE_Q}{\bar{Q}_{pump}}\%\right)^2} \quad (16)$$

Where ΔQ_{pump} is the uncertainty associated with the airflow rate through VOC sampling tubes (%); $AC_{flowmeter}$ is the average accuracy of airflow meter (± 1 cm^3/min); $\bar{Q}_{pump}$ is the average airflow rate passing through VOC sampling tubes (cm^3/min); and SE_Q is the standard error of mean measured airflow rate through VOC sampling tubes (cm^3/min).

We calculated the uncertainty of VOC concentration in background and printing periods based using Equation 17.

$$\Delta C_{VOC} = \sqrt{\left(AC_{M,VOC}\right)^2 + \left(\Delta Q_{pump}\right)^2} \quad (17)$$

Where ΔC_{VOC} is the uncertainty associated with VOC concentration in background and printing periods (%); and $AC_{M,VOC}$ is the accuracy of GC-MS technique to quantify collected mass of VOC in the sampling tubes (assumed to be ± 25% for a typical relative response factor between 0.75 and 1.25).

Finally, we calculated the uncertainty in the VOC emission rate estimate using Equation 18.

$$\Delta E_{VOC,i} = \sqrt{\left(\Delta C_{VOC,i,print}\right)^2 + \left(\Delta C_{VOC,i,bg}\right)^2 + (\Delta \mathrm{AER})^2} \quad (18)$$

Where $\Delta E_{VOC,i}$ is the uncertainty associated with estimated VOC emission for each component (%).

Printer and filament descriptions

We characterized UFP and VOC emissions from a total of 16 unique combinations of printers and filaments, including five popular commercially available makes and models of desktop 3D printers with up to nine different filament materials. The five printers included: (1) a FlashForge Creator dual extruder model compatible with ABS and PLA (both filaments were tested); (2) a Dremel 3D Idea Builder compatible with PLA only; (3) an XYZprinting da Vinci 1.0 compatible with ABS only; (4) a MakerBot Replicator 2X compatible with ABS only; and (5) a LulzBot Mini that was compatible with many different types of filaments. The LulzBot printer was tested with nine different filaments that are commonly used, including ABS, PLA, high impact polystyrene (HIPS), semitransparent nylon, laybrick (an imitation brick material of unknown

chemical composition), laywood (an imitation wood material of unknown chemical composition), transparent polycarbonate, a semitransparent nylon-based plasticized copolyamide thermoplastic elastomer (PCTPE), and a transparent polyester resin filament called T-Glase. The Dremel, XYZprinting, and MakerBot all had built-in plastic enclosures surrounding the apparatus (although they were not airtight), while the FlashForge and LulzBot did not have any enclosures. This list of printers is not meant to be exhaustive, but it is designed to span a reasonable range of currently popular printers with relatively generalizable characteristics such as filament type, nozzle and bed temperatures, and the presence or lack of a partial enclosure. Table 1 summarizes all experiments that were conducted.

Table 1. Summary of all experiments

Printer	Filaments	Extruder Temp. (°C)	Bed Temp. (°C)	Bed preparation	Test sample	Mass (g)	Encl.	Printing duration
FlashForge Creator	ABS-White	200	110	Glue	NIST	40.2	No	3hr 42min
	PLA-Red	200	110	Glue	NIST	53.2		3hr 42min
Dremel 3D Idea Builder	PLA-White*§	230	room temp.	Alcohol wipe	NIST	55.2	Yes	2hr 49min
XYZprinting da Vinci 1.0	ABS-Blue	230	100	Glue	NIST	40.4	Yes	2hr 26min
LulzBot Mini	ABS-Red*§ǂ	240	110	Alcohol wipe	NIST	44.5	No	2hr 33min
	ABS-Red	240	110	Alcohol wipe	Cube	56.7		2hr 42min
	PLA-Red	190	45	Alcohol wipe	NIST	53.1		3hr 25min
	HIPS-Black*	240	100	Alcohol wipe	NIST	47.4		2hr 28min
	Nylon Bridge-Semitransparent	230	65	Glue	NIST	46.5		2hr 55min
	Laybrick-White	200	65	Alcohol wipe	NIST	57.7		3hr 00min
	Laywood-Brown	200	65	Alcohol wipe	NIST	48.3		3hr 02min
	Polycarbonate-Transparent*	270	110	Glue	NIST	52.1		2hr 38min
	PCTPE-Semitransparent	235	65	Glue	NIST	47.8		3hr 02min
	T-Glase-Transparent red	240	60	Alcohol wipe	NIST	49.4		3hr 02min
MakerBot Replicator 2X	ABS-Whiteǂ	230	110	Glue	NIST	40.3	Yes	2hr 38min
	ABS-Whiteǂ	230	110	Glue	NIST	40.7	No	2hr 38min

* Experimental conditions with duplicate VOC emissions tests

§ Experimental conditions with duplicate UFP emissions tests

ǂ Experiments with simultaneous VOC sampling conducted outside of the chamber

Fifteen of the 16 printer and filament combinations were used to print the NIST test part, while one test combination (LulzBot-ABS) was also used to print a cube. The MakerBot with ABS filament was also tested twice: once with the plastic enclosure from the manufacturer installed as received from the factory and once with the enclosure intentionally removed. We also performed duplicate VOC measurements for four printer and filament combinations and two duplicate UFP measurements to evaluate the repeatability of our experiments.

Pilot study of a prototype sealed enclosure with gas and particle filtration

Subsequently, we also performed pilot testing to evaluate the effectiveness of a prototype sealed enclosure with a recirculating gas and particle filtration system (manufactured by 3DPrintClean) for reducing UFP and TVOC emissions from high-emitting combinations of desktop 3D printers and filaments (Figure 5). One printer was tested (LulzBot) with two of the highest UFP- and VOC-emitting filaments (Nylon and ABS filaments). The Nylon filament was previously shown to emit caprolactam as its primary speciated VOC, while ABS was shown to primarily emit styrene. We measured UFP concentrations using a TSI Model 3007 condensation particle counter (CPC) and TVOC concentrations with a RAE Systems ppbRAE 3000 TVOC monitor as indicators of these and other compounds.

Figure 5. 3DPrintClean enclosure and filtration system with a LulzBot printer in the controlled environmental chamber

Predicting concentrations of UFPs and VOCs resulting from 3D printer operation

After the measurement phase of this project, we then used a multi-zone airflow and contaminant transport analysis modeling software, CONTAM 3.2 (NIST, 2016), to predict concentrations resulting from gas and particle emissions from several combinations of desktop FFF 3D printers and filaments, assuming each printer is operated inside a one-story office building with a floor area of 511 m^2. The office building geometry and floor plan was taken from the Department of

Energy (DOE) Commercial Reference Building data set (Ng et al., 2012). However, we modified some of the building characteristics in the CONTAM model to represent more realistic scenarios. Figure 6 shows the building floor plan divided into multiple zones and the maximum occupancy in each zone (Ng et al., 2012).

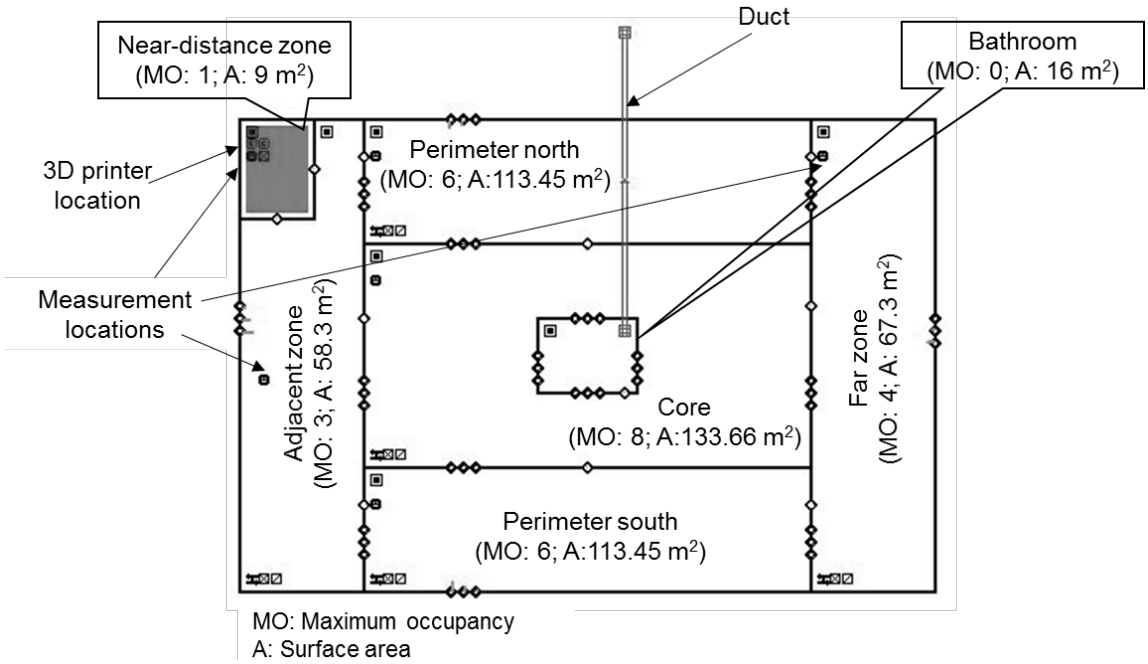

Figure 6. CONTAM model for the small office building (MO: maximum occupancy; A: floor area)

Each zone was assumed to be well-mixed with uniform temperature, relative humidity, and pollutant concentration. In all simulations, one desktop 3D printer was located in the small shaded zone in the top left corner of Figure 6. This zone does not have physical partitions like the other zones, but represents a 9 m^2 floor area space within the western perimeter zone in which the printer is contained. We refer to this zone as the "near-distance" zone, in which a person would be sitting within immediate proximity to an operating 3D printer (i.e., within ~3 m) for extending periods of time. We also refer to two other main zones in which occupants would be exposed to printer emissions only after the contaminants are transported from the printer location to those areas, including an immediately "adjacent zone" to the near-distance zone (within ~3-18 m) and a "far zone" that is on the far end of the building (between ~ 18 and ~33 m away).

Each zone (other than the bathroom and the "near-distance" zone) was modeled with its own air-handling unit (AHU) designed to recirculate indoor air and deliver outdoor air for ventilation. The total supply and return airflow rates were the same for each AHU. We assumed that all five AHUs were designed to meet ASHRAE Standard 62.1-2010 minimum ventilation requirements based on both floor area and occupancy (ASHRAE, 2010). One exhaust fan ducted to the exterior was also assumed to operate continuously in the bathroom at an airflow rate of 1.8 m^3/hr. The required outdoor air ventilation rate for each zone, $Q_{vent,i}$ (m^3/hr), was calculated using equation 19 (ASHRAE, 2010).

$$Q_{vent,i} = A \times N_{occupants,i} + B \times A_{zone,i} \quad (19)$$

Where A is the required outdoor air ventilation per person for a small office (9 m^3/hr per person); B is the required outdoor air ventilation per floor area (1.08 m^3/hr per m^2); $N_{occupants,i}$ is the maximum number of occupants in zone i (-); and $A_{zone,i}$ = the floor area of zone i (m^2).

For the baseline simulation conditions, we also assumed that the AHUs met minimum HVAC filtration efficiency requirements in ASHRAE Standard 62.1-2010 with MERV 8 particle filters and no gas-phase filtration (ASHRAE, 2012). We estimated the removal efficiency of MERV 8 filters for UFPs emitted from desktop 3D printers to be 43.5% by mapping the size-resolved removal efficiency of filters recently tested in Fazli and Stephens (2016) to the resulting size-resolved distribution of emitted particles from 3D printers in an office environment reported in Stephens et al. (2013) for particles less than 100 nm following a procedure described in Azimi et al. (2014).

We assumed default building occupancy and HVAC system runtime schedules from the NIST model, with the building occupied on weekdays from 7:00 am to 6:00 pm and the HVAC system operating from 6:00 am to 10:00 pm on weekdays. In all cases, we assumed that a single desktop 3D printer operated continuously for 8 hours from 9:00 am to 5:00 pm, representing a relatively high, albeit not uncommon, duration of operation. We assumed that the building was located in Chicago, IL and used Typical Meteorological Year (TMY) 3 data for Chicago (NSRDB: 1991-2005 Update: TMY3). Air infiltration through exterior walls was modeled using three characteristic openings in each wall representing various types of openings, including cracks and gaps in the walls, at the wall corners, and around large openings such as windows and doors. The effective leakage area was assumed to be 5.27 cm^2/m^2 at a reference pressure difference of 4 Pa for all three types of small openings (Emmerich and Persily, 2011). All of the zones were connected to at least one other zone by large openings with cross sectional areas of 1 m^2, which served to simulate doorway openings. The zone boundaries for the "near-distance" 3D printing zone were modeled as walls with large openings the same size as their cross sectional areas (9 m^2).

Given the breadth of our experimental work described above, we use the emission rates of UFPs and the primary speciated VOCs emitted from each of the 9 filaments that were tested to predict the time-varying concentrations of each pollutant that would likely be present in the previously defined near, adjacent, and far zones. We modeled the emitted pollutants "in addition" to what concentrations would have existed from other indoor sources. Thus, we assume that the concentrations of each pollutant in both outdoor and background indoor air are zero. In CONTAM, we assumed the diffusion coefficients of caprolactam and styrene in the office air are 0.065 and 0.071 cm^2/s (NJDEP, 2015), respectively, and kept the UFP and lactide diffusion coefficients equal to CONTAM defaults (0.2 cm^2/s). We also assumed default CONTAM values for the effective density and specific heat of UFP equal to 1 g/cm^3 and 1 kJ/kgK, respectively. Finally, the UFP decay rate was assumed 25×10^{-5} s^{-1}, equal to the median values measured in a recent study in UFP decay rates in residences (Wallace et al., 2013).

Modeling exposure control strategies

We also modeled the impacts of several control strategies on resulting pollutant concentrations in the office space, including: (i) upgrading the central HVAC filtration throughout the office; (ii) operating portable stand-alone air cleaners within close proximity to the 3D printer; (iii) installing spot ventilation systems within close proximity to the 3D printer; and (iv) operating the 3D printer inside a prototype sealed enclosure with recirculating gas and particle filtration. For this analysis, we modeled only the highest emission rates for each of the primary emitted pollutants to model the likely impacts of control strategies on only the worst-case scenarios of UFP and VOC emissions.

In the first exposure control scenario, we assumed that the HVAC filters installed in the central AHUs were upgraded to MERV 16 media impregnated with activated carbon to provide both gas and particle filtration. We estimated the UFP removal efficiency of the MERV 16 filter to be 97% using the same matching approach with data from Fazli and Stephens (2016) described earlier for MERV 8 filters. Because there is a lack of literature on the gas-phase removal efficiency of impregnated activated carbon filters for caprolactam, styrene, or lactide (which were the primary VOCs emitted from filaments herein), we relied on estimates from Sidheswaran et al. (2012) who reported VOC removal efficiencies of active carbon fiber filters for six speciated VOCs ranging between 60% and 80%. Therefore, we assumed that the removal efficiency of the HEPA filters with active carbon fibers for all of the emitted VOCs is equal to 70%.

Several previous studies have measured clean air delivery rates (CADRs) and/or single-pass removal efficiencies for UFPs from a number of commercial stand-alone air cleaners. Waring et al., (2008) reported a single-pass removal efficiency of ~60% for two HEPA air cleaners with average CADRs across all particle sizes of 188 and 324 m^3/hr, respectively. Other studies have reported CADRs for UFPs from other similar commercial air cleaner products ranging from ~100 to ~300 m^3/hr, with single-pass efficiencies typically ranging from ~45% to ~60% (Sultan et al., 2011; Mølgaard et al., 2014). Therefore, we modeled two distinct portable air cleaner scenarios with CADRs of 100 and 300 m^3/hr for UFPs. Assuming a single-pass efficiency of 60% for the HEPA filters, the airflow rates of the two air cleaners were calculated to be 167 m^3/hr and 500 m^3/hr, respectively. We assumed that the filters also contained impregnated carbon with 70% removal efficiency for each of the VOCs modeled herein (Sidheswaran et al., 2012), which yields CADRs for the modeled VOCs of 117 m^3/hr and 350 m^3/hr for the low- and high-efficiency air cleaner scenarios, respectively. Both air cleaners were modeled in CONTAM as an air handling system with equal supply and return air flows inside the "near-distance" zone and without any air exchange with outdoor air.

Next, we modeled the impacts of introducing spot ventilation in the "near-distance" zone within the immediate vicinity of the operating 3D printer. For lack of other data on exhaust systems that are designed specifically for 3D printer applications, we assumed that spot ventilation systems performed similar to exhaust hoods installed in small commercial or residential kitchens. We assumed that the hoods were located approximately 1.5 m above the desktop 3D printer and exhausted directly to the outdoors. A few recent studies in test kitchens have reported widely varying nominal and measured airflow rates, as well as capture efficiencies for both gas and particle emissions from cooking, that are achievable by a number of kitchen exhaust fans (Delp

and Singer, 2012; Singer et al., 2012; Logue, 2014). The nominal airflow rates in these studies ranged from 325 to 1300 m^3/hr (with measured airflow rates from 75 to 650 m^3/hr), and with low, moderate, and high pollutant capture efficiencies ranging from less than 50% to greater than 75%, generally scaling with airflow rates (Singer et al., 2012). Moreover, if we were to consider the 67.3 m^2 printing area in the office space as a "chemical storage room," ASHRAE Standard 62.1 would require a minimum exhaust airflow rate of 27 m^3/hr per m^2 of floor area (i.e., a total exhaust rate of 1817 m^3/hr) to meet minimum ventilation requirements (ASHRAE, 2010).

Given these bounds of reasonable airflow rates and capture efficiencies (CEs), we modeled three distinct spot ventilation scenarios with the following characteristics: (1) low effectiveness with 90 m^3/hr (25 L/s) and 25% CE; (2) medium effectiveness with 360 m^3/hr (100 L/s) and 63% CE; and (3) high effectiveness with 1800 m^3/hr (500 L/s) 100% CE. To model the spot ventilation scenarios in CONTAM, we defined a hypothetical 1 m^2 space inside the "near-distance" zone with an exhaust fan ducted to the outdoor air. We divided the emission sources between the zones based on the CE of the spot ventilation scenario. For example, if the CE was 25%, 75% of the total emissions of the four main pollutants were assumed to flow into the "near-distance" zone where they could be transported to other spaces and result in exposure, while 25% of the total emissions remained only in the 1 m^2 "spot ventilation zone." We divided the HVAC system supply airflow rates between the "near-distance" and "spot ventilation" zones in such a way that both zones have equal pollutant concentrations when the 3D printer operates and the spot ventilation airflow rate is zero.

Finally, we modeled the impacts of operating the 3D printers inside a prototype sealed enclosure with recirculating gas and particle filtration to reduce emissions. For this analysis, a pilot experimental chamber study was conducted with two high emitting filament and printer combinations installed inside a prototype enclosure that was tested herein (Figure 5). Average total VOC (i.e., TVOC) and UFP removal efficiencies of the enclosure were measured as ~90% and ~80%, respectively. For lack of other data, we assumed that the enclosure reduces the gas-phase emission rates equally (by 90%) for all speciated VOCs and all UFP emission rates equally (by 80%). The source emissions were simply reduced by 90% and 80% relative to the baseline scenario for gases and particles, respectively, in CONTAM. These inputs are summarized in the results and discussion section as well.

Results and Discussion

UFP emission rate measurements

Figure 7a shows an example of time-varying UFP concentrations resulting from just one test using one of the printers with ABS filament (LulzBot Mini), along with the smoothed fit to the UFP concentration data. The left guideline in Figure 7a shows the moment that printers began warming up prior to printing, which we considered part of the printing emissions period. Figure 7b shows the time-varying UFP emission rates estimated using Equation 7.

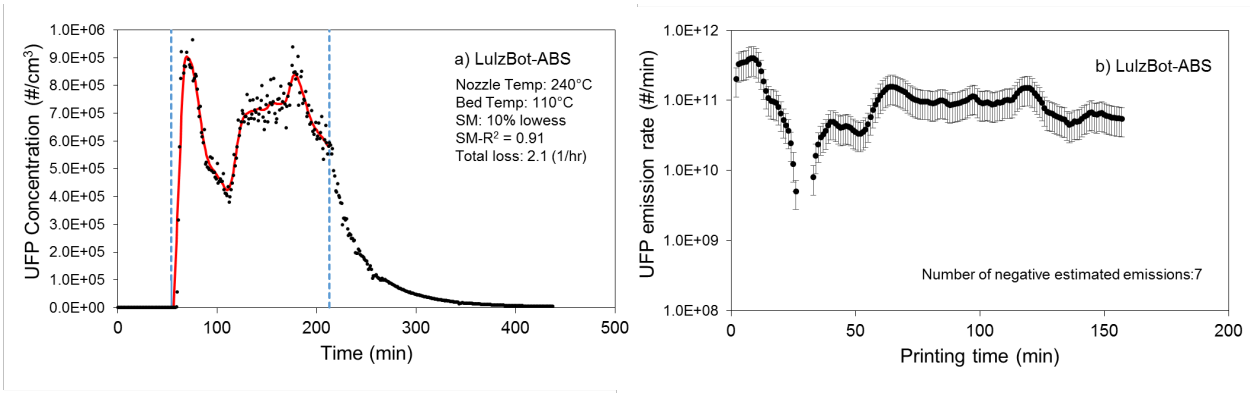

Figure 7. (a) Calibrated and smoothed UFP concentrations and (b) estimates of the time-varying UFP emission rates for one example test condition using a LulzBot Mini 3D printer and ABS filament. "SM" refers to the data smoothing method utilized.

Results in Figure 7a are similar to results from most of the experiments in that UFP concentrations typically rapidly increased just after printing began and persisted for the first 10-20 minutes, then decreased to a lower level, albeit typically to a level that was still higher than the background concentration. During some tests with other printer and filament combinations, UFP concentrations peaked again near the end of the print period as the thin protrusions on the printed object were created. However, the magnitude and shape of dynamic UFP concentrations varied widely depending on the printer, filament, shape of printed object, and nozzle and bed temperatures. In a few scenarios (e.g., Figure 7a), UFP concentrations reached an approximate steady state level toward the end of printing period. We used data from these periods to verify that the discretized time-varying emission rate calculation method (Equation 7) also yielded similar estimates of UFP emission rates as a simple steady state solution to the mass balance. Results from both solution methods were in good agreement for these periods, suggesting that the dynamic solution method provides reasonable emission rate estimates.

Figure 8 shows the range of time-varying UFP emission rates estimated for all 16 printer and filament combinations, grouped by (i) ABS filaments, (ii) PLA filaments, and (iii) all filaments other than ABS or PLA.

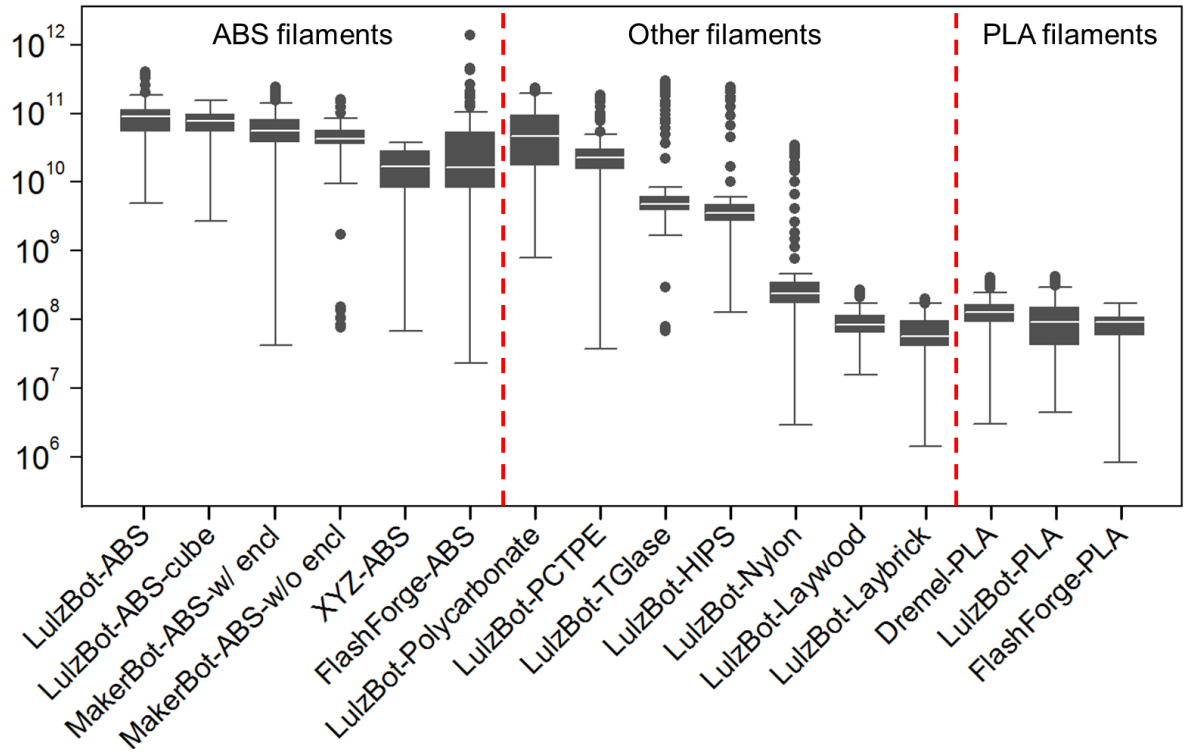

Figure 8. Summary of time-varying UFP emission rates estimated for 16 3D printer and filament combinations. Each data point represents data from 1-minute intervals and the combination of data points represents the entire printing period (typically between 2.5 and 4 hours). Boxes show the 25th and 75th percentile values with the 50th percentile (median) in between. Whiskers represent upper and lower adjacent values and circles represent outliers beyond those values.

UFP emission rates varied substantially depending on the make and model of the printer, the type of filament material, nozzle and bed temperatures, and the time of printing. The highest UFP emission rates typically occurred with the printers utilizing ABS filaments, with median values ranging from ~2×10^{10} to ~9×10^{10} #/min across all ABS printers with or without enclosures. The lowest UFP emission rates occurred with the three printers utilizing PLA filaments, regardless of printer make and model, with median UFP emission rates of ~10^{8} #/min. This was lower than what we estimated in our original study using a different make and model printer as well as a different study design (Stephens et al., 2013), but similar to other recent chamber tests (Kim et al., 2015). Median UFP emission rates for the other filaments were highest with the polycarbonate filament (~4×10^{10} #/min), followed by PCTPE (~2×10^{10} #/min), TGlase (~5×10^{9} #/min), HIPS (~4×10^{9} #/min), nylon (~2×10^{8} #/min), laywood (~8×10^{7} #/min), and laybrick (~6×10^{7} #/min), all printed using the LulzBot Mini printer.

Printing a cube instead of the NIST test part with ABS filament (in the LulzBot printer) did not meaningfully alter the magnitude of UFP emission rates, although it did slightly change the time-varying shape of the UFP emissions profile. Interestingly, the presence of an enclosure only moderately reduced UFP emission rates from the MakerBot-ABS combination, with a ~35% reduction in the median emission rate (although this variation is within the estimate of uncertainty). Larger reductions were not observed perhaps because the enclosure was not completely sealed and large gaps were visible. While these two comparisons provide preliminary

data on how printed shape and the presence of an enclosure may impact particle emissions from 3D printers, no other definitive conclusions can be drawn given this limited dataset. Finally, data from two sets of duplicate tests also demonstrated that there is some inherent variability in UFP emissions between repeated tests, as median emission rate estimates from these comparisons were within 57% and 48% of each other, respectively.

VOC emission rate measurements

Figure 9 summarizes estimates of individual speciated VOC and ΣVOC emission rates from each of the 16 printer and filament combinations. Only the top three speciated VOCs with the highest concentrations measured in each test are shown individually, while the remaining top-10 individual VOCs are summarized as "other" VOCs. The sum of these yields an estimate of the ΣVOC emission rate.

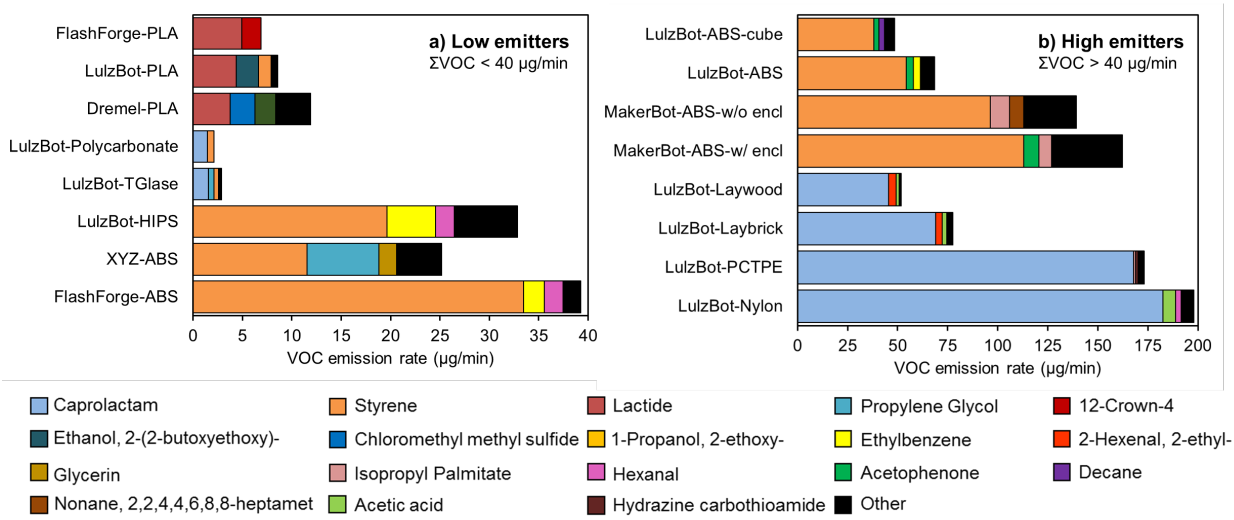

Figure 9. Estimates of emission rates for the top three highest concentration VOCs as well as sum of the top 10 detectable VOCs (i.e., ΣVOC) resulting from the operation of 16 3D printer and filament combinations. The figure is divided into (a) low emitters with $E_{\Sigma VOC}$ < 40 µg/min and (b) high emitters with $E_{\Sigma VOC}$ > 40 µg/min for visual clarity. Note that although no error bars are shown in the figure, we estimate the uncertainty in each individual VOC emission rate to be ~36%.

Filament material drove the majority of differences in the types of VOCs emitted, while printer make and model drove the majority of differences in the overall mass of VOCs emitted with the same filament. Estimates of total VOC emission rates (i.e., $E_{\Sigma VOC}$) ranged from as low as ~3 µg/min for the polycarbonate filament to nearly 200 µg/min for the nylon filament (both printed using the LulzBot). The top three highest emitted compounds accounted for at least 70% of ΣVOC emissions in all cases. For most of the printer and filament combinations, a single VOC dominated the ΣVOC emissions.

The primary individual VOC emitted from all six ABS filament and printer combinations and the only HIPS filament tested was styrene. Estimates of styrene emission rates with these filaments ranged from ~12 µg/min to ~113 µg/min, depending on the printer make and model. Interestingly, both the lowest and highest styrene emission rates were measured using printers with a partial enclosure (i.e., XYZprinting and MakerBot). Both styrene and total VOC emission

rates were slightly lower when the LulzBot-ABS combination printed a cube compared to the standard NIST test part, but they were actually slightly higher for the MakerBot-ABS combination with the plastic enclosure compared to results without the enclosure.

The primary individual VOC emitted from the nylon, PCTPE, laybrick, and laywood filaments was caprolactam. All of these filaments were installed in the LulzBot printer and all were classified as "high emitters" in Figure 9, with caprolactam emission rates as high as ~180 µg/min for the nylon filament. Caprolactam was also emitted from the polycarbonate and T-Glase filaments installed in the LulzBot printer, albeit at much lower levels. Finally, the primary individual VOC emitted from PLA filaments was lactide (1,4-dioxane-2,5-dione, 3,6-dimethyl), albeit at relatively low quantities, with emission rates ranging from ~4 µg/min to ~5 µg/min in the three printers using PLA filaments. We are confident that the majority of the identified VOCs originated from the filament materials for most of the printer tests, even for the tests that had glue applied to the bed, because the main components measured during the glue-only test (propylene glycol and glycerin) were only found in one filament/printer combination in Figure 9.

Impacts of nozzle and bed temperatures on measured emission rates

Next, we explored our estimates of both UFP and ΣVOC emission rates as a function of both nozzle temperatures and bed temperatures (Figure 10). The mean UFP and ΣVOC emission rates are split into three groups of bed temperature (less than 45°C, 60-65°C, and 100-110°C) and plotted versus nozzle temperature (which varied from 190°C to 270°C).

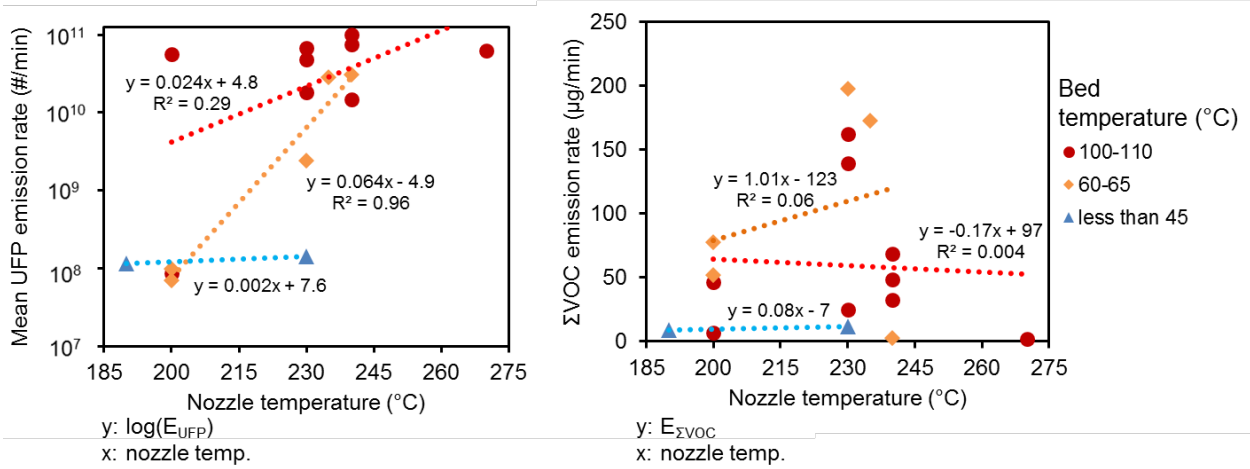

Figure 10. Impact of nozzle and bed temperature on mean UFP and TVOC emission rates

Nozzle temperatures did not have a large influence on UFP emission rates from this set of printers at either low bed temperatures or high bed temperatures. However, nozzle temperatures did appear to influence UFP emission rates at mid-range bed temperatures, as UFP emission rates were higher with increased nozzle temperatures. More importantly, bed temperatures alone appeared to influence UFP emission rates in this sample of printers. Most of the printer/filament combinations with the highest bed temperatures had the highest UFP emission rates while most of the printer/filament combinations with the lowest bed temperatures had the lowest UFP emission rates. There was no apparent relationship observed between ΣVOC emission rates and either bed or nozzle temperatures across this sample of printers and filaments. However, we should note that with this limited sample size, these relationships are only considered suggestive.

Correlations between total UFP and ΣVOC emissions per mass of filament

Figure 11 compares the total number of UFPs emitted (Equation 8) and the ΣVOC mass emitted (Equation 10) during printing, normalized by the mass of filament, for each of the 16 primary printer and filament combinations.

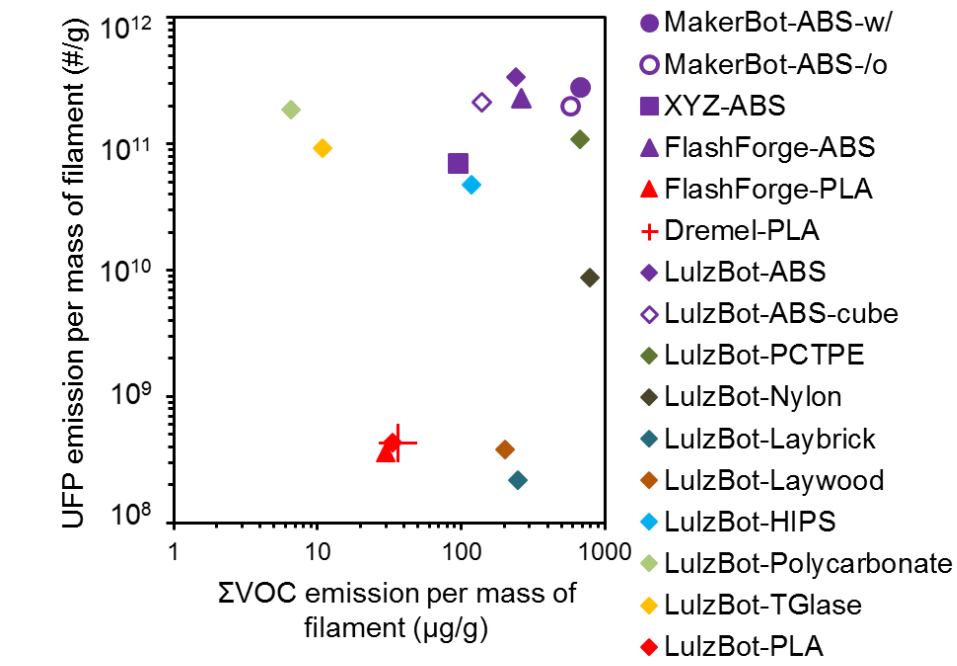

Figure 11. Comparison of total UFP and TVOC emissions per mass of filament

The total number of UFPs emitted per gram of filament printed ranged from a minimum of ~2×10^8 #/g for the LulzBot-Laybrick combination to a maximum of over 2×10^{11} #/g for multiple printers with ABS filaments. The ΣVOC mass emitted per gram of filament printed ranged from a minimum of ~6 µg/g with the LulzBot-Polycarbonate combination to nearly 800 µg/g with the LulzBot-Nylon combination. In general, ABS, PCTPE, and HIPS filaments had high mass-normalized emission rates of both UFPs and ΣVOCs, while PLA filaments had relatively low mass-normalized UFP and ΣVOC emission rates. Interestingly, both T-Glase and polycarbonate filaments (both used in the LulzBot printer) had low ΣVOC emissions but high UFP emissions. Conversely, both laywood and laybrick filaments (also used in the LulzBot printer) had relatively high ΣVOC emission rates but low UFP emission rates. These data suggest that filament material selection drives both UFP and ΣVOC emissions, although knowledge of one type of emissions may not necessarily be used to predict the other.

Pilot study of a prototype sealed enclosure with gas and particle filtration

Next, we investigated the impact of a custom sealed enclosure on UFP and VOC emissions from a high-emitting printer. Figure 12 shows time-varying UFP concentrations measured inside the chamber under four conditions: a LulzBot printer with ABS and Nylon filaments, each with and without the sealed enclosure installed with the filtration system operating continuously on a high speed setting. These concentrations are measured inside the chamber but outside the enclosure, thus representing only the UFPs that escape the enclosure system. The average reduction in time-varying UFP concentrations achieved by the enclosure and filtration system was 91% for the

ABS and 66% for the Nylon filament. Differences in these reductions may be attributable to differences in the sizes of UFPs emitted from the two filaments, although we do not have size-resolved concentration data for these filaments.

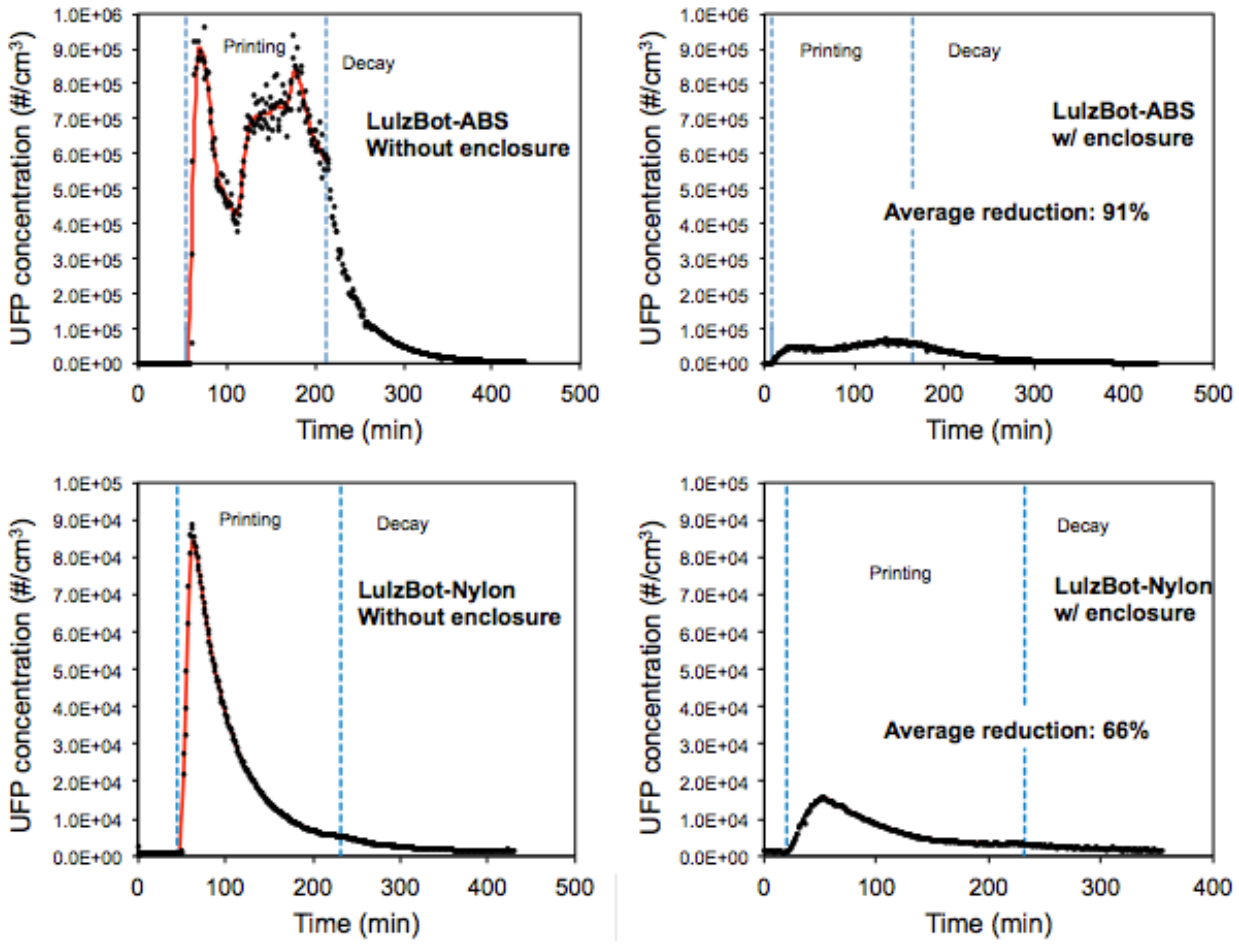

Figure 12. Time-varying UFP concentrations with and without a custom prototype enclosure with gas and particle filtration installed and operating continuously

Similarly, Figure 13 shows time-varying TVOC concentrations measured inside the chamber under the same four conditions. The average reduction in time-varying TVOC concentrations resulting from the use of the filtered enclosure was 85% for the ABS filament and 94% from the Nylon filament.

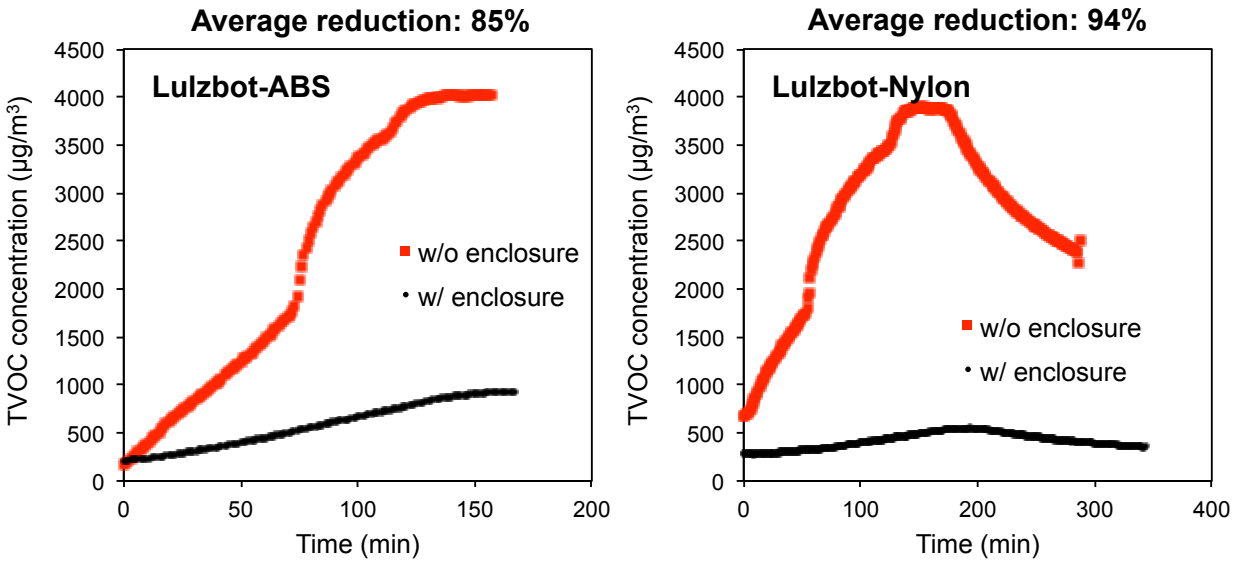

Figure 13. Time-varying TVOC concentrations with and without the enclosure installed and gas and particle filtration operating continuously

Figure 14 shows similar measurements made *inside* the sealed enclosure and filtration system for the duration of one printing period with ABS filament. These data demonstrate the time that is required for UFPs and TVOCs to decay inside the enclosure before it is safe to open. The printing period ended at approximately 200 minutes (marked on the figure). Subsequently, concentrations of UFPs decayed more rapidly than TVOCs: approximately 50 minutes for UFPs compared to more than 100 minutes for TVOCs. These data suggest that decreasing the time required for the flush out period could improve the practicality of the enclosure system.

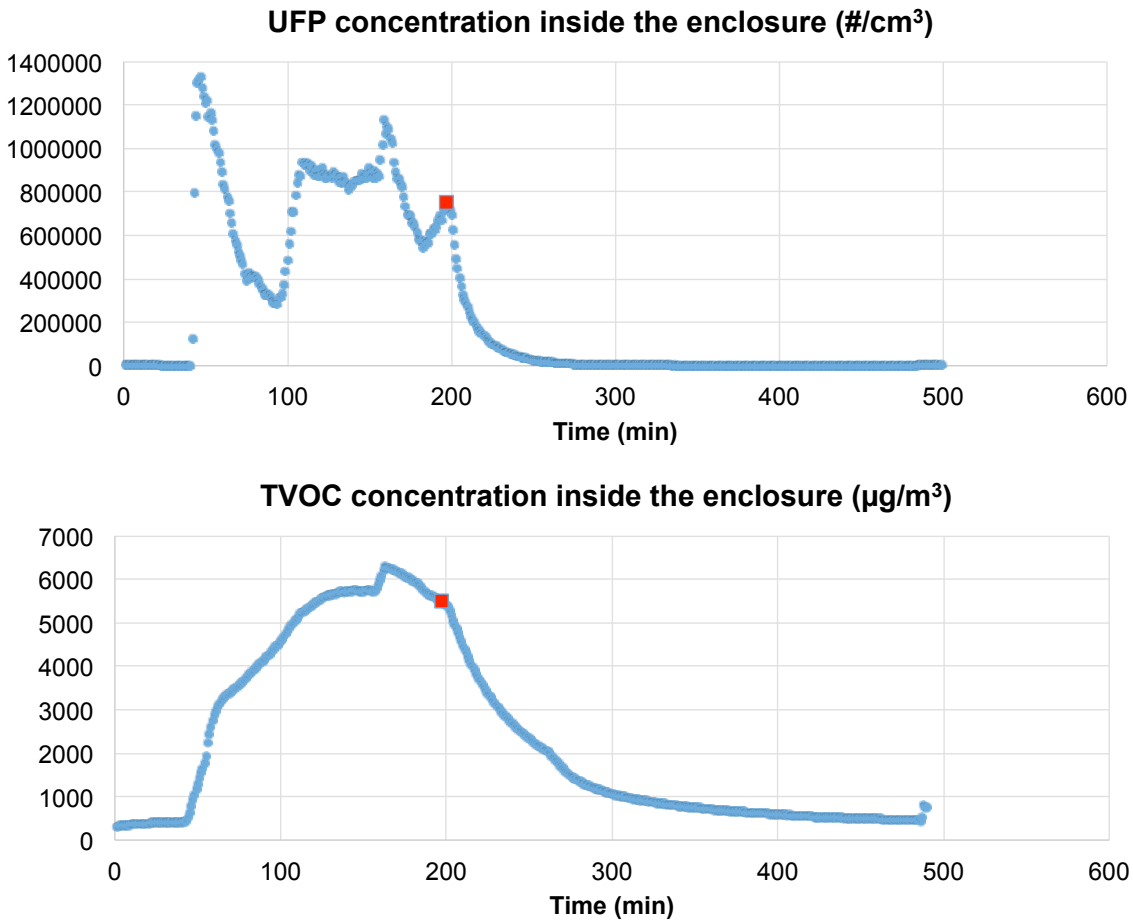

Figure 14. UFP and TVOC concentration data *inside* the sealed enclosure with a LulzBot+ABS filament combination (the red square marks when printing stopped)

Predicted concentrations of pollutants emitted from various 3D printer filaments

The next sections detail our findings from the modeling study in which we predicted concentrations of the various pollutants measured in phase 1 of this work inside a typical office environment. Figure 15 shows an example of modeled time-varying concentrations of UFPs and styrene in the three defined locations inside the small office environment during the weekdays of first week of January resulting from operating a single 3D printer with ABS filament (assuming the average ABS emission rate from data from the chamber emissions tests described herein).

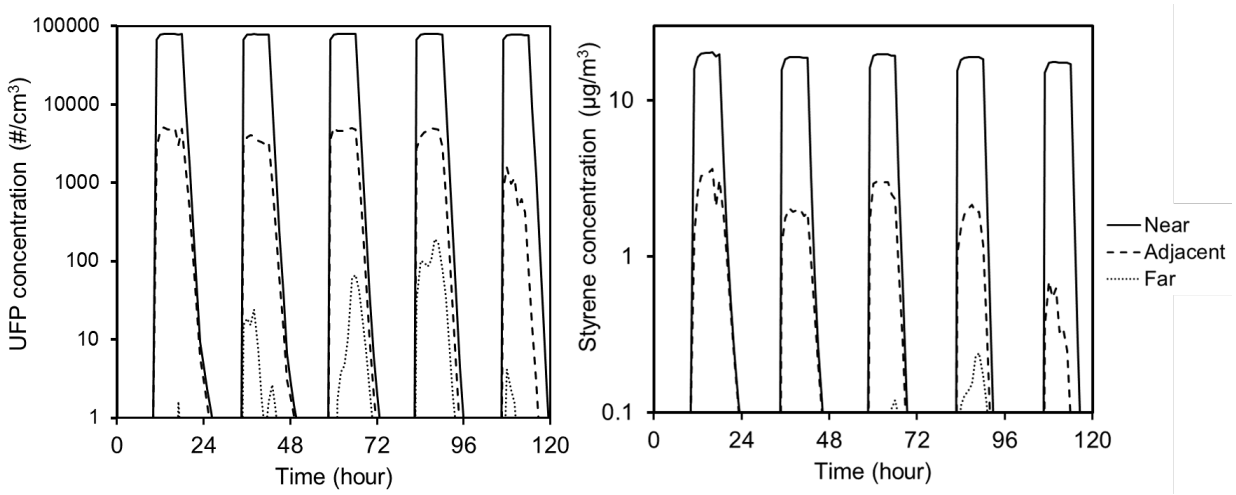

Figure 15. Typical hourly indoor concentration results from the CONTAM model with a single ABS printer operating in "near-distance", "adjacent", and "far" zones

The modeled time-varying concentration results demonstrate that the peak exposure to pollutants emitted by the 3D printer in the near-distance zone are typically more than 9 and 4 times higher than in the adjacent zone for UFPs and styrene, respectively, while a much smaller fraction of pollutants would actually reach the far-distance zone. The model results also reveal that the increase in both gas and particle concentrations in the near and adjacent zones occurs almost immediately after the printer begins operating, while concentrations peak much later in the far-distance zone. Modeled concentrations in the far zone are also more variable due to changes in air infiltration conditions. For example, the relative standard deviation of the predicted maximum 1-hour concentrations throughout the entire year is only 2% for UFPs and 15% for styrene in the near zone, slightly more variable in the adjacent zone (41% for UFPs and 58% for VOCs), and most variable for the far zone (114% for UFPs and 106% for VOCs). These profiles are repeated with reasonable consistency for all weekdays throughout the year.

Figure 16 and Figure 17 summarize the predicted time-varying concentrations of UFPs and speciated VOCs in all three zones over the course of an entire year for each printer and filament combination. Figure 16 shows concentrations predicted in the nearest zone and Figure 17 shows concentrations predicted in both the adjacent and far zones. Results are presented as ranges of daily maximum 1-hour, 8-hour and 24-hour concentrations (i.e., there is a total of 260 data points representing 260 weekdays in each series), as some of these metrics can be used to compare directly to regulatory limits. The daily maximum 8-hour concentrations during each weekday are calculated by taking 8-hour averages of the predicted hourly concentrations and selecting the highest average 8-hour concentration period for each day. The daily 24-hour concentrations are simply the daily averages for each weekday over the course of the entire year.

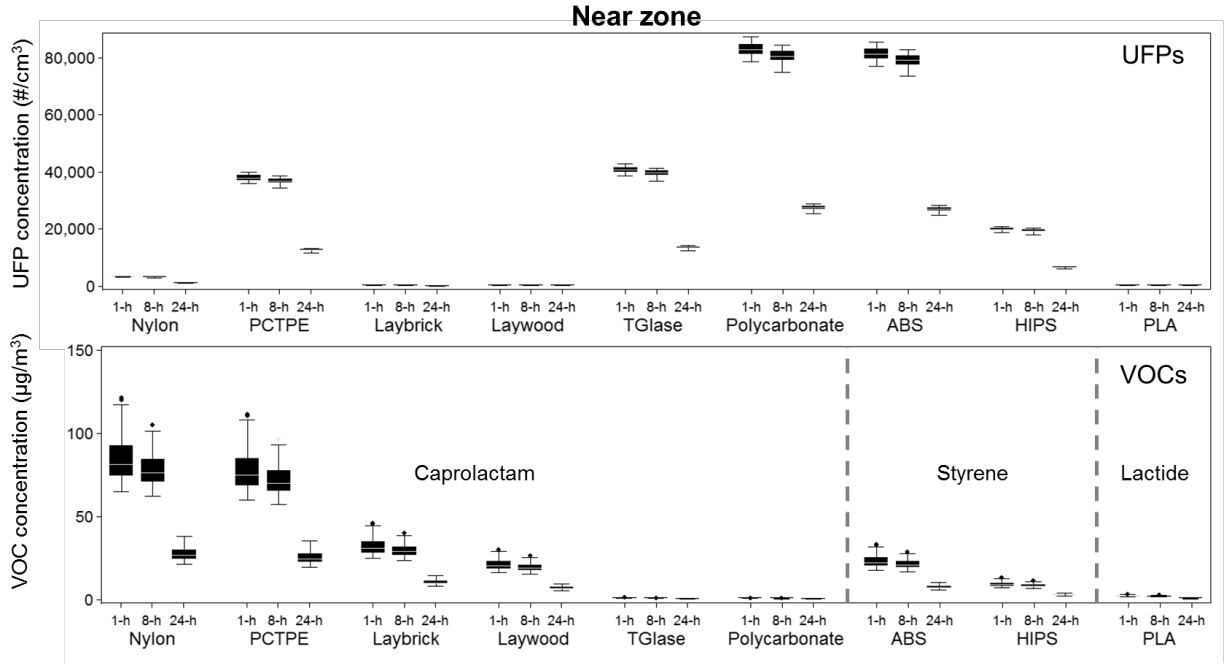

Figure 16. Ranges of predicted daily maximum 1-, 8-, and 24-hour concentrations of UFPs and speciated VOCs in the "near zone" for a typical year assuming a single desktop 3D printer with 9 different filaments operates continuously for 8 hours per day

The median values of daily maximum 1-hour UFP concentrations in the near zone ranged from just under 100 #/cm^3 for Laybrick, Laywood, and PLA filaments to nearly 80,000 #/cm^3 for ABS and Polycarbonate filaments. Median values of daily maximum 1-hour VOC concentrations ranged from 0.7 to 80 µg/m^3 with caprolactam-emitting filaments (highest with Nylon and PCTPE), from 8 to 22 µg/m^3 with styrene-emitting filaments (ABS and HIPS), and were consistently under 2 µg/m^3 for lactide-emitting filaments. Since we assumed that the printer operates 8 hours per day, the maximum 1-hour and 8-hour daily concentrations are relatively similar, while the average 24-hour concentrations are substantially lower, with median values approximately 3% and 67% lower than the maximum 1-hour concentration.

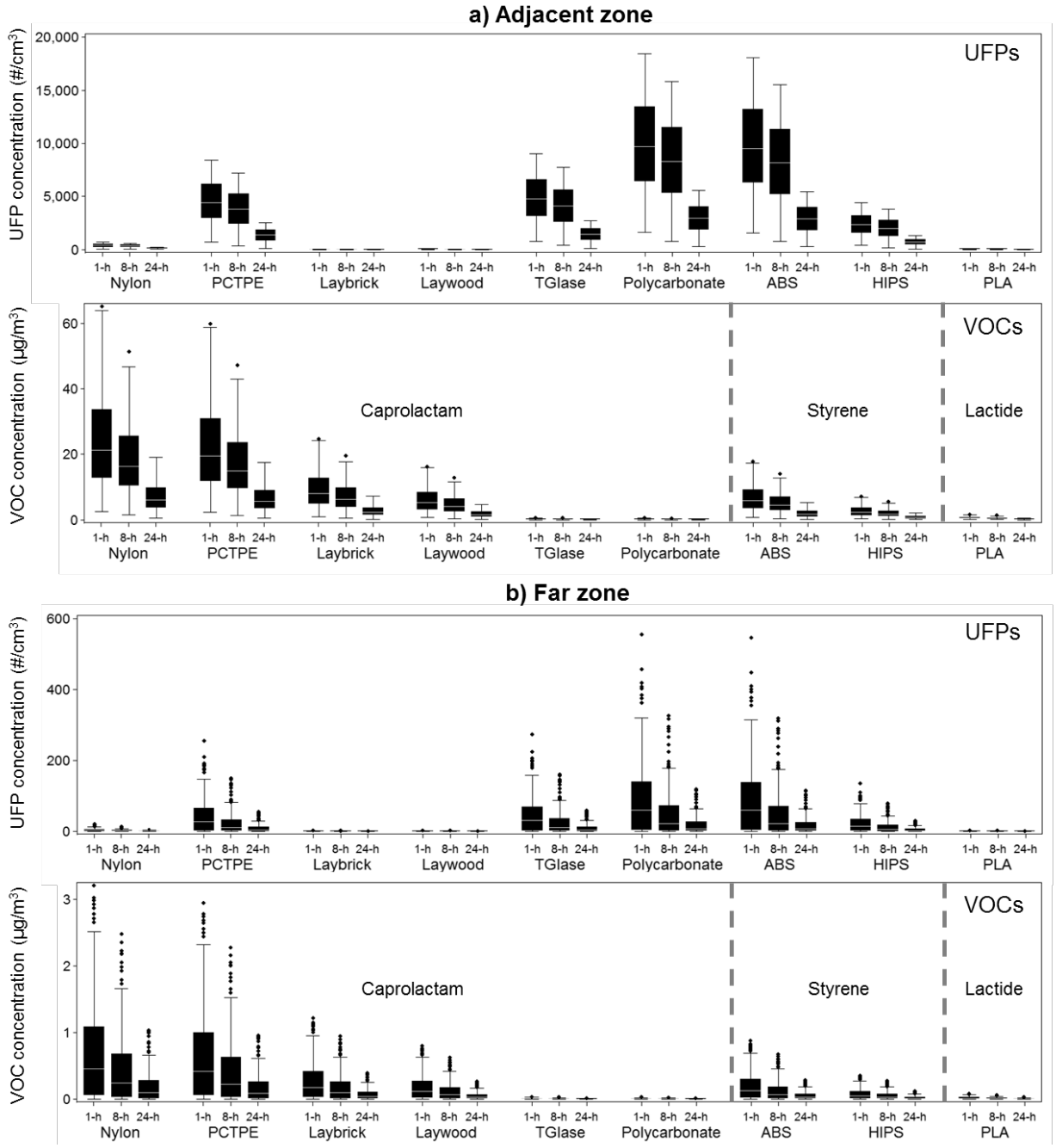

Figure 17. Ranges of predicted daily maximum 1-, 8-, and 24-hour concentrations of UFPs and speciated VOCs in the (a) "adjacent zone" and (b) "far zone" for a typical year assuming a single desktop 3D printer operates with 9 different filaments continuously for 8 hours per day

The median values of daily maximum 1-hour UFP concentrations in the adjacent zone ranged from less than 20 #/cm^3 for low-emitting filaments (e.g., Laybrick, Laywood, and PLA) to nearly 10,000 #/cm^3 for ABS and Polycarbonate filaments. The median values of daily maximum 1-hour VOC concentrations ranged from 0.2 to 20 µg/m^3 with caprolactam-emitting filaments, 2 to 6 µg/m^3 with styrene-emitting filaments, and were consistently lower than 1 µg/m^3 for lactide-emitting filaments. UFP and VOC concentration followed similar patterns in the far zone, albeit

at much lower absolute concentrations. The median 1-hour, 8-hour, and 24-hour UFP concentrations in the far zone were only 60, 20 and 7 #/cm^3, respectively, when the 3D printer was modeled with polycarbonate and ABS filaments. The highest median 1-hour maximum concentrations of caprolactam, styrene, and lactide were only 0.5, 0.1, and 0.01 μg/m^3 when the 3D printer was modeled with nylon, ABS, and PLA filaments, respectively. Thus, UFP and VOC emissions from the lowest-emitting filaments had essentially no impact on concentrations in the far distance zone.

Implications for human health

Measurements of UFP and individual VOC emission rates and predictions of their resulting concentrations in a typical workplace environment presented herein have important implications for human exposure and health effects. For example, styrene, which is classified as a *possible human carcinogen* by the International Agency for Research on Cancer (IARC Classification Group 2B) (IARC, 2002), was emitted in large amounts by all of the ABS filaments and the one HIPS filament. Caprolactam was also emitted in large amounts by four of the filaments: nylon, PCTPE, laybrick, and laywood. Although caprolactam is classified as *probably not carcinogenic to humans* (IARC, 1999), the California Office of Environmental Health Hazard Assessment (OEHHA) maintains acute, 8-hour, and chronic reference exposure levels (RELs) of only 50 μg/m^3, 7 μg/m^3, and 2.2 μg/m^3, respectively (OEHHA, 2014). Moreover, acute exposure to high concentrations of caprolactam is known to be "irritating to the eyes and the respiratory tract" and "may cause effects on the central nervous system" (CDC, 1994). We are not aware of any relevant information regarding the inhalation toxicity of lactide, the primary individual VOC emitted from PLA filaments.

The modeling results confirm some important implications of this work for human health. For example, results from the simulations herein suggest that operating a 3D printer with most of the nylon-based filaments (except TGlase and polycarbonate) would increase the concentration of caprolactam in both the adjacent and near zones to levels that would exceed both the 8-hour and chronic RELs set by OEHHA. Further, the predicted caprolactam concentration in the near zone during printing with nylon and PCTPE filaments would also exceed the acute OEHHA REL. The predicted caprolactam concentrations in the far distance zone consistently remain under all OEHHA RELs for all modeled nylon-based filaments.

Existing guidelines and recommendations for indoor styrene concentrations are limited to those set for industrial and workplace environments, including an 8-hour time-weighted-average (TWA) of 85 mg/m^3 and 426 mg/m^3 from the American Conference of Governmental Industrial Hygienists (ACGIH) and the Occupational Safety and Health Administration (OSHA) Standard # 29 CFR 1910.1000, respectively, and nearly 3000 mg/m^3 from the National Institute for Occupational Safety and Health (NIOSH). Further, the U.S. Environmental Protection Agency (EPA) maintains a Reference Concentration (RfC) for styrene of 1 mg/m^3 based on central nervous system effects in occupationally exposed workers (US EPA, 2000). However, other health impacts of styrene exposure have also been shown in epidemiology studies at much lower concentrations than these reference levels. For example, styrene concentrations as low as a few μg/m^3 have been associated with elevated risk of pulmonary infections in infants (Diez et al., 2000). Our results demonstrate that the median styrene concentrations in the near distance zone can easily reach more than 10 times this value, and can be as much as three times higher than the

highest measured styrene concentration of 7.5 μg/m^3 in typical commercial buildings in the U.S. EPA BASE study (Girman et al., 1999). These levels suggest that although the predicted styrene concentrations in all zones from all printer and filament combinations used herein are all lower than defined exposure limits, resulting concentrations still may pose a health risk to occupants.

Although we are not aware of any regulatory limits for indoor UFP concentrations, increases in UFP concentrations of ~80,000 #/cm^3 in the near-distance zone and ~10,000 #/cm^3 in the adjacent zone resulting from printing with polycarbonate and ABS filaments, as well as increases of ~40,000 #/cm^3 in the near-distance zone and ~5,000 #/cm^3 in the adjacent zone with some other filaments, are substantial, particularly given what is known about the health effects associated with outdoor UFPs. For example, UFP concentrations of ~80,000 #/cm^3 have been reported within 100 m of highly trafficked roadways (Zhu et al., 2002), and some of the observed associations of adverse health effects with proximity to busy roadways are likely attributable in part to elevated UFPs (Gauderman et al., 2005, 2007; McConnell et al., 2010). Further, recent studies have shown that increases in outdoor UFP concentrations of ~10,000 #/cm^3 are associated with a ~3% increase risk in daily mortality (Stölzel et al., 2007) and increases in outdoor UFP concentrations of only ~1,000 #/cm^3 are associated with increased blood pressure in children (Pieters et al., 2015).

Comparing the modeled UFP concentrations to levels measured in other indoor environments, 80,000 #/cm^3 is about 50% higher than the highest time-averaged UFP indoor concentrations that have been observed in schools in previous investigations (Diapouli et al., 2007). Printing with other filaments such as PCTPE, TGlase, and HIPS would also increase the near zone UFP concentrations to between 2 and 5 times higher than indoor UFP concentrations typically observed in other buildings in the adjacent and near-distance zones, respectively. Although much less is known about the adverse health effects of indoor-generated UFPs, recent studies of nanoparticles emitted from photocopiers and laser printers illustrate the potential hazard for human health. For example, ultrafine particles collected from a university copy center were recently shown to induce lung injury and inflammation in mice (Pirela et al., 2013) and upper airway inflammation and oxidative stress in healthy human volunteers (Khatri et al., 2013). These data suggest that controlling emissions and/or exposures from high emitting 3D printer and filament combinations is warranted in settings similar to the one modeled herein.

Impacts of control strategies on pollutant concentrations

Next, we chose the highest emitting printer and filament combinations for each pollutant and explored the impacts of various control strategies on the resulting concentrations in the same three locations within the modeled office environment. ABS, nylon, and PLA filaments were selected to represent the highest UFP and styrene, caprolactam, and lactide emissions, respectively. Figure 18 shows the predicted impacts of the various control strategies on maximum 1-hour UFP concentrations in the near, adjacent, and far distances with the 3D printer operating on the same schedule as all other simulations.

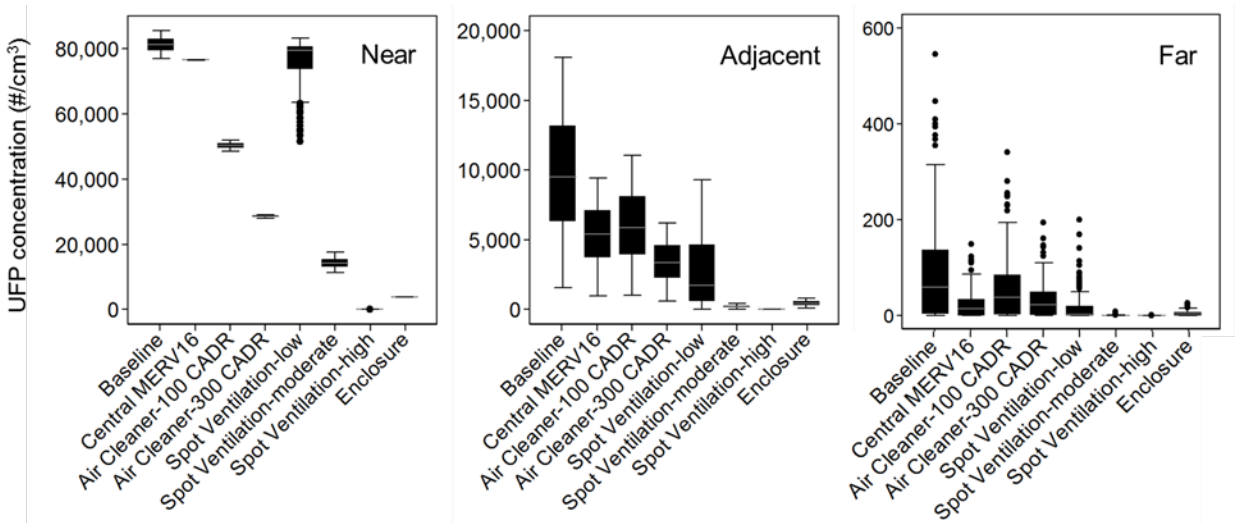

Figure 18. Modeled impacts of various control strategies on maximum 1-hour UFP concentrations in the near, adjacent, and far distances

Upgrading the central HVAC system filter to a MERV 16 with activated carbon and installing a low-flow (and low capture efficiency) spot ventilation system are predicted to yield the smallest reductions in daily maximum 1-hour UFP concentrations in the near zone. Conversely, installing a high-flow (and high capture efficiency) spot ventilation system has the greatest potential for reducing UFP concentrations in the near zone, followed by using the sealed enclosure with particle and gas filtration. Both are predicted to reduce median values of daily maximum 1-hour UFP concentrations from ~80,000 #/cm^3 to less than ~4000 #/cm^3. Both air cleaner scenarios have moderate impacts on UFP concentrations in the near zone. These results suggest that in order to reduce exposures in areas within immediate proximity to operating 3D printers, it is best to prioritize solutions that exhaust or control emissions directly at the source rather than attempting to lower UFP concentrations in the broader area with air cleaners and filtration.

Results are somewhat similar in the adjacent zone, albeit with some variability. Installing a low-CADR portable air cleaner and upgrading the central HVAC system filtration are predicted to yield the smallest reductions in UFP concentrations in the adjacent zone, although the relative reductions in this zone are higher than those in the immediate vicinity of the printer. Both moderate- and high-flow spot ventilation systems, as well as the sealed enclosure, are predicted to yield the largest reductions in median values of daily maximum 1-hour UFP concentrations (all below 500 #/cm^3). And although the air cleaners and low-flow spot ventilation system have lower UFP removal effectiveness, they can still limit increases in UFP concentrations to less than 5,000 #/cm^3 in the adjacent zone. Similar relative concentration profiles are also observed for the far zone, but the baseline UFP concentrations are already quite low (~60 #/cm^3) and thus may not necessitate further control strategies.

Figure 19 shows the impacts of the same control strategies for reducing daily maximum 1-hour concentrations of individual VOCs, including (a) caprolactam, (b) styrene, and (c) lactide emitted from nylon, ABS, and PLA filaments, respectively.

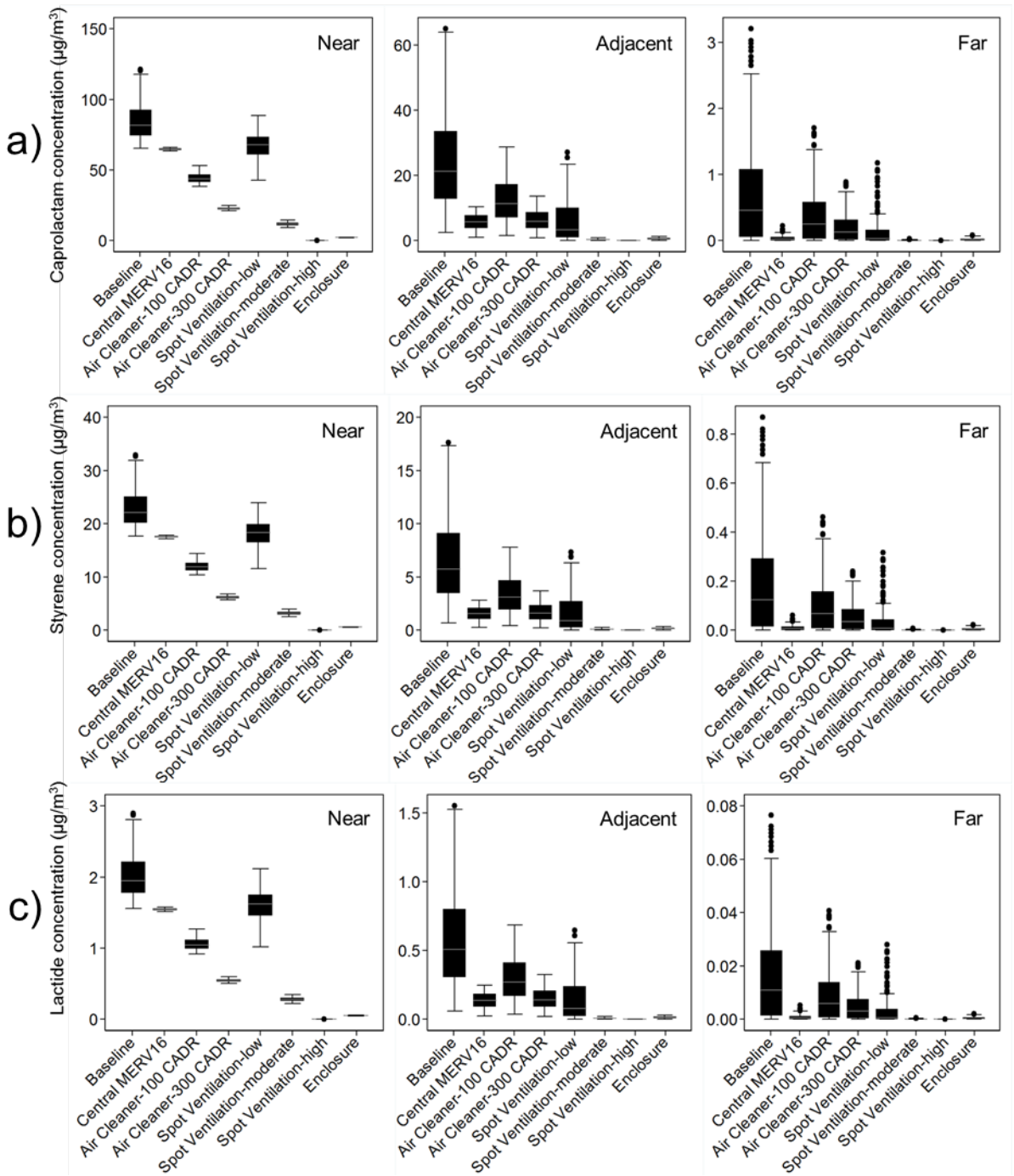

Figure 19. Modeled impacts of various control strategies on daily maximum 1-hour concentrations of (a) caprolactam, (b) styrene, and (c) lactide in the near, adjacent, and far zones

The relative reductions in daily maximum 1-hour concentrations with each control strategy are similar to those for UFP concentrations and are the same for all individual VOCs because most of the same assumptions for pollutant dynamics apply to each VOC. However, absolute concentrations vary based on the strength of the emission source. In the near zone, upgrading central HVAC filtration and installing low-flow spot ventilation again have the smallest impacts on VOC concentrations, allowing most of the daily maximum 1-hour caprolactam concentrations

from nylon-based filaments to still exceed the OEHHA acute REL of 50 μg/m^3. The remaining control strategies would all reduce the median daily maximum 1-hour caprolactam concentration below this level. Both the high-flow spot ventilation and the sealed enclosure with gas and particle filtration are predicted to reduce the median daily maximum 1-hour caprolactam concentration to less than 2 μg/m^3. Similarly, both moderate- and high-flow spot ventilation systems and the sealed enclosure are predicted to reduce the median daily maximum 1-hour styrene concentration to less than 7.5 μg/m^3 (i.e., the maximum level measured in U.S. commercial buildings in the BASE study).

Installing moderate- and high-flow spot ventilation systems and the sealed enclosure are predicted to yield the largest reductions in VOC concentrations in the adjacent zone, reducing daily maximum 1-hour caprolactam and styrene concentrations to less than 0.5 μg/m^3. The portable air cleaner scenarios yield smaller reductions in VOC concentrations in both the adjacent and far zones, but could still reduce peak caprolactam concentrations below the OEHHA acute REL for most days. All of the control strategies except for the low-CADR portable air cleaner are predicted to maintain the median daily maximum 1-hour styrene concentration in the adjacent zone below 2 μg/m^3. Median daily maximum 1-hour lactide concentrations remain below 2 μg/m^3 for all scenarios in all three zones, suggesting that lactide emissions from 3D printers using PLA filaments are likely not problematic for human exposure.

Pollutant removal effectiveness of the various control strategies

These same data were also used to calculate the effectiveness of each of the control strategies for reducing UFP and VOC concentrations in each zone using Equation 19.

$$E_{control,i} = 1 - \frac{\bar{C}_i}{\bar{C}_{baseline,i}} \tag{19}$$

Where $E_{control,i}$ = Effectiveness of a particular control strategy for removing UFPs/VOCs from a specific location (-); $\bar{C}_i$ = Median concentration of UFPs/VOCs in a specific location predicted with the use of a particular control strategy (#/cm^3 or μg/m^3); and $\bar{C}_{baseline,i}$ = Median concentration of UFPs/VOCs in a specific location predicted without the use of any control strategies (#/cm^3 or μg/m^3). Removal effectiveness values are shown in Figure 20.

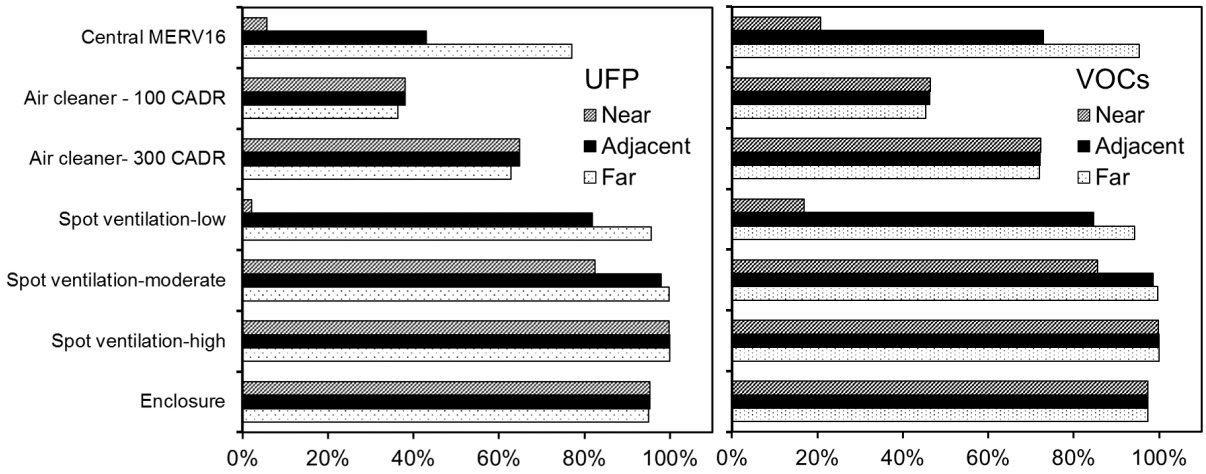

Figure 20. Removal effectiveness of each control strategy for reducing UFP and VOC concentrations in the near, adjacent, and far zones

Removal effectiveness values range from as little as 2% for the expected impact of a low-flow spot ventilation system on UFPs in the near zone to between 95% and 100% for the expected impact of a high-flow spot ventilation system or sealed and filtered enclosure on both UFPs and VOCs in all zones. Both portable air cleaner scenarios have similar UFP and VOC removal effectiveness for all zones: 38% for UFPs and 46% for VOCs with the low-CADR air cleaner, and 64% for UFPs and 72% for VOCs with the high-CADR air cleaner. The effectiveness of all other control strategies varied by zone. For example, the UFP and VOC removal effectiveness of upgraded central HVAC filtration is 6% and 21% in the near zone, 43% and 73% in the adjacent zone, and 77% and 95% in the far zone, respectively.

While these results provide insight into the likely impacts of realistic exposure control strategies on indoor concentrations of gas and particle emission products from desktop 3D printers, we should also note that some of these control strategies are more practical and cost-effective to apply than others. For example, high-flow rate spot ventilation systems that exhaust to the outdoors are likely cost prohibitive or impractical in many locations, and thus a sealed and filter enclosure may be a more appropriate solution in many environments. Further, operating a high-CADR stand-alone air cleaner with both gas and particle filtration can have a meaningful impact on both UFP and VOC concentrations in all zones, but could also come with a substantial energy penalty.

Recommendations for Future Work

Given the findings herein, we are prompted to make the following recommendations. First, additional measurements should be conducted to more accurately quantify personal exposures to both UFPs and speciated VOCs that account for proximity effects presented by typical 3D printer use patterns in a wide variety of realistic settings. Second, manufacturers should work towards designing low-emitting filament materials and/or printing technologies. Third, in the absence of new low-emitting filaments, manufacturers should work to evaluate the effectiveness of sealed enclosures on both UFP and VOC emissions and/or to introduce combined gas and particle filtration systems. Until then, we continue to suggest that caution should be used when operating

many printer and filament combinations in enclosed or poorly ventilated spaces or without the aid of gas and particle filtration systems. This is particularly true for both styrene- and nylon-based filaments based on data from the relatively large sample of printers and filament combinations evaluated here.

Conclusions

Previous research has shown that desktop 3D printers can emit large numbers of ultrafine particles (UFPs: particles less than 100 nm) and some hazardous volatile organic compounds (VOCs) during printing, although very few filament and 3D printer combinations had been tested to date prior to this project. In this work, we quantified emissions of UFPs and speciated VOCs from 5 commercially available filament extrusion desktop 3D printers utilizing up to 9 different filaments using controlled experiments in a test chamber. Median estimates of time-varying UFP emission rates ranged from ~10^8 to ~10^{11} #/min across all tested combinations, varying primarily by filament material and, to a lesser extent, bed temperature. The individual VOCs emitted in the largest quantities included: caprolactam from nylon-based and imitation wood and brick filaments (ranging ~2 to ~180 µg/min), styrene from acrylonitrile butadiene styrene (ABS) and high-impact polystyrene (HIPS) filaments (ranging ~10 to ~110 µg/min), and lactide from polylactic acid (PLA) filaments (ranging ~4 to ~5 µg/min). We also provide preliminary data on the impact of print object geometry and the use of partial and whole printer enclosures with and without a filtration system to mitigate printer emissions.

Subsequently, we also use our published measurements of emission rates of both UFPs and speciated VOCs from a wide variety of desktop FFF 3D printers and filaments to predict the magnitudes of human exposures to these same pollutants that would be expected in three spatial locations within a typical small office environment. We also use the worst case UFP and VOC emission scenarios to model the likely impacts of several potential control strategies for reducing exposures. Modeled concentrations in the three zones demonstrate that UFP and VOC concentrations within close or moderate proximity to some operating desktop 3D printers can exceed recommended exposure levels and may be cause for concern for both acute and chronic health effects. The results also suggest that the most effective control strategies for reducing both UFP and VOC concentrations in all zones from high emitters used in the modeled environment, in descending order of impact, include: (1) installing a high-flow spot ventilation system, (2) operating the printer in a sealed enclosure with high efficiency gas and particle filtration, (3) installing a moderate-flow spot ventilation system, and (4) operating a high-CADR stand-alone air cleaner with both gas and particle filtration within immediate proximity to the operating 3D printer. Upgrading central HVAC filtration, installing low-flow spot ventilation, and operating a low-CADR portable air cleaner are the least effective methods for reducing UFP and VOC concentrations resulting from 3D printer operation in this modeled environment. Results also demonstrate that some 3D printer and filament combinations with lower emissions (e.g., PLA filaments, which have both low UFP and VOC emissions) should be prioritized over higher emitting filaments to limit human exposures.

References

Allgood, C., Orlando, R., Munson, B., (1990). Correlations of relative sensitivities in gas chromatography electron ionization mass spectrometry with molecular parameters. *J. Am. Soc. Mass Spectrom.* 1, 397–404.

Andersen, Z.J., Olsen, T.S., Andersen, K.K., Loft, S., Ketzel, M., Raaschou-Nielsen, O., (2010). Association between short-term exposure to ultrafine particles and hospital admissions for stroke in Copenhagen, Denmark. *Eur. Heart J.* 31, 2034–2040.

ASHRAE, (2012). Standard 52.2: Method of testing general ventilation air-cleaning devices for removal efficiency by particle size.

ASHRAE, S., (2010). Standard 62.1-2010. *Vent. Accept. Indoor Air Qual. ASHRAE*.

Azimi, P., Zhao, D., Stephens, B., (2014). Estimates of HVAC filtration efficiency for fine and ultrafine particles of outdoor origin. *Atmos. Environ.* 98, 337–346.

CDC, (1994). The National Institute for Occupational Safety and Health (NIOSH) International Chemical Safety Cards (ICSC): Caprolactam.

Contos, D.A., Holdren, M.W., Smith, D.L., Brooke, R.C., Rhodes, V.L., Rainey, M.L., (1995). Sampling and Analysis of Volatile Organic Compounds Evolved During Thermal Processing of Acrylonitrile Butadiene Styrene Composite Resins. *J. Air Waste Manag. Assoc.* 45, 686–694.

Delfino, R.J., Sioutas, C., Malik, S., (2005). Potential role of ultrafine particles in associations between airborne particle mass and cardiovascular health. *Environ. Health Perspect.* 113, 934–946.

Delp, W.W., Singer, B.C., (2012). Performance Assessment of U.S. Residential Cooking Exhaust Hoods. *Environ. Sci. Technol.* 46, 6167–6173.

Diapouli, E., Chaloulakou, A., Spyrellis, N., (2007). Levels of ultrafine particles in different microenvironments--implications to children exposure. *Sci. Total Environ.* 388, 128–136.

Diez, U., Kroessner, T., Rehwagen, M., Richter, M., Wetzig, H., Schulz, R., Borte, M., Metzner, G., Krumbiegel, P., Herbarth, O., (2000). Effects of indoor painting and smoking on airway symptoms in atopy risk children in the first year of life results of the LARS-study. Leipzig Allergy High-Risk Children Study. *Int. J. Hyg. Environ. Health* 203, 23–28.

Emmerich, S.J., Persily, A.K., (2011). US Commercial Building Airtightness Requirements and Measurements, *in: AIVC Conference*.

Fazli, T., Stephens, B., (2016). Characterizing the in-Situ Size-Resolved Removal Efficiency of Residential and Light-Commercial HVAC Filters for Particle Sizes Between 0.01 and 10 μm (OR-16-C025). Presented at the ASHRAE Winter Conference.

Gauderman, W.J., Avol, E., Lurmann, F., Kuenzli, N., Gilliland, F., Peters, J., McConnell, R., (2005). Childhood Asthma and Exposure to Traffic and Nitrogen Dioxide. *Epidemiology* 16, 737–743.

Gauderman, W.J., Vora, H., McConnell, R., Berhane, K., Gilliland, F., Thomas, D., Lurmann, F., Avol, E., Kunzli, N., Jerrett, M., (2007). Effect of exposure to traffic on lung development from 10 to 18 years of age: a cohort study. *The Lancet* 369, 571–577.

Girman, J.R., Hadwen, G.E., Burton, L.E., (1999). Individual Volatile Organic Compound Prevalence and Concentrations in 56 Buildings of the Building Assessment Survey and Evaluation (BASE) Study, *in: In the Proceedings of Indoor Air 1999*. pp. 460–465.

Gross, B.C., Erkal, J.L., Lockwood, S.Y., Chen, C., Spence, D.M., (2014). Evaluation of 3D Printing and Its Potential Impact on Biotechnology and the Chemical Sciences. *Anal. Chem.* 86, 3240–3253.

HEI, (2013). Understanding the Health Effects of Ambient Ultrafine Particles (HEI Perspectives 3)*, HEI Review Panel on Ultrafine Particles*. Health Effects Institute, Boston, MA.

IARC, (1999). IARC Monographs on the Evaluation of Carcinogenic Risks to Humans Volume 71.

IARC, (2002). IARC Monographs on the Evaluation of Carcinogenic Risks to Humans Volume 82.

Khatri, M., Bello, D., Gaines, P., Martin, J., Pal, A.K., Gore, R., Woskie, S., (2013). Nanoparticles from photocopiers induce oxidative stress and upper respiratory tract inflammation in healthy volunteers. *Nanotoxicology* 7, 1014–1027.

Kim, Y., Yoon, C., Ham, S., Park, J., Kim, S., Kwon, O., Tsai, P.-J., (2015). Emissions of Nanoparticles and Gaseous Material from 3D printer Operation. *Environ. Sci. Technol.* 150924175328000.

Logue, J.M., (2014). Pollutant exposures from natural gas cooking burners: a simulation-based assessment for Southern California.

MatterHackers, (2015). 3D printer filament comparison guide. *MatterHackers Inc*.

McConnell, R., Islam, T., Shankardass, K., Jerrett, M., Lurmann, F., Gilliland, F., Gauderman, J., Avol, E., Künzli, N., Yao, L., Peters, J., Berhane, K., (2010). Childhood Incident Asthma and Traffic-Related Air Pollution at Home and School. *Environ. Health Perspect.* 118, 1021–1026.

Mølgaard, B., Koivisto, A.J., Hussein, T., Hämeri, K., (2014). A new clean air delivery rate test applied to five portable indoor air cleaners. *Aerosol Sci. Technol.* 48, 409–417.

Moylan, S., Slotwinski, J., (2012). Proposal for a standardized test artifact for additive manufacturing machines and processes. *Proc. 2012 Annu. Int. Solid Free. Fabr. Symp.* 6–8.

Ng, L.C., Musser, A., Persily, A.K., Emmerich, S.J., (2012). Airflow and indoor air quality models of DOE reference commercial buildings. *Gaithersburg MD Natl. Inst. Stand. Technol.* 163.

NIST, (2016). NIST Multizone Modeling Homepage [WWW Document]. URL http://www.bfrl.nist.gov/IAQanalysis/index.htm

NJDEP, (2015). Guidance: Remediation Standards [WWW Document]. URL http://www.nj.gov/dep/srp/guidance/rs/chemproperties.pdf

NSRDB: 1991- 2005 Update: TMY3 [WWW Document], (2016). . URL http://rredc.nrel.gov/solar/old_data/nsrdb/1991-2005/tmy3/

Oberdörster, G., Celein, R.M., Ferin, J., Weiss, B., (1995). Association of Particulate Air Pollution and Acute Mortality: Involvement of Ultrafine Particles?. *Inhal. Toxicol.* 7, 111–124.

Oberdorster, G., Oberdorster, E., Oberdorster, J., (2005). Nanotoxicology: An Emerging Discipline Evolving from Studies of Ultrafine Particles. *Environ. Health Perspect.* 113, 823–839.

Oberdörster, G., Sharp, Z., Atudorei, V., Elder, A., Gelein, R., Kreyling, W., Cox, C., (2004). Translocation of Inhaled Ultrafine Particles to the Brain. *Inhal. Toxicol.* 16, 437–445.

OEHHA, (2014). Table of All Acute, Chronic and 8 hour Reference Exposure Levels [WWW Document]. URL http://oehha.ca.gov/air/allrels.html

Pieters, N., Koppen, G., Van Poppel, M., De Prins, S., Cox, B., Dons, E., Nelen, V., Int Panis, L., Plusquin, M., Schoeters, G., Nawrot, T.S., (2015). Blood Pressure and Same-Day

Exposure to Air Pollution at School: Associations with Nano-Sized to Coarse PM in Children. *Environ. Health Perspect.*

Pirela, S., Molina, R., Watson, C., Cohen, J.M., Bello, D., Demokritou, P., Brain, J., (2013). Effects of copy center particles on the lungs: a toxicological characterization using a *Balb/c* mouse model. *Inhal. Toxicol.* 25, 498–508.

Ragan, S., (2013). Plastics for 3D printing. *Make:* 22.

Schaper, M.M., Thompson, R.D., Detwiler-Okabayashi, K.A., (1994). Respiratory Responses of Mice Exposed to Thermal Decomposition Products from Polymers Heated at and Above Workplace Processing Temperatures. *Am. Ind. Hyg. Assoc. J.* 55, 924–934.

Sidheswaran, M.A., Destaillats, H., Sullivan, D.P., Cohn, S., Fisk, W.J., (2012). Energy efficient indoor VOC air cleaning with activated carbon fiber (ACF) filters. *Build. Environ., International Workshop on Ventilation, Comfort, and Health in Transport Vehicles* 47, 357–367.

Singer, B.C., Delp, W.W., Price, P.N., Apte, M.G., (2012). Performance of installed cooking exhaust devices. *Indoor Air* 22, 224–234.

Stephens, B., Azimi, P., Orch, Z. El, Ramos, T., (2013). Ultrafine particle emissions from desktop 3D printers. *Atmos. Environ.* 79, 334–339.

Stölzel, M., Breitner, S., Cyrys, J., Pitz, M., Wölke, G., Kreyling, W., Heinrich, J., Wichmann, H.-E., Peters, A., (2007). Daily mortality and particulate matter in different size classes in Erfurt, Germany. *J. Expo. Sci. Environ. Epidemiol.* 17, 458–467.

Sultan, Z.M., Nilsson, G.J., Magee, R.J., (2011). Removal of ultrafine particles in indoor air: Performance of various portable air cleaner technologies. *HVACR Res.* 17, 513–525.

Unwin, J., Coldwell, M.R., Keen, C., McAlinden, J.J., (2013). Airborne Emissions of Carcinogens and Respiratory Sensitizers during Thermal Processing of Plastics. *Ann. Occup. Hyg.* 57, 399–406.

U.S. EPA, (1999). Compendium of Methods for the Determination of Toxic Organic Compounds in Ambient Air 2nd Edition Compendium Method TO-17 Determination of Volatile Organic Compounds in Ambient Air Using Active Sampling Onto Sorbent Tubes.

US EPA, O., (2000). Styrene | Technology Transfer Network Air Toxics Web site | US EPA [WWW Document]. URL http://www3.epa.gov/airtoxics/hlthef/styrene.html#ref5

Wallace, L., Kindzierski, W., Kearney, J., MacNeill, M., Héroux, M.-È., Wheeler, A.J., (2013). Fine and Ultrafine Particle Decay Rates in Multiple Homes. *Environ. Sci. Technol.* 47, 12929–12937.

Waring, M.S., Siegel, J.A., Corsi, R.L., (2008). Ultrafine particle removal and generation by portable air cleaners. *Atmos. Environ.* 42, 5003–5014.

Weichenthal, S., Dufresne, A., Infante-Rivard, C., (2007). Indoor ultrafine particles and childhood asthma: exploring a potential public health concern. *Indoor Air* 17, 81–91.

Westerdahl, D., Fruin, S., Sax, T., Fine, P.M., Sioutas, C., (2005). Mobile platform measurements of ultrafine particles and associated pollutant concentrations on freeways and residential streets in Los Angeles. *Atmos. Environ.* 39, 3597–3610.

Zhu, Y., Hinds, W.C., Kim, S., Shen, S., Sioutas, C., (2002). Study of ultrafine particles near a major highway with heavy-duty diesel traffic. *Atmos. Environ.* 36, 4323–4335.

Zitting, A., Savolainen, H., (1980). Effects of single and repeated exposures to thermo-oxidative degradation products of poly(acrylonitrile-butadiene-styrene) (ABS) on rat lung, liver, kidney, and brain. *Arch. Toxicol.* 46, 295–304.

Resulting Publications

1. Azimi, P., Fazli, T., Stephens, B. (Under review). Predicting concentrations of ultrafine particles and volatile organic compounds resulting from desktop 3D printer operation in a small office environment and the impact of potential control strategies. Returned with minor revisions to the *Journal of Industrial Ecology* Special Issue on the Environmental Dimensions of Additive Manufacturing and 3D Printing, October 2016.

2. Azimi, P., Zhao, D., Pouzet, C., Crain, N., Stephens, B. 2016. Emissions of ultrafine particles and volatile organic compounds from commercially available desktop 3D printers with multiple filaments. *Environmental Science and Technology* 50(3):1260-1268.

Materials Available for Other Investigators

All data and other products generated in this project are available to other investigators upon request.

Environmental Science & Technology

Article

pubs.acs.org/est

Emissions of Ultrafine Particles and Volatile Organic Compounds from Commercially Available Desktop Three-Dimensional Printers with Multiple Filaments

Parham Azimi,[†] Dan Zhao,[†] Claire Pouzet,[†,‡] Neil E. Crain,[§] and Brent Stephens*[,†]

[†]Department of Civil, Architectural and Environmental Engineering, Illinois Institute of Technology, Chicago, Illinois 60616, United States

[‡]Ecole des Ingénieurs de la Ville de Paris, 80 Rue Rebeval, 75019 Paris, France

[§]Department of Civil, Architectural and Environmental Engineering, The University of Texas at Austin, Austin, Texas 78712, United States

Supporting Information

ABSTRACT: Previous research has shown that desktop 3D printers can emit large numbers of ultrafine particles (UFPs, particles less than 100 nm) and some hazardous volatile organic compounds (VOCs) during printing, although very few filament and 3D printer combinations have been tested to date. Here we quantify emissions of UFPs and speciated VOCs from five commercially available filament extrusion desktop 3D printers utilizing up to nine different filaments by controlled experiments in a test chamber. Median estimates of time-varying UFP emission rates ranged from ~10^8 to ~10^{11} min^{-1} across all tested combinations, varying primarily by filament material and, to a lesser extent, bed temperature. The individual VOCs emitted in the largest quantities included caprolactam from nylon-based and imitation wood and brick filaments (ranging from ~2 to ~180 μg/min), styrene from acrylonitrile butadiene styrene (ABS) and high-impact polystyrene (HIPS) filaments (ranging from ~10 to ~110 μg/min), and lactide from polylactic acid (PLA) filaments (ranging from ~4 to ~5 μg/min). Results from a screening analysis of potential exposure to these products in a typical small office environment suggest caution should be used when operating many of the printer and filament combinations in poorly ventilated spaces or without the aid of combined gas and particle filtration systems.

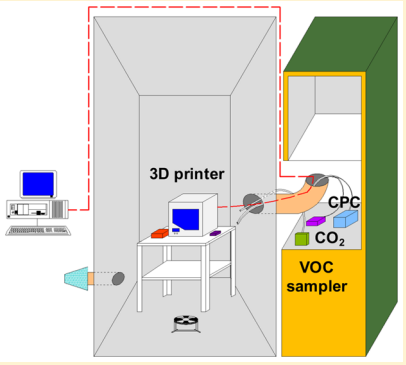

1. INTRODUCTION

Desktop three-dimensional (3D) printers are rapidly increasing in popularity. The majority of commercially available desktop 3D printers designed for the consumer market utilize an additive manufacturing technology called fused filament fabrication (FFF), also known as fused deposition modeling or molten polymer deposition. In the FFF process, a solid thermoplastic filament is forced through a heated extrusion nozzle, melted, and deposited in thin layers onto a moving bed.[1,2] A three-dimensional solid shape is formed layer-by-layer as the filament material cools and hardens. A wide variety of filament materials are now being used in desktop FFF 3D printers, including acrylonitrile butadiene styrene (ABS), poly(lactic acid) (PLA), poly(vinyl alcohol) (PVA), polycarbonate (PC), high-density polyethylene (HDPE), high-impact polystyrene (HIPS), nylon, and many other polymers, metals, ceramics, and other materials.[3] Filaments are melted at a variety of extruder nozzle temperatures and bed temperatures, and manufacturers typically recommend ranges of optimal temperatures for each filament material and thickness. ABS and PLA are currently the most commonly used filaments in desktop 3D printers, although others are also gaining popularity.[4]

It is well-known that both gases and particles are emitted during thermal processing of many thermoplastic materials.[5,6] However, little is known about the types and magnitudes of emissions from desktop FFF 3D printers and how they vary according to filament material or printer characteristics. In 2013, we published the first known measurements of emissions of ultrafine particles (UFPs: particles less than 100 nm in diameter) resulting from the operation of a single make and model of commercially available desktop FFF 3D printer using both ABS and PLA filaments.[7] These findings were crucial, as exposure to emissions from thermal decomposition of thermoplastics has been shown to have toxic effects in animals,[8−10] and exposure to UFPs from other sources has been linked to a variety of adverse human health effects.[11−17] We are aware of only one other published study to date that has investigated emissions from extrusion-based desktop 3D printers. Kim et al.[18] measured emissions of particles, total volatile organic compounds (TVOCs), several aldehydes and phthalates, and

Received: October 12, 2015
Revised: December 12, 2015
Accepted: January 7, 2016
Published: January 7, 2016

DOI: 10.1021/acs.est.5b04983
Environ. Sci. Technol. 2016, 50, 1260−1268

benzene, toluene, ethylbenzene, and *m*-,*p*-xylene (BTEX) from two different FFF printers operating in a small chamber, again using both ABS and PLA filaments. They confirmed that particle emissions were higher for printers utilizing ABS filaments compared to PLA filaments, and they also demonstrated higher VOC emissions from the printers using ABS filaments compared to PLA.

Despite these two studies, important gaps in our knowledge of emissions from 3D printers still remain. Only a very limited number of makes and models of printers have been tested to date, and even fewer filament materials have been characterized for gas and/or particle emissions (i.e., only ABS and PLA). Further, we hypothesize that Kim et al.[18] may have missed some individual VOCs that are emitted with some filaments because they were not specifically targeted or identified by a mass spectral library compound search. We also have no information to date on how the design or shape of printed materials, or printer characteristics such as the presence of enclosures, may influence gas and/or particle emissions.

Therefore, we advance these previous studies by quantifying emission rates of particles and a broad range of speciated VOCs from five popular commercially available desktop FFF 3D printers utilizing as many as nine different filaments to print standardized test objects in a medium-sized test chamber. We use the results to explore differences in particle and VOC emissions based on filament material and printer characteristics. We also provide preliminary data on the impact of print object geometry and the use of a partial enclosure.

2. EXPERIMENTAL METHODS

2.1. Emissions Testing Procedure. All measurements were conducted inside a 3.6 m^3 stainless steel chamber with a small stainless steel mixing fan operating as described in Supporting Information (Figure S1). Each printer was connected to a desktop computer located outside the chamber. Before each experiment began, filtered supply air was delivered to the chamber at a constant ventilation rate of approximately 1 h^{-1} for a period of at least 8 h to achieve initial steady-state background conditions. The 3D printer beds were prepared for printing before sealing the chamber by wiping with isopropyl alcohol, or, in some cases, depending on the printer and filament combination, by applying small amounts of adhesive from glue sticks following manufacturer recommendations. The printer was then powered on and began printing a small object.

For all tests but one, we printed a 10 × 10 × 1 cm standardized sample from the National Institute of Standards and Technology (NIST), as shown in Figure 1.[19] The sample was chosen because it was developed as a standardized test part to evaluate the performance of additive manufacturing technologies, and it has a range of features that were thought to potentially influence dynamic printer emissions, including a combination of solid volumes, thin protrusions, holes, and indentations. We also repeated one test with a single printer and filament combination, printing a ∼195 cm^3 cube of approximately the same printing duration as the NIST sample, allowing for an evaluation of the impact of print object shape on emissions. Nozzle and bed warm-up periods typically lasted between 5 and 10 min depending on the printer and filament, and the printing time varied from 2.5 to 4 h depending on the combination of printer, filament, and object shape.

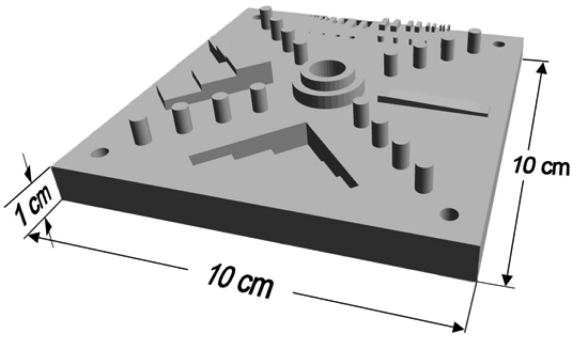

Figure 1. Shape file image of the NIST 3D printer test part used for emissions testing.

2.2. Air Sampling and Analysis. Particle concentrations were continuously measured inside the exhaust port of the chamber by use of a TSI model 3007 condensation particle counter (CPC) logging at 1 min intervals. The CPC was located inside an external exhaust hood and connected to the chamber exhaust port by a 0.9 m long piece of conductive tubing 0.6 cm in diameter. The CPC measures the total number concentrations of particles between 10 nm and 1 μm with a reported maximum concentration of $10^5/cm^3$ and a sample flow rate of 0.7 L/min. Particle concentrations were measured during all phases of the experiment, beginning with the last 45−60 min of background measurements, spanning the 2.5−4 h print period (which includes the 5−10 min warm-up phase), and ending with a final ∼3-h decay period during which particle concentrations were allowed to decrease toward background concentrations with the printer off.

We should note that although the measurement range of the CPC is 10 nm to 1 μm, the vast majority of particles emitted from most FFF printers were assumed to be in the UFP size range, as demonstrated by preliminary data in Supporting Information (Figure S4).[7,18] Thus, we consider these measurements largely representative of UFPs and use this nomenclature from here on. We periodically calibrated the CPC used for the chamber measurements via colocation measurements with a TSI model 3910 NanoScan scanning mobility particle sizer (SMPS) that had been recently calibrated by the manufacturer. We considered the SMPS to be the most accurate for UFP measurements, but it was not available for use during all of the tests. Thus, we calibrated the CPC to the SMPS using a polynomial regression from these periodic colocation experiments. The calibration between CPC particle counts and total UFP counts from the SMPS (Figure S2) was nearly linear throughout the manufacturer-reported measurement range of the CPC (up to $10^5/cm^3$) but increased exponentially beyond this range, as is typical for this instrument.[20] This was important to account for because several of the highest UFP emitters yielded raw CPC concentrations greater than $10^5/cm^3$ in the experimental chamber.

Chamber air was also sampled during the tests for VOC analysis using Tenax-GR sorbent tubes during two periods: once during the last ∼45 min prior to printing (with a printer in the chamber but not powered on or operating), and again during the last ∼45 min of printing after VOC concentrations reached approximately steady state. We used the differences in concentrations between the two samples to estimate emission rates both for speciated VOCs and for the sum of the 10 highest detectable VOCs (∑VOC). Total VOC (TVOC) concentrations inside the chamber were also continuously measured during a subset of experiments by use of a TSI Q-Trak model 7575 indoor air quality monitor with a model 982

DOI: 10.1021/acs.est.5b04983
Environ. Sci. Technol. 2016, 50, 1260−1268

photoionization detection (PID) probe to verify that TVOC concentrations achieved approximately steady state by the time air sampling for VOC analysis was conducted. These measurements were used to verify that approximately steady-state conditions were typically achieved within 2 h from the beginning of printing and that TVOC emissions followed a characteristic constant emission rate profile (Figure S3). Thus, we consider air sampling for VOC analysis during the final 45 min of printing each object reasonably representative of steady-state concentrations.

The procedure for sampling and analyzing the sorbent tubes was based on a modified version of U.S. EPA Method TO-17.[21] Sorbent tubes were inserted into a small hole in the exhaust port of the chamber and connected to a Buck VSS-1 low-flow air sampling pump located outside the chamber and operating at ~20 mL/min. Airflow rates of the sampling pumps and tubes were measured after each test by use of a Gilian Gilibrator 2 and combined with the recorded sampling duration to estimate the total air volume passed through the tubes during sampling. All sorbent tubes were shipped in a freezer pack overnight to the University of Texas at Austin and analyzed by thermal desorption followed by gas chromatography and electron ionization mass spectrometry (TD/GC/MS). An internal standard, 4-bromofluorobenzene, was used for all analysis. Individual VOCs were statistically identified and quantified by a NIST library compound search (LCS). The mass of the identified compounds was estimated from the response of the internal standard and a relative response factor of 1. The majority of the uncertainty associated with these calculations is related to the assumption that the relative response factor is 1. Relative response factors for this method have been shown to commonly range from approximately 0.75 to 1.25 for most VOCs;[22] thus we use 25% as an approximate estimate of the uncertainty in our VOC quantification method. Individual VOCs may not have the same response factors, but this provides a reasonable base estimate of the uncertainty in the reported concentrations.

We also sampled for VOCs outside the chamber during several tests. These sorbent samples were taken during the entire printing period to ensure that there were no unexpected external sources of VOCs transported into the chamber. Blank sorbent tubes were also collected outside the chamber without connecting them to the air pumps during each test to characterize adsorption of any unexpected compounds during shipping and storage. Finally, temperature and relative humidity (RH) were measured during each test with an Onset HOBO U12 data logger recording at 1 min intervals, and ventilation rates were measured during each test with CO_2 as a tracer gas. CO_2 was injected from a small tank into the chamber at the beginning of each test, and the subsequent decay of chamber CO_2 concentrations was measured by a PP Systems SBA-5 CO_2 monitor connected to an Onset HOBO U12 data logger, also recording at 1 min intervals. The ventilation rate calculation procedure is described fully in Supporting Information.

2.3. Ultrafine Particle Emission Rate Estimation. Because there was a large amount of scatter in the resulting UFP concentration data, we first applied a smoothing function to the UFP data using the "smooth" function in MATLAB R2015a, as described in Supporting Information. These smoothed concentration data were then used to estimate the time-varying UFP emission rate for each printer and filament combination via a discrete solution to a dynamic well-mixed number balance applied on the total particle number concentrations measured inside the chamber, as shown in eq 1 and derived in Supporting Information:

$$\frac{E_{\mathrm{UFP}}(t_{n+1})}{V} = \frac{[C_{\mathrm{UFP,in}}(t_{n+1}) - C_{\mathrm{UFP,in}}(t_n)]}{\Delta t} - L_{\mathrm{UFP}}\bar{C}_{\mathrm{UFP,bg}} + L_{\mathrm{UFP}}C_{\mathrm{UFP,in}}(t_n) \quad (1)$$

where $E_{\mathrm{UFP}}(t)$ is the time-varying UFP emission rate from a single 3D printer at time t (per minute), V is the chamber volume (cubic meters), $C_{\mathrm{UFP,in}}(t)$ is the UFP concentration inside the chamber at time t (per cubic meter), Δt is the time step for UFP measurements (1 min), L_{UFP} is the total UFP loss rate constant (per minute), and $\bar{C}_{\mathrm{UFP,bg}}$ is the average background UFP concentration inside the chamber prior to emissions testing. L_{UFP} was estimated from a log−linear regression with the first 60 min of data from the final decay period after printing finished, as described in Supporting Information. We should note that eq 1 makes several important assumptions that may lead to inaccuracies in estimates of UFP emission rates, such as ignoring size-resolved particle dynamics, ignoring coagulation, and assuming constant particle loss rates. Potential impacts of these assumptions are discussed in more detail in Supporting Information. We estimate the uncertainty in our time-varying UFP emission rate calculations to be approximately 45%, as described in Supporting Information.

The time-varying UFP emission rate estimates were also used to quantify the total number of UFPs emitted during printing, normalized by the mass of filament used, as shown in eq 2:

$$\dot{E}_{\mathrm{UFP}} = \frac{\sum_{k=1}^{N} E_{\mathrm{UFP}}(t_k)\Delta t}{m_{\mathrm{object}}} \quad (2)$$

where $\dot{E}_{\mathrm{UFP}}$ is the total number of UFPs emitted during printing per mass of filament used (per gram), N is the total number of time intervals during printing (minutes), and m_{object} is the mass of filament used (i.e., mass of final printed object, in grams).

2.4. Volatile Organic Compound Emission Rate Estimation. The TD/GC/MS library compound searches (LCS) identified and quantified approximately 50 speciated VOCs inside the chamber during the initial background periods and the last ~45 min of the printing periods. The emission rate of each identified VOC was estimated by use of eq 3, which assumes that ventilation was the only removal mechanism in the chamber, that the concentrations of top 10 measured emitted VOCs from 3D printers were negligible outside the chamber (verified by measurements), and that VOC concentrations achieved steady state during the final sampling period. These assumptions are discussed in more detail in Supporting Information.

$$E_{\mathrm{VOC,i}} = (C_{\mathrm{VOC,i,print}} - C_{\mathrm{VOC,i,bg}})\lambda V \quad (3)$$

$E_{\mathrm{VOC,i}}$ is the estimated constant emission rate of an individual VOC (micrograms per minute), $C_{\mathrm{VOC,i,print}}$ is the steady-state concentration of an individual VOC inside the chamber during the last ~45 min of printing (micrograms per cubic meter), and $C_{\mathrm{VOC,i,bg}}$ is the background concentration of an individual VOC inside the chamber prior to printing (micrograms per cubic meter). We estimate the uncertainty in our speciated VOC emission rate calculations to be approximately 36%, as described in Supporting Information.

The emission rate of each printer for the sum of the 10 highest detectable VOCs ($\sum$VOC) was estimated by adding all positive individual VOC emission rates of the top 10

DOI: 10.1021/acs.est.5b04983
Environ. Sci. Technol. 2016, 50, 1260−1268

Table 1. Summary of All Experiments[a]

printer	filament	extruder temp (°C)	bed temp (°C)	bed prep	mass (g)	enclosure	printing duration
FlashForge Creator	ABS white	200	110	glue	40.2	no	3 h 42 min
	PLA red	200	110	glue	53.2	no	3 h 42 min
Dremel 3D Idea Builder	PLA white[b,c]	230	room temperature	alcohol wipe	55.2	yes	2 h 49 min
XYZprinting da Vinci 1.0	ABS blue	230	100	glue	40.4	yes	2 h 26 min
LulzBot Mini	ABS red[b,c,d]	240	110	alcohol wipe	44.5	no	2 h 33 min
	ABS red[e]	240	110	alcohol wipe	56.7	no	2 h 42 min
	PLA red	190	45	alcohol wipe	53.1	no	3 h 25 min
	HIPS black[b]	240	100	alcohol wipe	47.4	no	2 h 28 min
	nylon bridge semitransparent	230	65	glue	46.5	no	2 h 55 min
	laybrick white	200	65	alcohol wipe	57.7	no	3 h 0 min
	laywood brown	200	65	alcohol wipe	48.3	no	3 h 2 min
	polycarbonate transparent[b]	270	110	glue	52.1	no	2 h 38 min
	PCTPE semitransparent	235	65	glue	47.8	no	3 h 2 min
	T-Glase transparent red	240	60	alcohol wipe	49.4	no	3 h 2 min
MakerBot Replicator 2X	ABS white[d]	230	110	glue	40.3	yes	2 h 38 min
	ABS white[d]	230	110	glue	40.7	no	2 h 38 min

[a]For all tests but one, we printed a 10 × 10 × 1 cm standardized sample from NIST. [b]Experimental conditions with duplicate VOC emissions tests. [c]Experimental conditions with duplicate UFP emissions tests. [d]Experiments with simultaneous VOC sampling conducted outside the chamber. [e]In this case we printed a ∼195 cm^3 cube with approximately the same printing duration as the NIST sample.

compounds with the highest concentrations inside the chamber during the last 45 min of the printing period. We limited to the top 10 highest concentration compounds because compounds below the top 10 added negligible amounts to the overall detectable $\sum VOC_i$ mass. We also normalized $\sum VOC$ emission rates by the mass of filament consumed by use of eq 4:

$$\dot{E}_{\sum VOC} = \frac{\sum_{k=1}^{N} E_{\sum VOC}(t_k)\Delta t}{m_{object}} \quad (4)$$

where $E_{\sum VOC}$ is the total VOC emission rate of a printer for the top 10 identified compounds and $\dot{E}_{\sum VOC}$ is the total VOC emission rate per mass of filament used (micrograms per gram).

2.5. Printer and Filament Descriptions. We characterized UFP and VOC emissions from a total of 16 unique combinations of printers and filaments, including five popular commercially available makes and models of desktop 3D printers with up to nine different filament materials. The five printers included (1) a FlashForge Creator dual extruder model compatible with ABS and PLA (both filaments were tested); (2) a Dremel 3D Idea Builder compatible with PLA only; (3) an XYZprinting da Vinci 1.0 compatible with ABS only; (4) a MakerBot Replicator 2X compatible with ABS only; and (5) a LulzBot Mini that was compatible with many different types of filaments. The LulzBot printer was tested with nine different filaments that are commonly used, including ABS, PLA, high-impact polystyrene (HIPS), semitransparent nylon, laybrick (an imitation brick material of unknown chemical composition), laywood (an imitation wood material of unknown chemical composition), transparent polycarbonate, a semitransparent nylon-based plasticized copolyamide thermoplastic elastomer (PCTPE), and a transparent polyester resin filament called T-Glase. The Dremel, XYZprinting, and MakerBot printers all had built-in plastic enclosures surrounding the apparatus (although they were not airtight), while the FlashForge and LulzBot did not have any enclosures. This list of printers is not meant to be exhaustive, but it is designed to span a reasonable range of currently popular printers with relatively generalizable characteristics such as filament type, nozzle and bed temperatures, and the presence or absence of a partial enclosure. Table 1 summarizes all experiments that were conducted.

Fifteen of the 16 printer and filament combinations were used to print the NIST test part, while one test combination (LulzBot-ABS) was also used to print a cube. The MakerBot with ABS filament was also tested twice: once with the plastic enclosure from the manufacturer installed as received from the factory and once with the enclosure intentionally removed. We also performed duplicate VOC measurements for four printer and filament combinations and two duplicate UFP measurements to evaluate the repeatability of our experiments.

3. RESULTS AND DISCUSSION

3.1. Ultrafine Particle Emission Rates. Figure 2a shows an example of time-varying UFP concentrations resulting from just one test of one of the printers with ABS filament (LulzBot Mini), along with the smoothed fit to the UFP concentration data. The left guideline in Figure 2a shows the moment that printers began warming up prior to printing, which we considered part of the printing emissions period. Figure 2b shows the time-varying UFP emission rates estimated from eq 1. Figures S6−S23 show similar time-series profiles of both UFP concentrations and emission rates for all 16 experimental combinations, as well as two duplicates.

Results in Figure 2a are similar to results from most of the experiments in that UFP concentrations typically rapidly increased just after printing began and persisted for the first 10−20 min, then decreased to a lower level, albeit typically to a level that was still higher than the background concentration. During some tests with other printer and filament combinations, UFP concentrations peaked again near the end of the print period as the thin protrusions on the printed object were

DOI: 10.1021/acs.est.5b04983
Environ. Sci. Technol. 2016, 50, 1260−1268

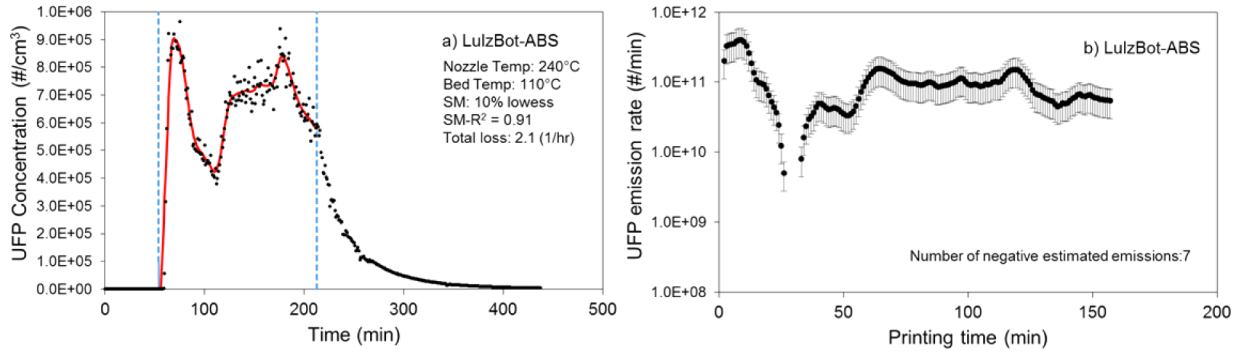

Figure 2. (a) Calibrated and smoothed UFP concentrations and (b) estimates of time-varying UFP emission rates for one sample test condition with LulzBot Mini 3D printer and ABS filament. SM refers to the data smoothing method utilized.

created. However, the magnitude and shape of dynamic UFP concentrations varied widely depending on the printer, filament, shape of printed object, and nozzle and bed temperatures. In a few scenarios (e.g., Figure 2a), UFP concentrations reached an approximate steady-state level toward the end of printing period. We used data from these periods to verify that the discretized time-varying emission rate calculation method (eq 1) also yielded similar estimates of UFP emission rates as the simple steady-state solution to the mass balance, as described in Supporting Information. Results from both solution methods were in good agreement for these periods, suggesting that the dynamic solution method provides reasonable emission rate estimates.

Figure 3 shows the range of time-varying UFP emission rates estimated for all 16 printer and filament combinations, grouped by (i) ABS filaments, (ii) PLA filaments, and (iii) all filaments other than ABS or PLA.

UFP emission rates varied substantially depending on make and model of the printer, type of filament material, nozzle and bed temperatures, and time of printing. The highest UFP emission rates typically occurred with the printers utilizing ABS filaments, with median values ranging from $\sim 2 \times 10^{10}$ to $\sim 9 \times 10^{10}$ min^{-1} across all ABS printers with or without enclosures. The lowest UFP emission rates occurred with the three printers

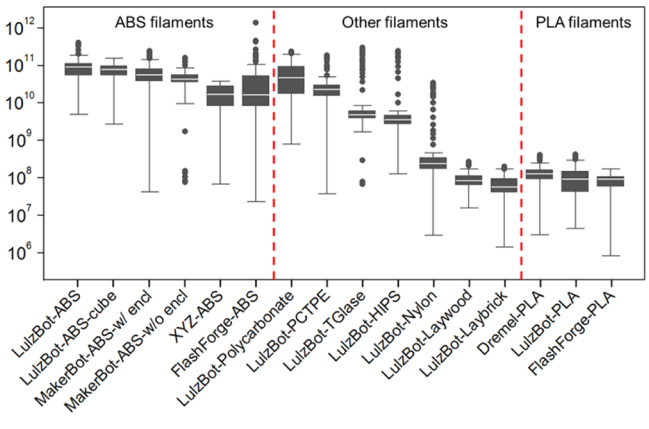

Figure 3. Summary of time-varying UFP emission rates estimated for 16 3D printer and filament combinations. Each data point represents data from 1 min intervals, and the combination of data points represents the entire printing period (typically between 2.5 and 4 h). Boxes show the 25th and 75th percentile values with the 50th percentile (median) in between. Whiskers represent upper and lower adjacent values, and circles represent outliers beyond those values.

utilizing PLA filaments, regardless of printer make and model, with median UFP emission rates of $\sim 10^8$ min^{-1}. This is lower than what we estimated in our original study with a different make and model printer as well as a different study design[7] but is similar to other recent chamber tests.[18] Median UFP emission rates for other filaments were highest for polycarbonate filament ($\sim 4 \times 10^{10}$ min^{-1}), followed by PCTPE ($\sim 2 \times 10^{10}$ min^{-1}), T-Glase ($\sim 5 \times 10^{9}$ min^{-1}), HIPS ($\sim 4 \times 10^{9}$ min^{-1}), nylon ($\sim 2 \times 10^{8}$ min^{-1}), laywood ($\sim 8 \times 10^{7}$ min^{-1}), and laybrick ($\sim 6 \times 10^{7}$ min^{-1}), all printed with the LulzBot Mini printer.

Printing a cube instead of the NIST test part with ABS filament (in the LulzBot printer) did not meaningfully alter the magnitude of UFP emission rates, although it did slightly change the time-varying shape of the UFP emissions profile (Figure S8). Interestingly, the presence of an enclosure only moderately reduced UFP emission rates from the MakerBot–ABS combination, with a ~35% reduction in the median emission rate (although this variation is within the estimate of uncertainty). Larger reductions were not observed, perhaps because the enclosure was not completely sealed and large gaps were visible. While these two comparisons provide preliminary data on how printed shape and presence of an enclosure may impact particle emissions from 3D printers, no other definitive conclusions can be drawn given this limited data set. Finally, data from two sets of duplicate tests (Figures S6 and S7and Figures S17 and S18) also demonstrated that there is some inherent variability in UFP emissions between repeated tests, as median emission rate estimates from these comparisons were within 57% and 48% of each other, respectively.

3.2. Volatile Organic Compound Emission Rates.

Figure 4 summarizes estimates of individual speciated VOC and ∑VOC emission rates from each of the 16 printer and filament combinations. Only the top three speciated VOCs with the highest concentrations measured in each test are shown individually, while the remaining top 10 individual VOCs are summarized as other VOCs. The sum of these yields an estimate of the ∑VOC emission rate. We also provide a list of the top 10 individual VOCs with the highest measured concentrations during the printing periods for all 16 experimental combinations inside the chamber and four duplicate experiments for VOC sampling in Table S2, as well as during four periods of VOC sampling outside the chamber in Table S3.

Filament material drove the majority of differences in the types of VOCs emitted, while printer make and model drove the majority of differences in the overall mass of VOCs emitted

DOI: 10.1021/acs.est.5b04983
Environ. Sci. Technol. 2016, 50, 1260−1268

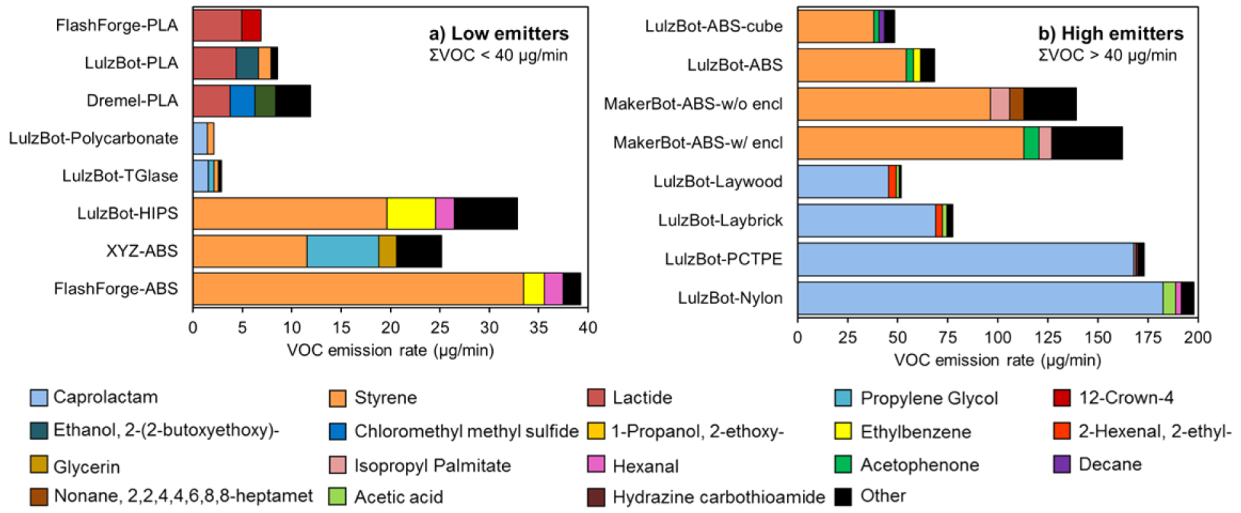

Figure 4. Estimates of emission rates for the top three highest-concentration VOCs as well as sum of the top 10 detectable VOCs (∑VOC) resulting from operation of 16 3D printer and filament combinations. The figure is divided into (a) low emitters, with $E_{\sum VOC}$ < 40 μg/min, and (b) high emitters, with $E_{\sum VOC}$ > 40 μg/min, for visual clarity. Note that although no error bars are shown in the figure, we estimate the uncertainty in each individual VOC emission rate to be ∼36% as described in Supporting Information.

with the same filament. Estimates of total VOC emission rates ($E_{\sum VOC}$) ranged from as low as ∼3 μg/min for the polycarbonate filament to nearly 200 μg/min for the nylon filament (both printed with the LulzBot). The top three highest emitted compounds accounted for at least 70% of ∑VOC emissions in all cases. For most of the printer and filament combinations, a single VOC dominated the ∑VOC emissions.

The primary individual VOC emitted from all six ABS filament and printer combinations and the only HIPS filament tested was styrene. Estimates of styrene emission rates with these filaments ranged from ∼12 to ∼113 μg/min, depending on the printer make and model. Interestingly, both the lowest and highest styrene emission rates were measured for printers with a partial enclosure (XYZprinting and MakerBot). Both styrene and total VOC emission rates were slightly lower when the LulzBot−ABS combination printed a cube compared to the standard NIST test part, but they were actually slightly higher for the MakerBot−ABS combination with the plastic enclosure compared to results without the enclosure.

The primary individual VOC emitted from nylon, PCTPE, laybrick, and laywood filaments was caprolactam. All of these filaments were installed in the LulzBot printer and all were classified as high emitters in Figure 4b, with caprolactam emission rates as high as ∼180 μg/min for the nylon filament. Caprolactam was also emitted from the polycarbonate and T-Glase filaments installed in the LulzBot printer, albeit at much lower levels (Figure 4a). Finally, the primary individual VOC emitted from PLA filaments was lactide (1,4-dioxane-2,5-dione, 3,6-dimethyl), albeit in relatively low quantities, with emission rates ranging from ∼4 to ∼5 μg/min in the three printers using PLA filaments. We are confident that the majority of the identified VOCs originated from the filament materials for most of the printer tests, even for the tests that had glue applied to the bed, because the main components measured during the glue-only test (propylene glycol and glycerin, as shown in Table S2) were found only in one filament/printer combination in Figure 4.

3.3. Impacts of Nozzle and Bed Temperatures. Next, we explored our estimates of both UFP and ∑VOC emission rates as a function of both nozzle and bed temperatures (Figure 5). The mean UFP and ∑VOC emission rates are split into three groups of bed temperature (less than 45, 60−65, and 100−110 °C) and plotted versus nozzle temperature (which varied from 190 to 270 °C, as described in Table 1).

Nozzle temperatures did not have a large influence on UFP emission rates from this set of printers at either low or high bed temperatures. However, nozzle temperatures did appear to influence UFP emission rates at midrange bed temperatures, as UFP emission rates were higher with increased nozzle temperatures. More importantly, bed temperatures alone appeared to influence UFP emission rates in this sample of printers. Most of the printer/filament combinations with the highest bed temperatures had the highest UFP emission rates, while most of the printer/filament combinations with the lowest bed temperatures had the lowest UFP emission rates. There was no apparent relationship observed between ∑VOC emission rates and either bed or nozzle temperatures across this sample of printers and filaments. However, we should note that with this limited sample size, these relationships are only considered suggestive.

3.4. Correlations between Total Ultrafine Particle and Sum of Volatile Organic Compound Emissions per Mass of Filament. Figure 6 compares the total number of UFPs emitted (eq 2) and the ∑VOC mass emitted (eq 4) during printing, normalized by the mass of filament, for each of the 16 primary printer and filament combinations.

The total number of UFPs emitted per gram of filament printed ranged from a minimum of ∼2×10^8 g^{-1} for the LulzBot−laybrick combination to a maximum of over 2×10^{11} g^{-1} for multiple printers with ABS filaments. The ∑VOC mass emitted per gram of filament printed ranged from a minimum of ∼6 μg/g for the LulzBot−polycarbonate combination to nearly 800 μg/g for the LulzBot−nylon combination. In general, ABS, PCTPE, and HIPS filaments had high mass-normalized emission rates of both UFPs and ∑VOCs, while PLA filaments had relatively low mass-normalized UFP and ∑VOC emission rates. Interestingly, both T-Glase and polycarbonate filaments (both used in the LulzBot printer) had low ∑VOC emissions but high UFP emissions. Conversely, both laywood and laybrick filaments (also used

DOI: 10.1021/acs.est.5b04983
Environ. Sci. Technol. 2016, 50, 1260−1268

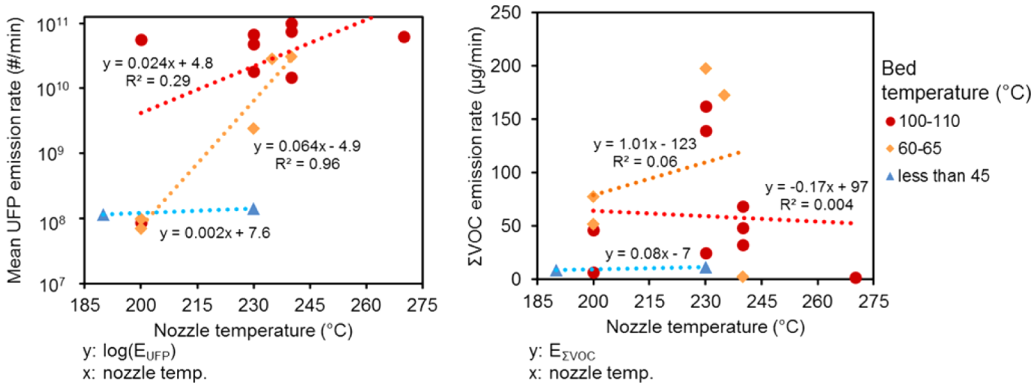

Figure 5. Impact of nozzle and bed temperature on mean UFP and TVOC emission rates.

in the LulzBot printer) had relatively high ∑VOC emission rates but low UFP emission rates. These data suggest that filament material selection drives both UFP and ∑VOC emissions, although knowledge of one type of emissions may not necessarily be used to predict the other.

3.5. Implications for Human Exposure and Health Effects. Measurements of UFP and individual VOC emission rates presented here have important implications for human exposure and health effects. For example, styrene, which is classified as a possible human carcinogen by the International Agency for Research on Cancer (IARC classification group 2B),[23] was emitted in large amounts by all ABS filaments and the one HIPS filament. Caprolactam was also emitted in large amounts by four of the filaments: nylon, PCTPE, laybrick, and laywood. Although caprolactam is classified as probably not carcinogenic to humans,[24] the California Office of Environmental Health Hazard Assessment (OEHHA) maintains acute, 8-h, and chronic reference exposure levels (RELs) of only 50, 7, and 2.2 $\mu g/m^3$, respectively.[25] We are not aware of any relevant information regarding the inhalation toxicity of lactide, the primary individual VOC emitted from PLA filaments.

To provide a basis for comparison to regulatory exposure limits and to help understand potential implications for human health, we used these estimates of UFP and individual VOC emission rates to predict steady-state concentrations that would likely result from constant printer operation in a typical small well-mixed office environment. This effort is not meant to serve as a detailed exposure model but rather as a screening analysis for potential health implications. We should also note that this analysis does not take into account proximity effects that could serve to substantially elevate exposures to both UFPs and VOCs in certain microenvironments compared to well-mixed conditions.

Let us assume that one desktop 3D printer operates continuously in a well-mixed 45 m^3 furnished and conditioned office space (i.e., the same office space reported by Stephens et al.[7] Let us assume a worst-case scenario in which a single printer has the maximum median UFP and individual VOC emission rates from the findings herein, which include ~10^{11} min^{-1} for UFPs, 183 $\mu g/min$ for caprolactam, 113 $\mu g/min$ for styrene, and 5 $\mu g/min$ for lactide. Let us assume a typical office ventilation rate of 1 h^{-1},[26] no sorption losses for the three VOCs (likely a conservative estimate),[27,28] and a typical UFP deposition loss rate constant of 1.3 h^{-1}.[29] Under these conditions, steady-state indoor concentrations of each of these constituents would be elevated to ~58 000 cm^{-3} for

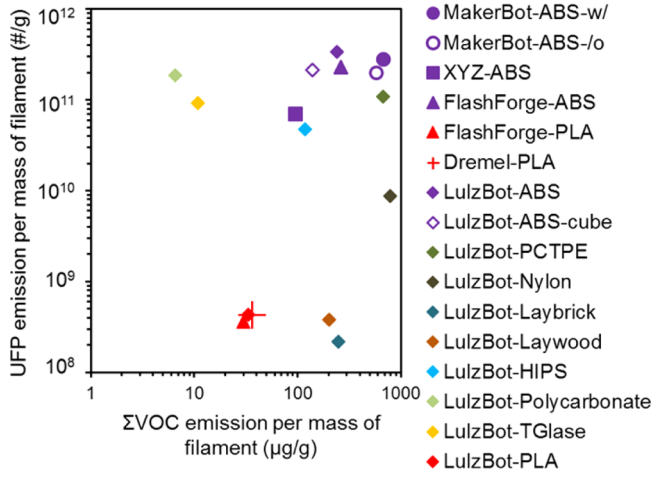

Figure 6. Comparison of total UFP and TVOC emissions per mass of filament.

UFPs, ~244 $\mu g/m^3$ for caprolactam, ~150 $\mu g/m^3$ for styrene, and ~6 $\mu g/m^3$ for lactide.

The predicted caprolactam concentration (244 $\mu g/m^3$) would exceed all three RELs identified by the California OEHHA,[25] which suggests that although there is considerable uncertainty in this estimate, exposure to caprolactam from desktop 3D printing in a typical office environment with nylon and nylon-based filaments could lead to adverse health outcomes, particularly for susceptible individuals. Acute exposure to high concentrations of caprolactam is known to be "irritating to the eyes and the respiratory tract" and "may cause effects on the central nervous system", according to the Centers for Disease Control and Prevention (CDC).[30]

The predicted styrene concentration in this configuration (150 $\mu g/m^3$) would be approximately 20 times higher than the highest styrene concentration measured in commercial buildings in the U.S. EPA BASE study[31] and more than 20 times higher than the average concentration in U.S. residences.[32] There are also reports that suggest exposure to styrene at these concentrations could be problematic for human health. For example, high indoor styrene concentrations have been estimated to yield relatively high lifetime cancer risks in previous studies that assumed typical potency factors,[33] and even moderate styrene concentrations (i.e., greater than only 2 $\mu g/m^3$) have been associated with elevated risk of pulmonary infections in infants.[34]

Although we are not aware of any regulatory limits for indoor UFP concentrations, an increase in UFP concentrations to

DOI: 10.1021/acs.est.5b04983
Environ. Sci. Technol. 2016, 50, 1260−1268

~58 000 cm^{-3} would be approximately 10 times higher than what we typically observe in indoor air in our office and laboratory environments and what has been reported as a typical 8-h average indoor concentration in schools.[35] However, it would only be moderately higher than typical time-averaged concentrations in homes[36] but lower than what is often observed in other microenvironments.[37]

Given these findings, we are prompted to make the following recommendations. First, additional measurements should be conducted to more accurately quantify personal exposures to both UFPs and speciated VOCs that account for proximity effects presented by typical 3D printer use patterns. Second, manufacturers should work toward designing low-emitting filament materials and/or printing technologies. Third, in the absence of new low-emitting filaments, manufacturers should work to evaluate the effectiveness of sealed enclosures on both UFP and VOC emissions or to introduce combined gas and particle filtration systems. Until then, we continue to suggest that caution should be used when operating many printer and filament combinations in enclosed or poorly ventilated spaces or without the aid of gas and particle filtration systems. This is particularly true for both styrene- and nylon-based filaments, based on data from the relatively large sample of printers and filament combinations evaluated here.

■ ASSOCIATED CONTENT

Supporting Information

The Supporting Information is available free of charge on the ACS Publications website at DOI: 10.1021/acs.est.5b04983.

Additional text, 23 figures, and four tables with descriptions of solution methods, experimental setup details, calibrations, uncertainty analysis, and all resulting UFP and VOC data (PDF)

■ AUTHOR INFORMATION

Corresponding Author

*Phone (312) 567-3356; e-mail brent@iit.edu.

Notes

The authors declare no competing financial interest.

■ ACKNOWLEDGMENTS

This research was funded by the Centers for Disease Control and Prevention through the National Institute for Occupational Safety and Health (Grant ROH010699). Its contents are solely the responsibility of the authors and do not necessarily represent the official views of the Centers for Disease Control and Prevention or the Department of Health and Human Services.

■ REFERENCES

(1) Getting Started with a 3D Printer. *2013 MAKE Ultimate Guide to 3D Printing*; http://makezine.com/2012/11/13/getting-started-with-a-3d-printer/.

(2) Gross, B. C.; Erkal, J. L.; Lockwood, S. Y.; Chen, C.; Spence, D. M. Evaluation of 3D Printing and Its Potential Impact on Biotechnology and the Chemical Sciences. *Anal. Chem.* **2014**, *86* (7), 3240−3253.

(3) *MatterHackers 3D printer filament comparison guide*, 2015; https://www.matterhackers.com/3d-printer-filament-compare.

(4) Ragan, S. Plastics for 3D Printing. *2013 MAKE Ultimate Guide To 3D Printing*, Winter **2013**; page 22; http://makezine.com/2012/11/13/plastics-for-3d-printing/.

(5) Contos, D. A.; Holdren, M. W.; Smith, D. L.; Brooke, R. C.; Rhodes, V. L.; Rainey, M. L. Sampling and Analysis of Volatile Organic Compounds Evolved During Thermal Processing of Acrylonitrile Butadiene Styrene Composite Resins. *J. Air Waste Manage. Assoc.* **1995**, *45* (9), 686−694.

(6) Unwin, J.; Coldwell, M. R.; Keen, C.; McAlinden, J. J. Airborne Emissions of Carcinogens and Respiratory Sensitizers during Thermal Processing of Plastics. *Ann. Occup. Hyg.* **2013**, *57* (3), 399−406.

(7) Stephens, B.; Azimi, P.; El Orch, Z.; Ramos, T. Ultrafine particle emissions from desktop 3D printers. *Atmos. Environ.* **2013**, *79*, 334−339.

(8) Zitting, A.; Savolainen, H. Effects of single and repeated exposures to thermo-oxidative degradation products of poly-(acrylonitrile-butadiene-styrene) (ABS) on rat lung, liver, kidney, and brain. *Arch. Toxicol.* **1980**, *46* (3−4), 295−304.

(9) Schaper, M. M.; Thompson, R. D.; Detwiler-Okabayashi, K. A. Respiratory Responses of Mice Exposed to Thermal Decomposition Products from Polymers Heated at and Above Workplace Processing Temperatures. *Am. Ind. Hyg. Assoc. J.* **1994**, *55* (10), 924−934.

(10) Oberdorster, G.; Oberdorster, E.; Oberdorster, J. Nanotoxicology: An Emerging Discipline Evolving from Studies of Ultrafine Particles. *Environ. Health Perspect.* **2005**, *113* (7), 823−839.

(11) Oberdörster, G.; Sharp, Z.; Atudorei, V.; Elder, A.; Gelein, R.; Kreyling, W.; Cox, C. Translocation of Inhaled Ultrafine Particles to the Brain. *Inhalation Toxicol.* **2004**, *16* (6−7), 437−445.

(12) Oberdörster, G.; Celein, R. M.; Ferin, J.; Weiss, B. Association of Particulate Air Pollution and Acute Mortality: Involvement of Ultrafine Particles? *Inhalation Toxicol.* **1995**, *7* (1), 111−124.

(13) Delfino, R. J.; Sioutas, C.; Malik, S. Potential role of ultrafine particles in associations between airborne particle mass and cardiovascular health. *Environ. Health Perspect.* **2005**, *113* (8), 934−946.

(14) HEI. *Understanding the Health Effects of Ambient Ultrafine Particles*; HEI Review Panel on Ultrafine Particles; HEI Perspectives 3; Health Effects Institute: Boston, MA, 2013; http://pubs.healtheffects.org/getfile.php?u=893.

(15) Weichenthal, S.; Dufresne, A.; Infante-Rivard, C. Indoor ultrafine particles and childhood asthma: exploring a potential public health concern. *Indoor Air* **2007**, *17* (2), 81−91.

(16) Stölzel, M.; Breitner, S.; Cyrys, J.; Pitz, M.; Wölke, G.; Kreyling, W.; Heinrich, J.; Wichmann, H.-E.; Peters, A. Daily mortality and particulate matter in different size classes in Erfurt, Germany. *J. Exposure Sci. Environ. Epidemiol.* **2007**, *17* (5), 458−467.

(17) Andersen, Z. J.; Olsen, T. S.; Andersen, K. K.; Loft, S.; Ketzel, M.; Raaschou-Nielsen, O. Association between short-term exposure to ultrafine particles and hospital admissions for stroke in Copenhagen, Denmark. *Eur. Heart J.* **2010**, *31* (16), 2034−2040.

(18) Kim, Y.; Yoon, C.; Ham, S.; Park, J.; Kim, S.; Kwon, O.; Tsai, P.-J. Emissions of Nanoparticles and Gaseous Material from 3D Printer Operation. *Environ. Sci. Technol.* **2015**, *49*, 12044−12053.

(19) Moylan, S.; Slotwinski, J.; Cooke, A.; Jurrens, K.; Donmez, M. A. Proposal for a standardized test artifact for additive manufacturing machines and processes. *Solid Freeform Fabr. Symp. Proc.* **2012**, 6−8, http://sffsymposium.engr.utexas.edu/Manuscripts/2012/2012-69-Moylan.pdf.

(20) Westerdahl, D.; Fruin, S.; Sax, T.; Fine, P. M.; Sioutas, C. Mobile platform measurements of ultrafine particles and associated pollutant concentrations on freeways and residential streets in Los Angeles. *Atmos. Environ.* **2005**, *39* (20), 3597−3610.

(21) U.S. EPA. Compendium Method TO-17: Determination of Volatile Organic Compounds in Ambient Air Using Active Sampling Onto Sorbent Tubes. In *Compendium of Methods for the Determination of Toxic Organic Compounds in Ambient Air*, 2nd ed.; EPA/625/R-96/010b; U.S. Environmental Protection Agency, 1999; http://www3.epa.gov/ttnamti1/files/ambient/airtox/to-17r.pdf.

(22) Allgood, C.; Orlando, R.; Munson, B. Correlations of relative sensitivities in gas chromatography electron ionization mass spectrometry with molecular parameters. *J. Am. Soc. Mass Spectrom.* **1990**, *1* (5), 397−404.

DOI: 10.1021/acs.est.5b04983
Environ. Sci. Technol. 2016, 50, 1260−1268

(23) IARC. *Some Traditional Herbal Medicines, Some Mycotoxins, Naphthalene and Styrene*; IARC Monographs on the Evaluation of Carcinogenic Risks to Humans, Vol. *82*; International Agency for Research on Cancer, 2002; http://monographs.iarc.fr/ENG/Monographs/vol82/mono82.pdf.
(24) IARC. *Re-evaluation of Some Organic Chemicals, Hydrazine and Hydrogen Peroxide*; IARC Monographs on the Evaluation of Carcinogenic Risks to Humans, Vol. *71*; International Agency for Research on Cancer, 1999; http://monographs.iarc.fr/ENG/Monographs/vol71/mono71.pdf.
(25) Office of Environmental Health Hazard Assessment. Table of All OEHHA Acute, Chronic and 8 h Reference Exposure Levels; http://oehha.ca.gov/air/allrels.html (accessed October 7, 2015).
(26) Bennett, D.; Apte, M.; Wu, X.; Trout, A.; Faulkner, D.; Maddalena, R.; Sullivan, D. *Indoor environmental quality and heating, ventilating, and air conditioning survey of small and medium size commercial buildings*; CEC-500-2011-043; California Energy Commission: 2011; http://www.energy.ca.gov/2011publications/CEC-500-2011-043/CEC-500-2011-043.pdf.
(27) Singer, B. C.; Revzan, K. L.; Hotchi, T.; Hodgson, A. T.; Brown, N. J. Sorption of organic gases in a furnished room. *Atmos. Environ.* **2004**, *38* (16), 2483−2494.
(28) Singer, B. C.; Hodgson, A. T.; Hotchi, T.; Ming, K. Y.; Sextro, R. G.; Wood, E. E.; Brown, N. J. Sorption of organic gases in residential rooms. *Atmos. Environ.* **2007**, *41* (15), 3251−3265.
(29) Wallace, L.; Kindzierski, W.; Kearney, J.; MacNeill, M.; Héroux, M.-È.; Wheeler, A. J. Fine and Ultrafine Particle Decay Rates in Multiple Homes. *Environ. Sci. Technol.* **2013**, *47* (22), 12929−12937.
(30) CDC. The National Institute for Occupational Safety and Health (NIOSH) International Chemical Safety Cards (ICSC), Caprolactam; Centers for Disease Controls and Prevention, 1994; http://www.cdc.gov/niosh/ipcsneng/neng0118.html.
(31) Girman, J. R.; Hadwen, G. E.; Burton, L. E.; et al. Individual Volatile Organic Compound Prevalence and Concentrations in 56 Buildings of the Building Assessment Survey and Evaluation (BASE) Study. *Proc. Indoor Air* **1999**, Vol. *II*, pp 460−465; http://www.epa.gov/sites/production/files/2014-08/documents/base_2_460.pdf.
(32) Logue, J. M.; Price, P. N.; Sherman, M. H.; Singer, B. C. A method to estimate the chronic health impact of air pollutants in U.S. residences. *Environ. Health Perspect.* **2012**, *120* (2), 216−222.
(33) Guo, H.; Lee, S. C.; Chan, L. Y.; Li, W. M. Risk assessment of exposure to volatile organic compounds in different indoor environments. *Environ. Res.* **2004**, *94* (1), 57−66.
(34) Diez, U.; Kroessner, T.; Rehwagen, M.; Richter, M.; Wetzig, H.; Schulz, R.; Borte, M.; Metzner, G.; Krumbiegel, P.; Herbarth, O. Effects of indoor painting and smoking on airway symptoms in atopy risk children in the first year of life results of the LARS-study. Leipzig Allergy High-Risk Children Study. *Int. J. Hyg. Environ. Health* **2000**, *203* (1), 23−28.
(35) Diapouli, E.; Chaloulakou, A.; Spyrellis, N. Levels of ultrafine particles in different microenvironments–implications to children exposure. *Sci. Total Environ.* **2007**, *388* (1−3), 128−136.
(36) Bhangar, S.; Mullen, N. A.; Hering, S. V.; Kreisberg, N. M.; Nazaroff, W. W. Ultrafine particle concentrations and exposures in seven residences in northern California. *Indoor Air* **2011**, *21*, 132−144.
(37) Wallace, L.; Ott, W. Personal exposure to ultrafine particles. *J. Exposure Sci. Environ. Epidemiol.* **2011**, *21* (1), 20−30.

DOI: 10.1021/acs.est.5b04983
Environ. Sci. Technol. 2016, 50, 1260−1268

Supporting Information (SI) for:

Emissions of ultrafine particles and volatile organic compounds from commercially available desktop 3D printers with multiple filaments

Parham Azimi,[1] Dan Zhao,[1] Claire Pouzet,[1,2] Neil E. Crain,[3] Brent Stephens[1,*]

[1]Department of Civil, Architectural and Environmental Engineering, Illinois Institute of Technology, Chicago, IL USA
[2]Ecole des Ingénieurs de la Ville de Paris (EIVP), 80 Rue Rebeval, 75019 Paris, France
[3]Department of Civil, Architectural, and Environmental Engineering, The University of Texas at Austin, Austin, TX 78712, USA

*Corresponding author:
Dr. Brent Stephens
Civil, Architectural and Environmental Engineering
Illinois Institute of Technology
Alumni Memorial Hall 212
3201 S Dearborn St
Chicago, IL 60616
Phone: (312) 567-3356
Email: brent@iit.edu

30 pages, 23 figures, 4 tables

Table of Contents

1. Experimental setup details

Measurements were conducted inside a 3.6 m^3 chamber (dimensions of 1.2×1.2×2.4 m) located in the Built Environment Research Group Laboratory at the Illinois Institute of Technology. The exterior walls of the chamber were made of 1.1 cm plywood sheets and the interior walls, floor, and ceiling were covered with 0.25 cm stainless steel sheets cut to the same size as the walls, floors, and ceiling. Gaps and edges inside the chamber were sealed with adhesive PTFE film tape (3M 5490). Each printer was tested while operating on a 0.6×0.9×0.9 m stainless steel table at the center of the chamber. A small stainless steel mixing fan was operated to achieve well-mixed conditions in the chamber, which were confirmed prior to the experiments with CO_2 concentration measurements in four locations throughout the chamber. Each printer was connected to a desktop computer located outside the chamber so that it could be operated without opening the chamber door during the test period.

Filtered room air was supplied to the chamber using a 10 cm 12 VDC diameter blower connected to a fibrous activated carbon filter to remove both gases and particulate matter. A DC power supply was used to control the speed of the blower to keep the ventilation rate of the chamber constant near 1 hr^{-1} throughout each test (the ventilation rate was also measured during each test using CO_2 injection and decay as described in the next section). The chamber exhaust port was connected to a 20 cm diameter sheet metal duct that vented directly to a powered fume hood. Figure S1 shows details of the experiment setup.

The interior walls of the chamber were cleaned with distilled water after each experiment and the entire chamber was cleaned with isopropyl alcohol on a weekly basis. The chamber was left unused for at least 2 days after each alcohol cleaning to avoid contamination of VOC samples.

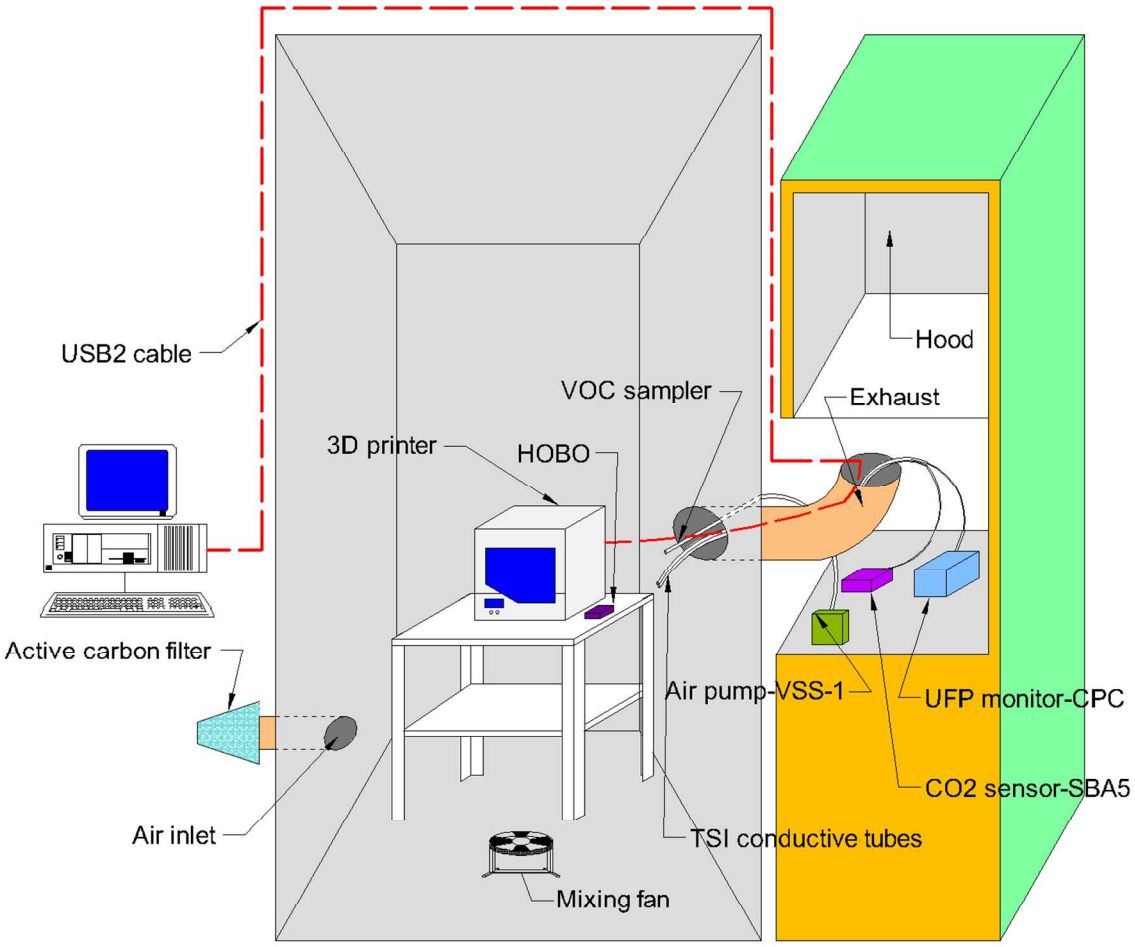

Figure S1: Schematic of the experimental test chamber. All acronyms are defined in the main text.

2. Ventilation rate estimation

We estimated the air exchange rate (AER) of the chamber during each experiment using a CO_2 injection and decay method, which involved increasing the CO_2 concentration inside the chamber by injection from a filtered compressed CO_2 cylinder and measuring the subsequent decay. We applied a dynamic mass balance equation for change in CO_2 concentration inside the chamber as shown in Equation S1.

$$\frac{dC_{co2,in}(t)}{dt} = \lambda C_{CO2,out} - \lambda C_{CO2,in}(t) \quad \text{(S1)}$$

Where
$C_{co2,in}(t)$ = concentration of CO_2 inside the chamber during an experiment (ppm)
t = time (min)
λ = air exchange rate of the chamber during an experiment (1/min)
$C_{CO2,out}$ = concentration of CO_2 outside the chamber during an experiment (ppm)

We also measured the background chamber CO_2 concentrations when it achieved steady state levels prior to the printing experiment and used this value for the concentration outside the chamber. Thus, Equation S1 can be re-written for background period as Equation S2.

$$C_{CO2,out} = \bar{C}_{CO2,in,bg} \quad \text{(S2)}$$

Where
$\bar{C}_{CO2,in,bg}$ = average background CO_2 concentration during an experiment (ppm)

We estimated the AER of the chamber by re-arranging and integrating Equation S1, as shown in Equation S3.

$$-ln\frac{C_{CO2,in}(\mathrm{t}) - \bar{C}_{CO2,in,bg}}{C_{CO2,in}(\mathrm{t}=0) - \bar{C}_{CO2,in,bg}} = \lambda \times t \quad \text{(S3)}$$

We plotted the left hand side of Equation S3 versus time for the first 60 minutes of the decay periods and considered the slope of linear regression line through the data points as the air exchange rate of the chamber during the entire experiment.

3. CPC calibration

We periodically calibrated the TSI Model 3007 Condensation Particle Counter (CPC) used in all experiments via co-location with a TSI Model 3910 NanoScan Scanning Mobility Particle Sizer (SMPS) that had been recently calibrated by the manufacturer. Three printer and filament combinations were operated in the chamber with both monitors logging at 1-minute intervals to provide data for the calibration. Figure S2 shows the raw particle readings from the CPC on the x-axis and the total UFP readings from the SMPS on the y-axis for the three tested combinations of printer and filaments inside the test chamber. Data from the three tests were used to generate a polynomial relationship between the two (R^2 = 0.989). This equation was then applied to all raw CPC concentrations prior to solving for emission rates.

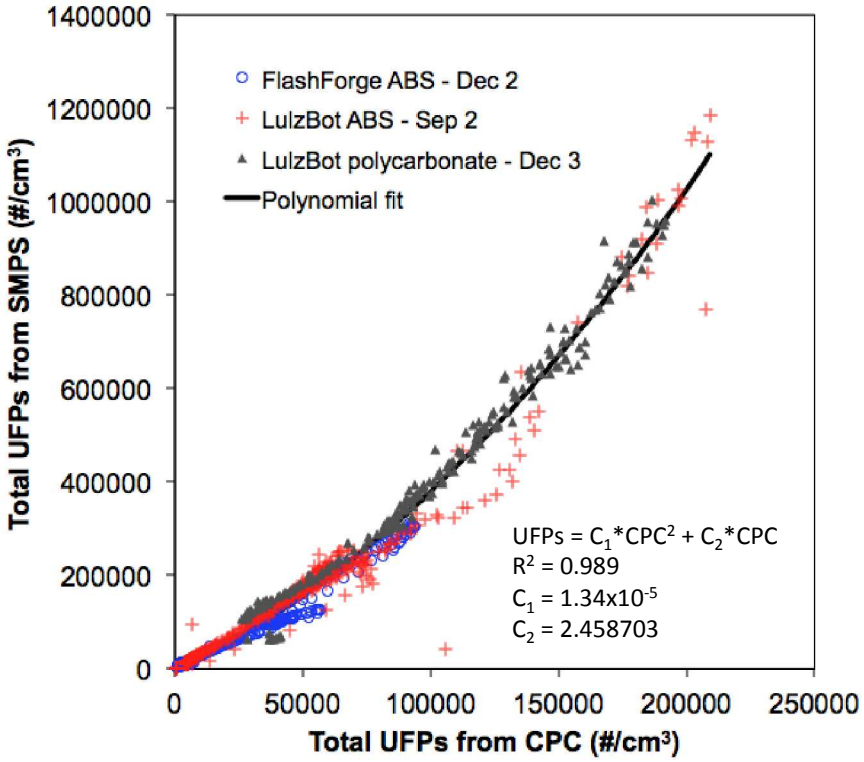

Figure S2: Measured UFP concentration inside the chamber using CPC and SMPS

4. Evaluating the time to reach steady state for TVOCs and the loss rate of TVOCs to chamber walls

TVOC concentrations inside the chamber were continuously measured during a limited subset of experiments using a TSI Q-Trak Indoor Air Quality Monitor Model 7575 with a Model 982 PID-based TVOC probe to verify that TVOC concentrations achieved approximately steady state by the time air sampling for VOC analysis was conducted. As an example, Figure S3 shows time-resolved TVOC concentrations measured during printing the standard NIST sample from using just one printer and filament combination (FlashForge with ABS filament).

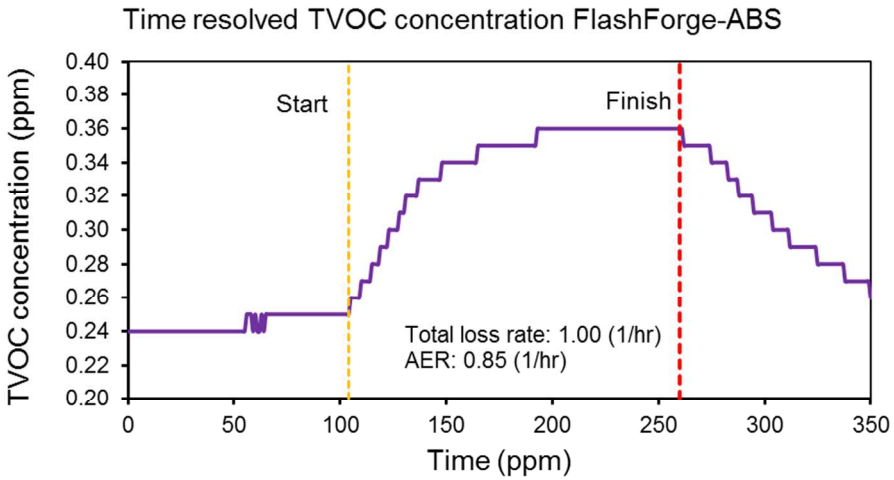

Figure S3: Time resolved TVOC concentration inside the test chamber

Figure S3 shows that the TVOC concentration reached to approximately steady state conditions ~100 minutes after printing started. Two other similar experiments with different printers/filaments were also similar. These measurements verified that approximately steady state conditions were typically achieved within 2 hours from the beginning of printing. Thus we consider air sampling for VOC analysis during the final 45 minutes of printing each object (the printing durations were at least 2 hr 26 min for all experiments) a reasonable assessment of steady state concentrations and can use the difference between the two samples to make reasonable estimates of speciated VOC emission rates.

Additionally, we also used these data to investigate the potential for sorption effects to the stainless steel chamber walls by estimating the total TVOC loss rate from the final decay period in Figure S3 (i.e., after printing stopped around 260 mins). The total TVOC loss rate was approximately 1.0 hr^{-1} using these data while the measured air exchange rate (AER) was 0.85 hr^{-1}. Thus, it appears that in this case, other removal mechanisms such as sorption on the chamber walls may have contributed an additional 0.15 hr^{-1}. However, when we applied the same method to two other experiments the results varied. The total TVOC loss rates were 1.12 and 1.22 hr^{-1}, with corresponding AERs of 1.04 and 1.24 hr^{-1}, respectively. These corresponded with the total loss rate being 7% higher and 2% lower than the chamber air exchange rate. Thus, we consider it reasonable to assume that sorption effects were negligible herein and that ventilation is indeed the major loss mechanism.

5. UFP emission rate estimation

We applied a dynamic well-mixed number balance on the total particle number concentrations measured inside the chamber (Equation S4) to estimate time-varying particle emission rates, which we considered largely representative of UFPs.

$$\frac{dC_{UFP,in}(t)}{dt} = P_{UFP}\lambda C_{UFP,out} - L_{UFP}C_{UFP,in}(\mathrm{t}) + \frac{E_{UFP}(t)}{V} \quad \text{(S4)}$$

where $C_{UFP,in}(t)$ is the UFP concentration inside the chamber at time t (#/m^3), P_{UFP} is the UFP penetration factor of the chamber (-), λ is the air exchange rate of the chamber (1/min), $C_{UFP,out}$ is the UFP concentration outside of the chamber (#/m^3), L_{UFP} is the total UFP loss rate constant inside the chamber (1/min), $E_{UFP}(t)$ is the time-varying UFP emission rate from a single 3D printer at time t (#/min), and V is the chamber volume (m^3).

The UFP concentration inside the chamber prior to testing (i.e., during the background period) reached steady state conditions prior to all experiments. Therefore, the average measured background concentration $\bar{C}_{UFP,bg}$ was used in place of $P_{UFP}\lambda C_{UFP,out}$ using Equation S5.

$$P_{UFP}\lambda C_{UFP,out} = \bar{C}_{UFP,bg}L_{UFP} \quad \text{(S5)}$$

The total UFP loss rate (L_{UFP}) was estimated using a log-linear regression with data from the final decay period after printing finished, as shown in Equation S6. We plotted the left hand side of Equation S6 versus time for the first 60 minutes of the decay period and used the slope of the linear regression as the total UFP loss rate during the entire experiment.

$$-ln\frac{C_{UFP,in}(\mathrm{t}) - \bar{C}_{UFP,bg}}{C_{UFP,in}(\mathrm{t}=0) - \bar{C}_{UFP,bg}} = L_{UFP}t \quad \text{(S6)}$$

Next, we estimated the time-varying UFP emission rate for each 3D printer using a discrete solution to the number balance in Equation S4, as shown in Equation S7.

$$\frac{E_{UFP}(t_{n+1})}{\mathrm{V}} = \frac{\left[C_{UFP,in}(\mathrm{t_{n+1}}) - C_{UFP,in}(\mathrm{t_n})\right]}{\Delta \mathrm{t}} - L_{UFP}\bar{C}_{UFP,bg} + L_{UFP}C_{UFP,in}(t_n) \quad \text{(S7)}$$

where Δt was the time step for UFP measurements (1 min).

We should note that Equations S4 through S7 make several important assumptions that may lead to inaccuracies in estimates of UFP emission rates. We do not consider size-resolved particle dynamics because we did not have access to the SMPS for every test. We assume that particle loss rates were constant throughout each test period, although one would expect them to vary depending on the particle size distribution in the chamber, which may vary at any given time based on size-dependent loss mechanisms such as deposition or coagulation. We have also assumed that the impact of coagulation on total UFP concentrations is negligible, which may not be the case. However, we estimate the likely magnitude of the impact of this assumption on total UFP emission rates to be relatively small (i.e., less than 30%, on average, using the most

conservative estimates of coagulation, as described later herein). While these are important limitations to this work, results can still provide a reasonable quantitative measure of particle emission rates resulting from 3D printer operation that can be used to compare one printer to another.

Further, there was a large amount of scatter in most of the resulting UFP concentration data from one minute to the next, particularly at high concentrations, which led to unreasonable numbers of negative emission rate estimates using the discretized solution method with raw UFP data. This was likely due to high uncertainty beyond the upper limit of the CPC. Therefore, we first applied a smoothing function to the resulting UFP concentration data using the '*smooth*' function in MATLAB R2015a. These smoothed concentration data were then used with Equation S7 to estimate time-varying emission rates with minimal negative values. We applied a number of smoothing function options (e.g., loess, lowess, and others) to each highly varying data set and selected smoothed data from the method that yielded a combination of the fewest negative emission rate estimates and the highest correlation between actual and smoothed UFP concentrations (i.e., R^2 was typically above 0.90, as described later herein). Any remaining periods of negative UFP emission rate estimates, which were likely due to time-varying and size-dependent loss rates that we were not able to account for, were simply excluded from analysis (the average number of negative values excluded was 10 data points out of a total of between ~150 and ~250 data points for each test).

6. VOC emission rate estimation

The TD/GC/MS library compound searches (LCS) identified and quantified approximately 50 speciated VOCs inside the chamber during the initial background periods and at the last ~45 minutes of the printing periods. The estimated mass of each individual VOC was converted to a chamber air concentration using Equation S8.

$$C_{VOC,i} = \frac{m_{VOC,i}}{\bar{Q}_{pump} \times t_{pump}} \quad \text{(S8)}$$

where $m_{VOC,i}$ is the total collected mass of an individual VOC in the sampling tube (μg), $\bar{Q}_{pump}$ is the average sampling pump airflow rate (m^3/min), and t_{pump} is the total VOC sampling time (min) for each sampling period.

Similar to the previous section, we applied a dynamic well-mixed mass balance on the speciated VOC mass concentrations measured inside the chamber, as shown in Equation S9.

$$\frac{dC_{VOC,i}(t)}{dt} = P_{VOC,i}\lambda C_{VOC,i,out} - L_{VOC,i}C_{VOC,i}(\mathrm{t}) + \frac{E_{VOC,i}}{V} \quad \text{(S9)}$$

where $C_{VOC,i}(t)$ is an individual VOC concentration inside the chamber at time t (μg/m^3), $P_{VOC,i}$ is an individual VOC penetration factor of the chamber (-),$C_{VOC,i,out}$ is an individual VOC concentration outside of the chamber (μg/m^3), $L_{VOC,i}$ is the total loss rate constant of an individual VOC inside the chamber (1/min), $E_{VOC,i}$ is the estimated constant emission rate of an individual VOC (μg/min).

Next, the emission rate of each identified VOC was estimated using Equation S10, assuming that ventilation was the only removal mechanism in the chamber, the concentration of 10 top measured emitted VOCs from 3D printers is negligible outside the chamber (verified by measuring individual VOC concentrations outside the chamber), and that VOC concentrations achieved steady state during the final sampling period.

$$E_{VOC,i} = \left(C_{VOC,i,print} - C_{VOC,i,bg}\right)\lambda V \quad \text{(S10)}$$

where $C_{VOC,i,print}$ is the steady state concentration of an individual VOC inside the chamber during the last ~45 minutes of printing (μg /m^3), and $C_{VOC,i,bg}$ is the background concentration of an individual VOC inside the chamber prior to printing (μg/m^3). We estimated the uncertainty in individual VOC emission rates to be approximately 36% based on the likely uncertainty in the GC/MS quantification method (~25%) combined with the uncertainty in pump flow rate measurements in quadrature (calculated later in Section 8 of the SI). Adsorption and desorption effects were assumed to be negligible given that the interior of the chamber was stainless steel.[1,2] This assumption was further verified by comparing TVOC loss rate estimates from multiple post-printing decay periods measured by the Q-Trak TVOC probe to the air exchange loss rate measured using CO_2 decay, as shown in Section 4 of the SI. Loss rates were similar, suggesting that sorption effects were indeed minor.

7. Impact of coagulation on UFP emission rate estimates

Given that UFP concentrations were often elevated to very high concentrations in the chamber, it is important to consider the potential for particle coagulation to influence our results, even though we did not have size resolved data. Here, we evaluate the likely impact of coagulation on UFP emission rates from the highest UFP emitter in the study: the LulzBot-ABS combination. We used a number balance equation based on our calibrated UFP measurements using the Condensation Particle Counter (CPC). Our assumptions serve to simplify the calculations while maximizing the likely impact of coagulation on estimates of the dynamic UFP emission rate in order to provide an upper bound of the likely impact of neglecting coagulation.

The rate of change of the particle number concentration due to just coagulation can be expressed as Equation S11 for particles with similar aerodynamic diameter:

$$\frac{dC_i(t)}{dt} = -K_{coag}C_i^2(t) \quad \text{(S11)}$$

Where
K_{coag} = corrected coagulation coefficient (cm^3/min)
C_i (t) = number of particles with aerodynamic diameter of i (#/cm^3)

As the CPC measures the number concentration of particles with diameters smaller than 1 μm, we assumed all particles inside the chamber have a similar coagulation coefficient of 6.9×10^{-8} cm^3/min, which is the highest coagulation coefficient for particles smaller than 1 μm.[3] For simplicity, we also assumed that particles collide with just one other particle in each collision and form new particles that are still smaller than 1 μm, which is reasonable given that the majority of particles emitted inside the chamber are smaller than 0.1 μm (demonstrated by early measurements with a combination of TSI Nanoscan SMPS Nanoparticle Sizer 3910 and TSI Optical Particle Sizer 3330, as shown in Figure S4).

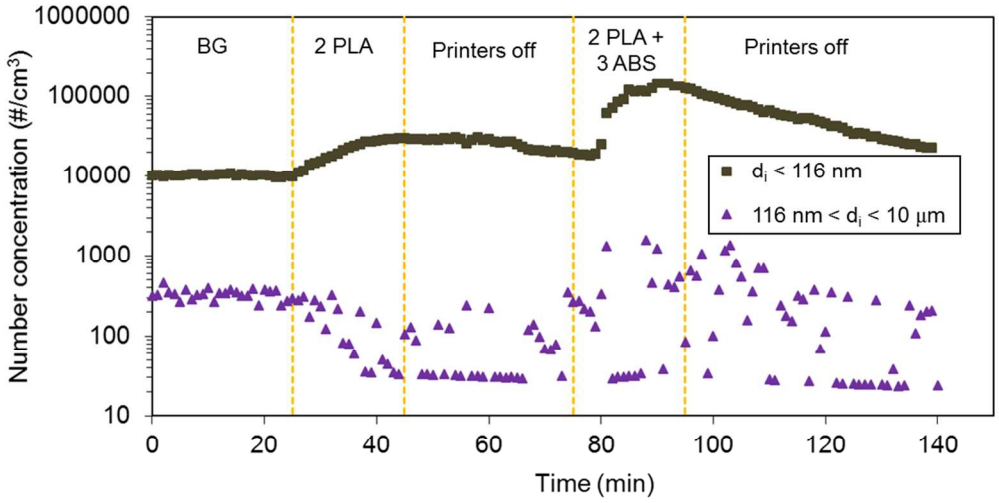

Figure S4: Comparison of total number concentration of particles smaller than 116 nm and between 116 nm and 10 μm in the Stephens et al. (2013) study

Figure S4 compares the total number concentration of particles smaller than 116 nm to those summed between 116 nm and 10 μm inside an office environment in downtown Chicago.[4] Five time periods are defined: (1) background measurements without printers operating for approximately 25 min; (2) two identical 3D printers using PLA filament operating for approximately 20 min; (3) a time period of approximately 30 minutes in which all printers were turned off; (4) the same two PLA-based printers operating simultaneously with three of the same make and model printers operating with ABS filament for approximately 20 min; and (5) a concentration decay period lasting approximately 40 min. The results demonstrate that the vast majority of particles emitted during printing are smaller than 116 nm (i.e., UFPs).

Therefore, the number balance equation for particles inside the chamber considering coagulation can be written as Equation S12.

$$\frac{dC_{UFP,in}(t)}{dt} = P_{UFP}\lambda C_{UFP,out} - L_{UFP}C_{UFP,in}(\mathrm{t}) + \frac{E_{UFP}(t)}{V} - \frac{1}{2}K_{coag}C_{UFP,in}^2(t) \quad \text{(S12)}$$

$C_{UFP,in}$= total concentration of UFPs inside the chamber (#/cm^3)
P_{UFP} = UFP penetration factor of chamber (-)
$C_{UFP,out}$= total concentration of UFPs outside the chamber (#/cm^3)
L_{UFP}= UFP loss rate inside the chamber due to AER and deposition (1/min)
$E_{UFP}(t)$ = emission rate of UFP from 3D printer (#/min)
V = chamber volume (cm^3)

We assumed that during the background period there was no UFP emission source inside the chamber and that UFP concentrations reached steady state conditions. Therefore, the number balance equation for background periods can be written as Equation S13.

$$\frac{P_{UFP}\lambda C_{UFP,out}}{L_{UFP}} = C_{UFP,bg} + \frac{K_{coag}}{2L_{UFP}}\, C_{UFP,bg}^2 \quad \text{(S13)}$$

In this equation $P_{UFP}\lambda C_{UFP,out}$ and L_{UFP} are unknown. We then used a dynamic number balance equation for the decay period, as shown in Equation S14, in which we assumed that the emission of particles from 3D printers stopped completely after the printing period.

$$\frac{dC_{UFP,in}(t)}{dt} = P_{UFP}\lambda C_{UFP,out} - L_{UFP}C_{UFP,in}(\mathrm{t}) - \frac{1}{2}K_{coag}C_{UFP,in}^2(t) \quad \text{(S14)}$$

Equation S14 can be solved by taking an integral as shown in Equation S15.

$$\int_{C_{UFP,in}(t=0)}^{C_{UFP,in}(t)} \frac{dC_{UFP,in}(t)}{\frac{K_{coag}}{2L_{UFP}}C_{UFP,in}^2(t) + C_{UFP,in}(\mathrm{t}) - \frac{P_{UFP}\lambda C_{UFP,out}}{L_{UFP}}} = \int_0^t -L_{UFP}dt \quad \text{(S15)}$$

Using a trial and error method, we estimated the UFP loss rate due to AER and deposition (L_{UFP}) combined, as follows:

- First, we chose a reasonable value for L_{UFP} without considering coagulation with the same method as described in Equations S4-S6 in Section 5.
- Second, we calculated $\frac{K_{coag}}{2L_{UFP}}$ and $\frac{P_{UFP}\lambda C_{UFP,out}}{L_{UFP}}$ values in Equation S15 by knowing the average UFP concentration during the background period.
- Third, we plotted the left hand side values of Equation S15 versus time for the first 60 minutes of the decay periods and considered the slope of linear regression line assigned to the data points as L_{UFP}. The left hand side values were calculated using MATLAB R2015a.
- Finally, we compared the calculated UFP loss rate and the value we chose at the first step. We ended the trial and error cycle once the two values were within 0.001 1/min of each other; otherwise, we used the new estimation of UFP loss rate due to AER and deposition in the first step and repeated the trial and error solution.

We estimated the time-varying UFP emission rate with and without considering coagulation using a discrete solution to the number balance in Equation S12, similar to the solution described in Equation S7. Figure S5 shows estimates of time resolved UFP emission rates from the LulzBot-ABS combination with and without considering coagulation in this manner.

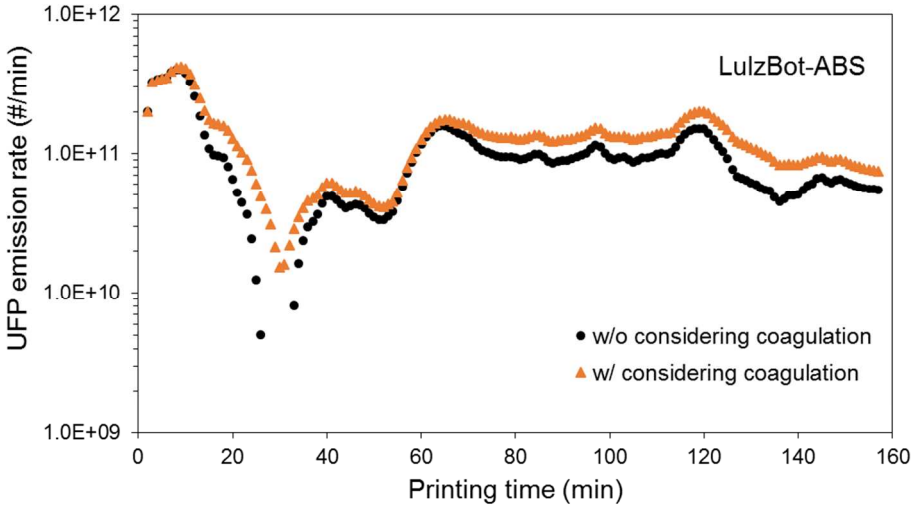

Figure S5: Comparison between UFP emission rate estimations with and without considering coagulation

In this analysis, although we assumed the highest coagulation coefficient for particles less than 1 μm, and considered the printer and filament combination with the highest average UFP concentration during printing period, the mean impact of coagulation was ~28% (changing from -1% to 90%). The average difference between estimated UFP emission values with and without considering coagulation was ~3×10^{10} #/min (ranges from -3×10^{9} to 7×10^{10} #/min) which is about an order of magnitude smaller than average estimated UFP emission, (~10^{11} #/min). The results demonstrate that although the coagulation might impact the UFP emission rate estimates, specifically for the highest concentrations of UFPs, the impact is likely smaller in most cases and generally within the uncertainty of our estimates. Thus we consider it reasonable to neglect coagulation impacts herein.

8. Uncertainty analysis

We estimated the uncertainty in our UFP and VOC emission rate estimates using a variety of approaches. First, we calculated the uncertainty in each smoothed concentration of UFP data, the average background concentration of UFPs, the chamber air exchange rate (AER), and the total UFP loss rate by adding standard errors of regression coefficients from related equations and the accuracy of each monitoring device in quadrature.

The uncertainty associated with the smoothed concentration of UFP is a function of the reported accuracy of the TSI CPC model 3007 (±20%) and the standard error due to both calibration (R^2_{calib} = 0.981) and smoothing (R^2_{smooth} > 0.9, varied depend on the experiment), which was calculated using Equation S16.

$$\Delta C_{UFP,smooth} = \sqrt{(AC_{CPC})^2 + \left(\frac{SE_{UFP,calib}}{\bar{C}_{UFP,calib}}\%\right)^2 + \left(\frac{SE_{UFP,smooth}}{\bar{C}_{UFP,smooth}}\%\right)^2} \quad \text{(S16)}$$

Where:

$\Delta C_{UFP,smooth}$ = uncertainty associated with smoothed UFP concentration inside the chamber for each combination of 3D printer, filament and printing object shape (%)

AC_{CPC} = average accuracy of TSI CPC model 3007 (±20%)

$SE_{UFP,calib}$ = standard error of the calibration (± 933 #/cm^3)

$\bar{C}_{UFP,calib}$ = average concentration of UFP inside the chamber during the calibration measured by SMPS (± 183444 #/cm^3)

$SE_{UFP,smooth}$ = standard error of the smoothing procedure for each studied combination (#/cm^3)

$\bar{C}_{UFP,smooth}$ = average smoothed concentration of UFP inside the chamber during the printing period for each studied combination (#/cm^3)

The uncertainty associated with the background concentration of UFPs is a function of the average accuracy of the CPC, the standard error of the mean, and the standard error due to calibration, which was calculated using Equation S17.

$$\Delta C_{UFP,bg} = \sqrt{(AC_{CPC})^2 + \left(\frac{SE_{UFP,calib}}{\bar{C}_{UFP,calib}}\%\right)^2 + \left(\frac{SE_{UFP,bg}}{\bar{C}_{UFP,bg}}\%\right)^2} \quad \text{(S17)}$$

Where

$\Delta C_{UFP,bg}$ = uncertainty associated with average background UFP concentration inside the chamber for each combination of 3D printer, filament and printing object shape (%)

$SE_{UFP,bg}$ = standard error of the mean background UFP concentration inside the chamber for each studied combination (#/cm^3)

$\bar{C}_{UFP,smooth}$ = average background concentration of UFP inside the chamber during the printing period for each studied combination (#/cm^3)

We estimated the air exchange rate of the chamber from Equations S1-S3 using a CO_2 inject-decay method. The uncertainty associated with the AER of chamber is a function of the average accuracy of SBA-5 CO_2 anazlyer, the standard error of the mean CO_2 background, and the standard error due to fitting a linear regression line to the left hand side (LHS) of Equation S3, which was calculated using Equation S18.

$$\Delta AER = \sqrt{\left(\frac{AC_{SBA5}}{\bar{C}_{CO2,decay}}\%\right)^2 + \left(\frac{AC_{SBA5}}{\bar{C}_{CO2,bg}}\%\right)^2 + \left(\frac{SE_{CO2,bg}}{\bar{C}_{CO2,bg}}\%\right)^2 + \left(\frac{SE_{CO2,LHS}}{\overline{LHS}_{CO2}}\%\right)^2} \quad \text{(S18)}$$

Where
ΔAER = uncertainty associated with AER of the chamber for various experiments (%)
AC_{SBA5} = average accuracy of SBA5 CO_2 monitor (± 20 ppm)
$\bar{C}_{CO2,decay}$ = average concentration of CO_2 during the decay period for each experiment (ppm)
$\bar{C}_{CO2,bg}$ = average concentration of background CO_2 for each experiment (ppm)
$SE_{CO2,bg}$= standard error of the mean CO_2 background concentration for each experiment (ppm)
$SE_{CO2,LHS}$= standard error of linear regression line fitted to left hand side values of Equation S3 to estimate AER for each experiment (-)
$\overline{LHS}_{CO2}$ = left hand side values average in Equation S3 to estimate AER for each experiment (-)

We also estimated the uncertainty associated with the total loss rate for each combination of printer, filament, and printing object shape based on the regression coefficients from Equation S6 in Section 5. The total loss rate uncertainty is a function of the background and smoothed UFP concentrations and the standard error of the linear regression between to the left hand side (LHS) of Equation S6 versus time, which was calculated using Equation S19.

$$\Delta L_{UFP} = \sqrt{\left(\Delta C_{UFP,smooth}\right)^2 + \left(\Delta C_{UFP,bg}\right)^2 + \left(\frac{SE_{UFP,LHS}}{\overline{LHS}_{UFP}}\%\right)^2} \quad \text{(S19)}$$

ΔL_{UFP} = uncertainty associated with the UFP loss rate for various experiments (%)
$SE_{UFP,LHS}$= standard error of linear regression line fitted to left hand side values of Equation S6 to estimate UFP total loss rate for various experiments (-)
$\overline{LHS}_{UFP}$ = average of left hand side values in Equation S6 to estimate UFP total loss rate for various experiments (-)

Finally, we estimated the uncertainty associated with the air flow rate of the VOC sampling pumps. For each VOC sampling tube and pump combination, we measured the air flow rate through the tube five times, and calculated the uncertainty in this airflow rate as a function of the average accuracy of the air flow meter and the standard error of the mean measured air flow rate, as shown in Equation S20.

$$\Delta Q_{pump} = \sqrt{\left(\frac{AC_{flowmeter}}{\bar{Q}_{pump}}\%\right)^2 + \left(\frac{SE_Q}{\bar{Q}_{pump}}\%\right)^2} \quad \text{(S20)}$$

Where

ΔQ_{pump} = uncertainty associated with air flow passing through VOC sampling tubes (%)

$AC_{flowmeter}$= average accuracy of air flow meter (± 1 cm^3/min)

$\bar{Q}_{pump}$ = average air flow passing through VOC sampling tubes (cm^3/min)

SE_Q = Standard error of mean measured air flow passing through VOC sampling tubes (cm^3/min)

Next, we used the previous uncertainty estimations to calculate uncertainty associated with time varying UFP emission rate, VOC concentration in background and printing periods, and VOC emission rate from each printer. We calculated the uncertainty of time-varying UFP emission rates based on Equation S7, as shown in Equation S21.

$$\Delta E_{UFP}(t_{n+1}) = \sqrt{\left(\Delta C_{UFP,in}(t_{n+1})\right)^2 + \left(\Delta C_{UFP,in}(t_n)\right)^2 + (\Delta L_{UFP})^2 + \left(\Delta \bar{C}_{UFP,bg}\right)^2} \quad \text{(S21)}$$

Where

$\Delta E_{UFP}(t_{n+1})$ = uncertainty associated with UFP emission rate (%)

We calculated the uncertainty of VOC concentration in background and printing periods based on the Equation S8 in Section 6, as shown in Equation S22.

$$\Delta C_{VOC} = \sqrt{\left(AC_{M,VOC}\right)^2 + \left(\Delta Q_{pump}\right)^2} \quad \text{(S22)}$$

Where

ΔC_{VOC} = uncertainty associated with VOC concentration in background and printing periods (%)

$AC_{M,VOC}$ = Accuracy of GC-MS technique to quantify collected mass of VOC in the sampling tubes (assumed to be ± 25% for a typical relative response factor between 0.75 and 1.25)

Finally, we calculated the uncertainty in the VOC emission rate estimate based on the Equation S10 in Section 6, as shown in Equation S23.

$$\Delta E_{VOC,i} = \sqrt{\left(\Delta C_{VOC,i,print}\right)^2 + \left(\Delta C_{VOC,i,bg}\right)^2 + (\Delta \mathrm{AER})^2} \quad \text{(S23)}$$

Where

$\Delta E_{VOC,i}$ = uncertainty associated with estimated VOC emission for each component (%)

9. Time varying UFP concentration data and estimated emission rates

As described briefly in the main text, we applied a number of smoothing function options (e.g., loess, lowess, and others) to each highly varying data set and selected smoothed data from the method that yielded a combination of the fewest negative emission rate estimates (fewer than 5%) and the highest correlation between actual and smoothed UFP concentrations (R^2 was mostly above 0.90). However, in four case studies (i.e. LulzBot-HIPS, LulzBot-Nylon, LulzBot-TGlase, and FlashForge-ABS) the number of negative estimated emissions were higher than 5%, as shown in the following figures. The negative emission estimations may be due to a combination of coagulation impacts and UFP loss rate underestimation. In most of the cases, the negative emission estimations were happened during high concentrations of UFP (~10^5 #/cm^3 and higher), where the coagulation impacts are considerable. In Section 7 we demonstrated that without considering coagulation we might underestimate the emission estimations up to 90% at UFP pick concentrations in extreme case scenarios, although in average, the impacts would be lower than 28%, specifically for low UFP emitter combinations of printer and filament. Moreover, in the all four cases the loss rates were estimated when the UFP concentrations in decay period were about three orders of magnitude lower than the corresponding UFP pick concentrations. This might cause an underestimation in particle loss rates due to changes in particles' size distribution and deposition rate.

We used the *'smooth'* function in MATLAB-R2015a with various smoothing methods (SM), as shown in Table 1.

Table S1: Description of various smoothing methods used herein

method	Description
'moving'	Moving average (default). A lowpass filter with filter coefficients equal to the reciprocal of the span.
'lowess'	Local regression using weighted linear least squares and a 1st degree polynomial model
'loess'	Local regression using weighted linear least squares and a 2nd degree polynomial model
'sgolay'	Savitzky-Golay filter. A generalized moving average with filter coefficients determined by an unweighted linear least-squares regression and a polynomial model of specified degree (default is 2). The method can accept nonuniform predictor data.
'rlowess'	A robust version of 'lowess' that assigns lower weight to outliers in the regression. The method assigns zero weight to data outside six mean absolute deviations.
'rloess'	A robust version of 'loess' that assigns lower weight to outliers in the regression. The method assigns zero weight to data outside six mean absolute deviations.

Figures S6(a) - S23(a) show calibrated and smoothed UFP concentrations inside the chamber, nozzle and bed temperatures during printing, smoothing method (SM), coefficient of determination between smoothed and calibrated data (SM-R^2), and our estimate of the total UFP loss rate. Figures S6(b) - S23(b) show the estimates of time-varying UFP emission rates during each printing period as well as the number of negative estimated emissions (NNEE) for all tested combinations.

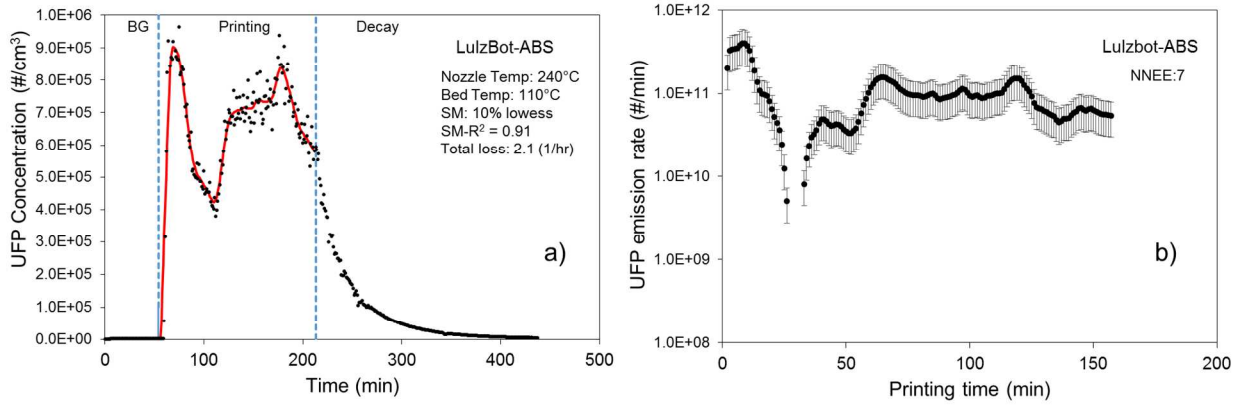

Figure S6: (a) Calibrated and smoothed UFP concentration inside the chamber and (b) Time varied UFP emission rate for LulzBot-ABS

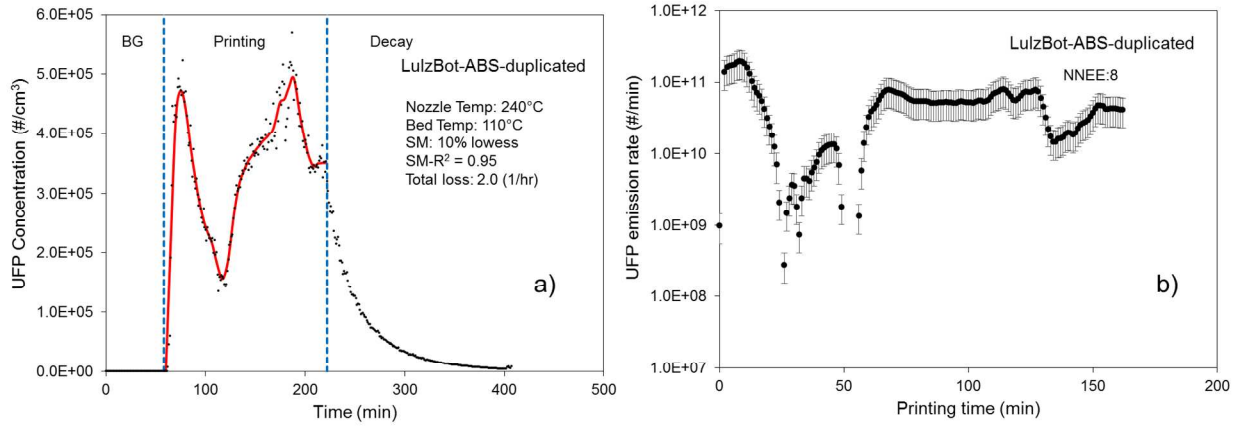

Figure S7: (a) Calibrated and smoothed UFP concentration inside the chamber and (b) Time varied UFP emission rate for LulzBot-ABS (Duplicated)

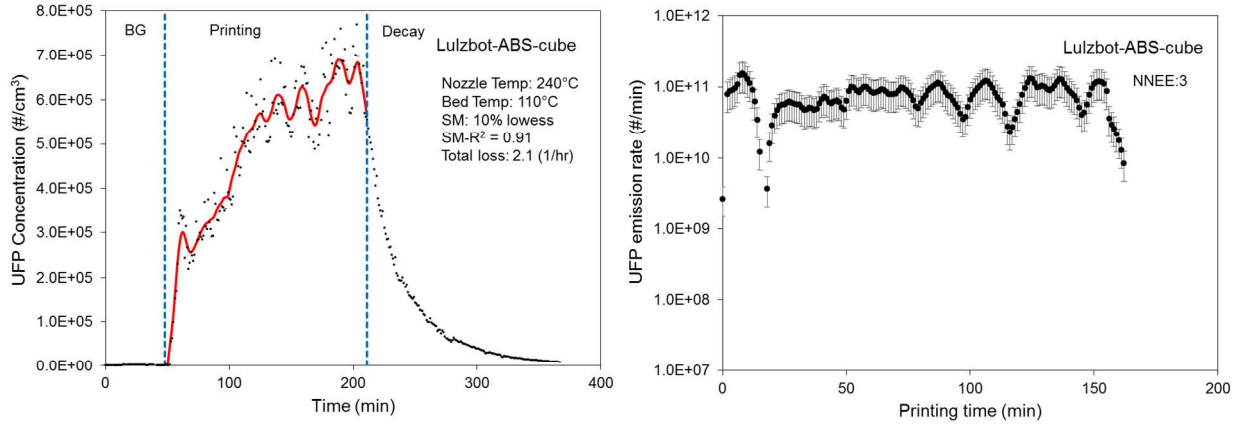

Figure S8: (a) Calibrated and smoothed UFP concentration inside the chamber and (b) Time varied UFP emission rate for LulzBot-ABS (Cube)

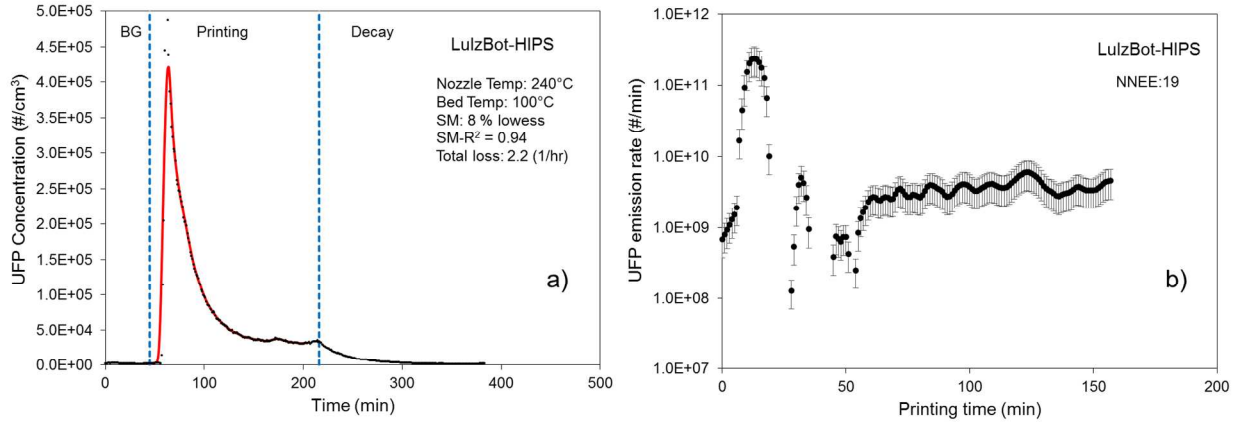

Figure S9: (a) Calibrated and smoothed UFP concentration inside the chamber and (b) Time varied UFP emission rate for LulzBot-HIPS

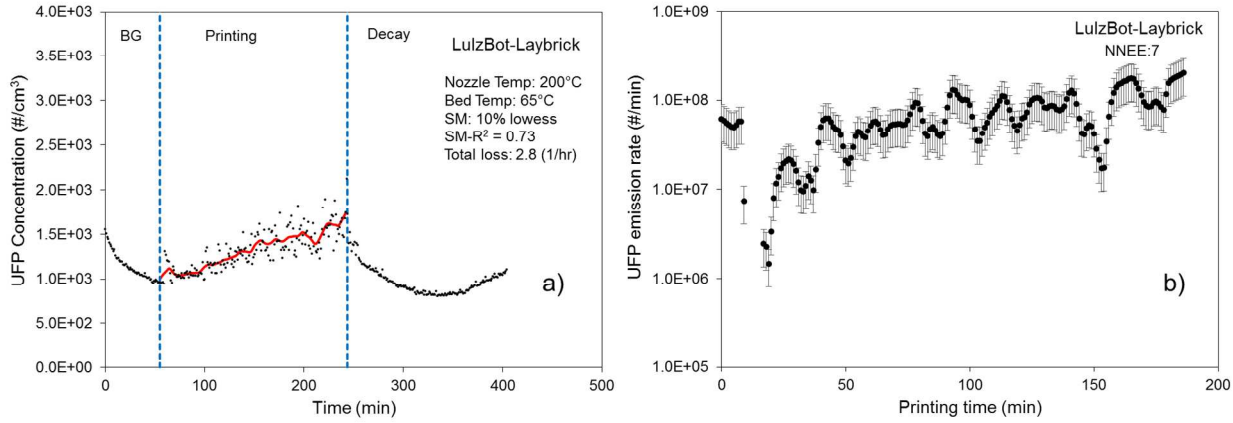

Figure S10: (a) Calibrated and smoothed UFP concentration inside the chamber and (b) Time varied UFP emission rate for LulzBot-Laybrick

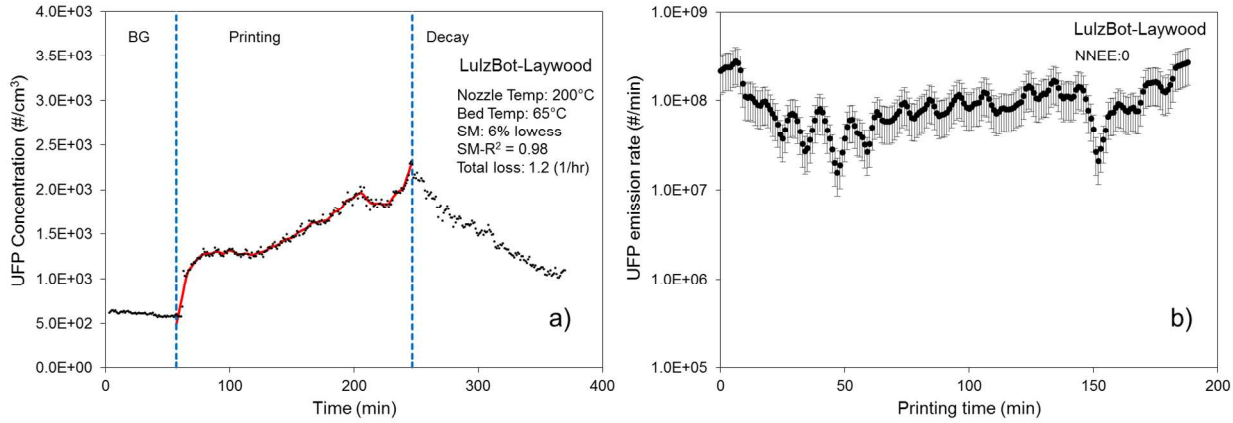

Figure S11: (a) Calibrated and smoothed UFP concentration inside the chamber and (b) Time varied UFP emission rate for LulzBot-Laywood

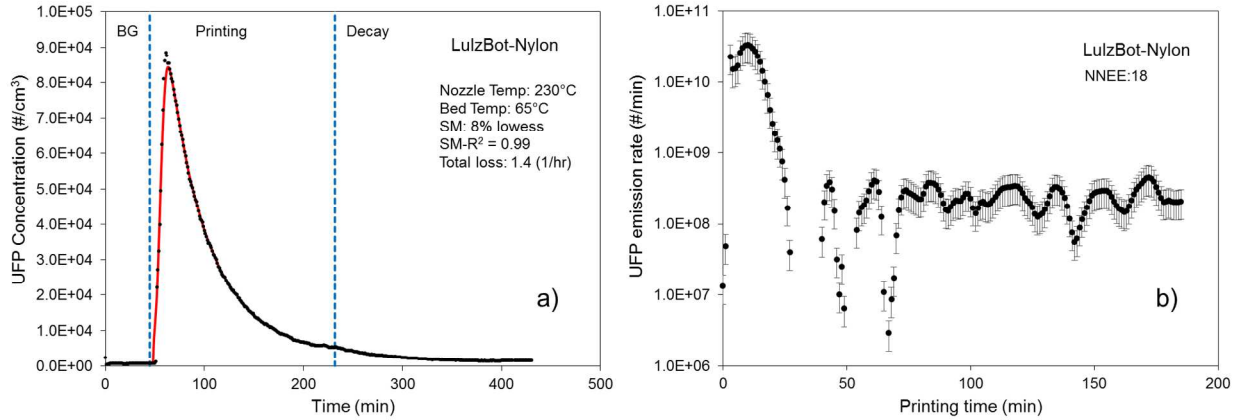

Figure S12: (a) Calibrated and smoothed UFP concentration inside the chamber and (b) Time varied UFP emission rate for LulzBot-Nylon

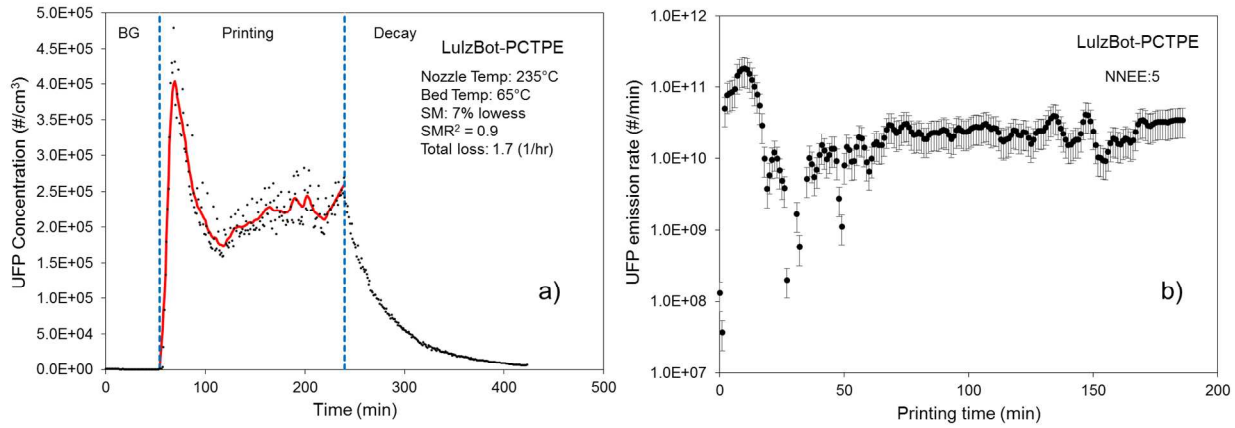

Figure S13: (a) Calibrated and smoothed UFP concentration inside the chamber and (b) Time varied UFP emission rate for LulzBot-PCTPE

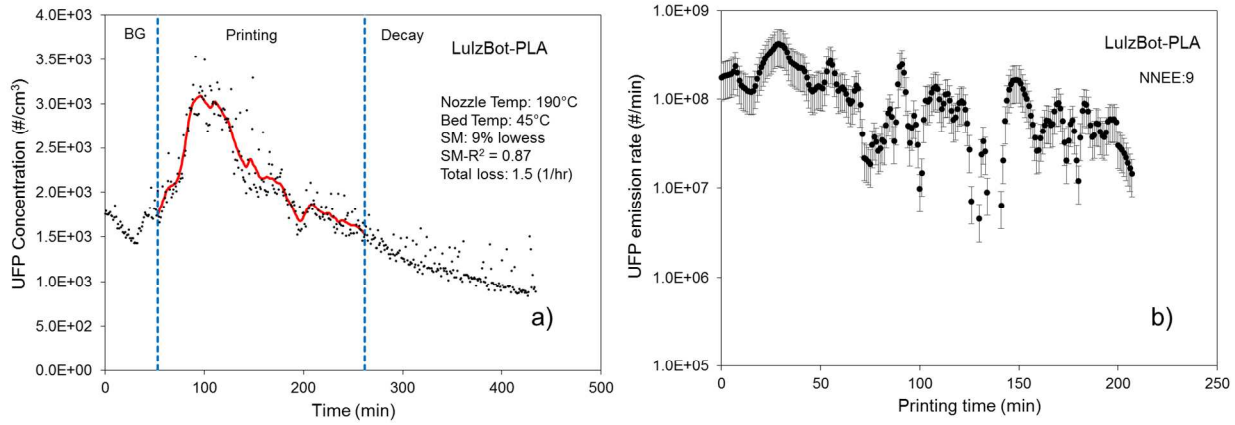

Figure S14: (a) Calibrated and smoothed UFP concentration inside the chamber and (b) Time varied UFP emission rate for LulzBot-PLA

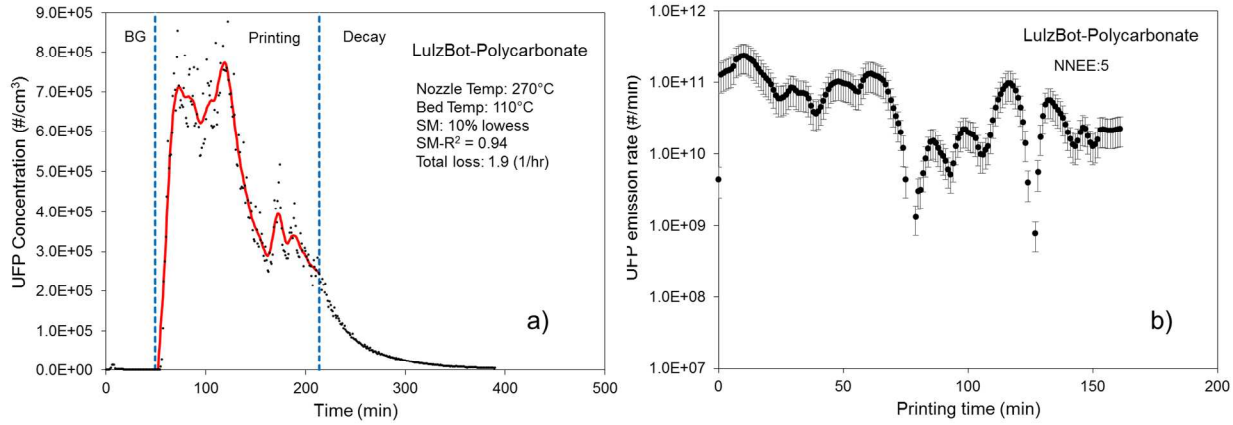

Figure S15: (a) Calibrated and smoothed UFP concentration inside the chamber and (b) Time varied UFP emission rate for LulzBot-Polycarbonate

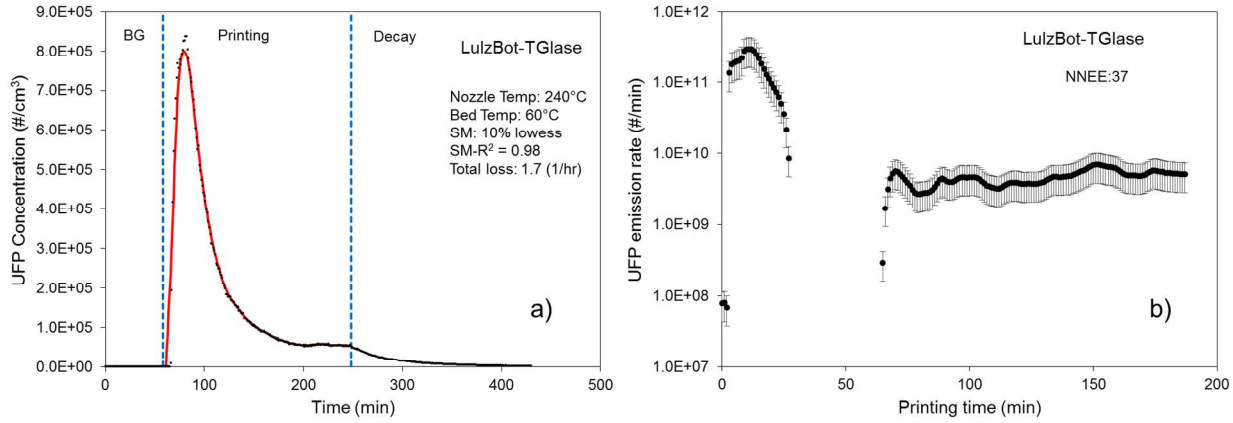

Figure S16: (a) Calibrated and smoothed UFP concentration inside the chamber and (b) Time varied UFP emission rate for LulzBot-TGlase

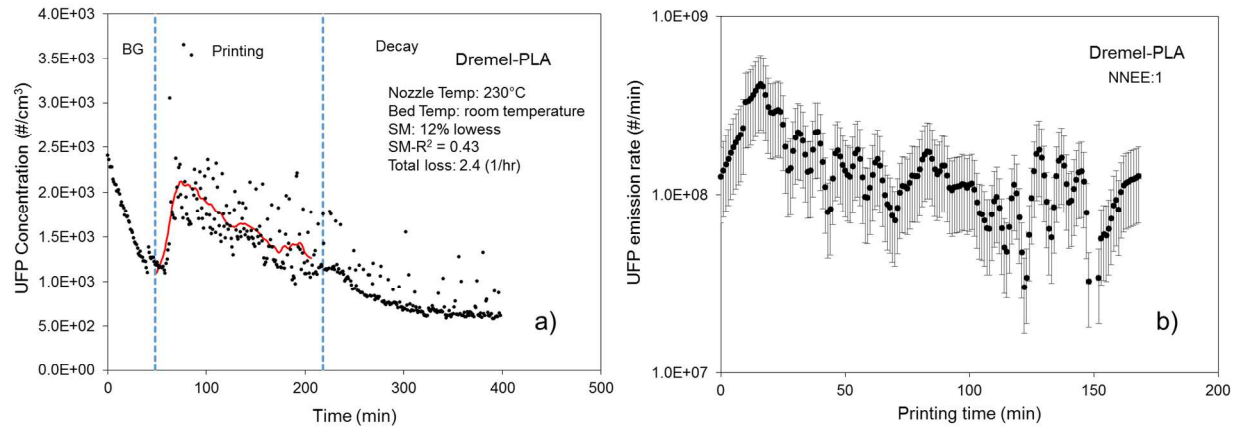

Figure S17: (a) Calibrated and smoothed UFP concentration inside the chamber and (b) Time varied UFP emission rate for Dremel-PLA

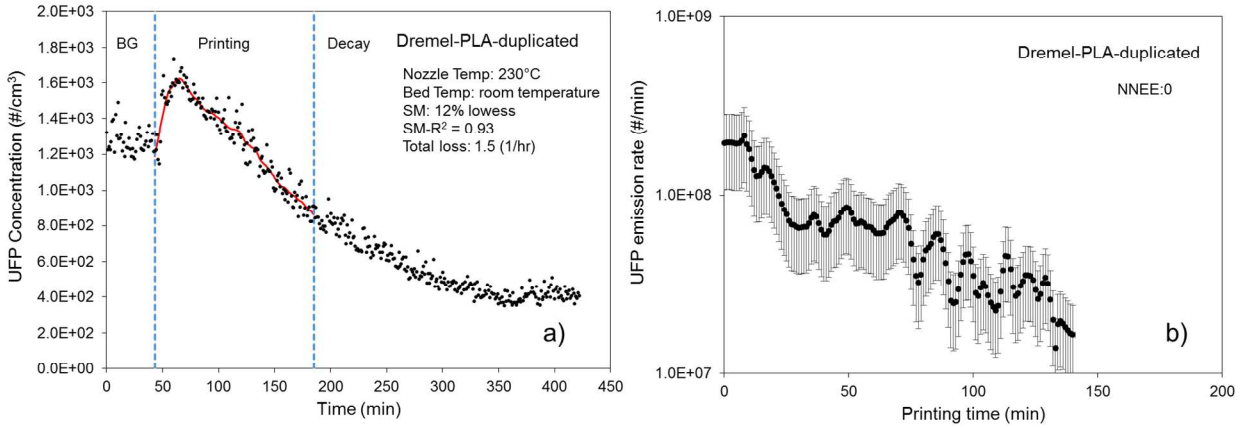

Figure S18: (a) Calibrated and smoothed UFP concentration inside the chamber and (b) Time varied UFP emission rate for Dremel-PLA (Duplicated)

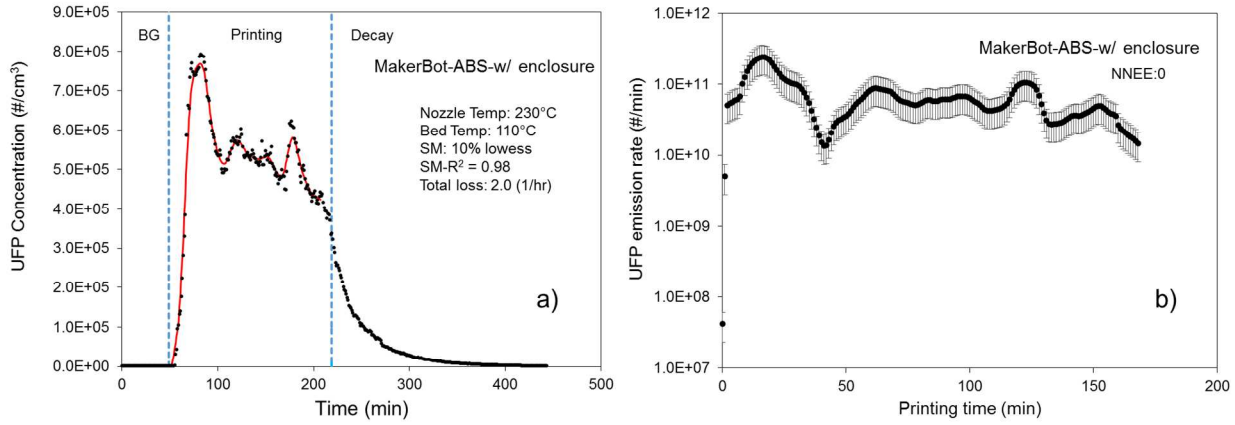

Figure S19: (a) Calibrated and smoothed UFP concentration inside the chamber and (b) Time varied UFP emission rate for Makerbot-ABS (w/ enclosure)

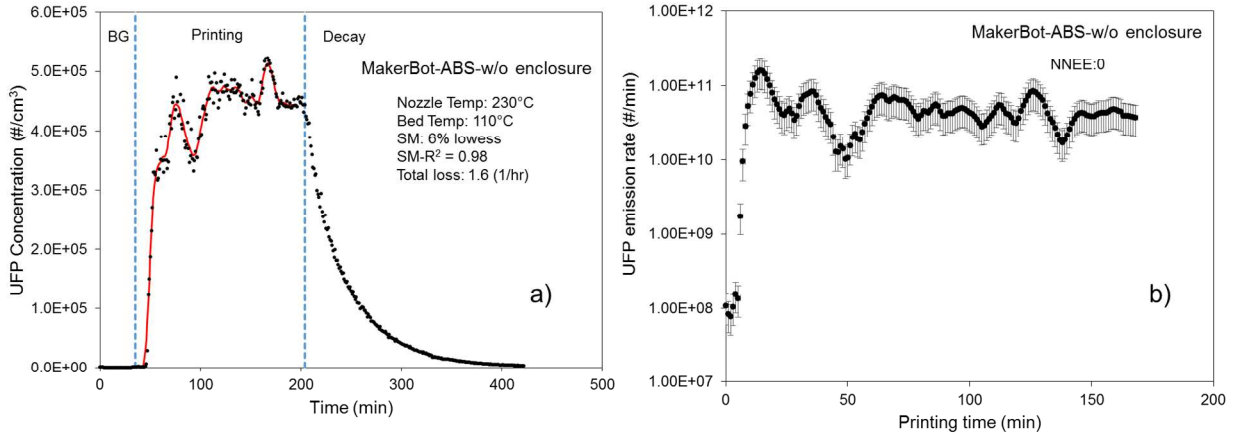

Figure S20: (a) Calibrated and smoothed UFP concentration inside the chamber and (b) Time varied UFP emission rate for Makerbot-ABS (w/o enclosure)

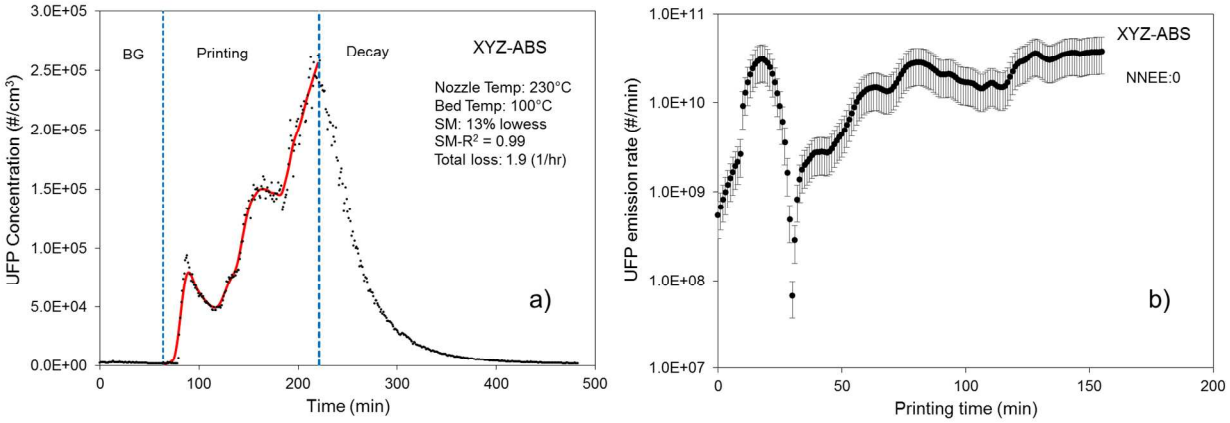

Figure S21: (a) Calibrated and smoothed UFP concentration inside the chamber and (b) Time varied UFP emission rate for XYZ-ABS

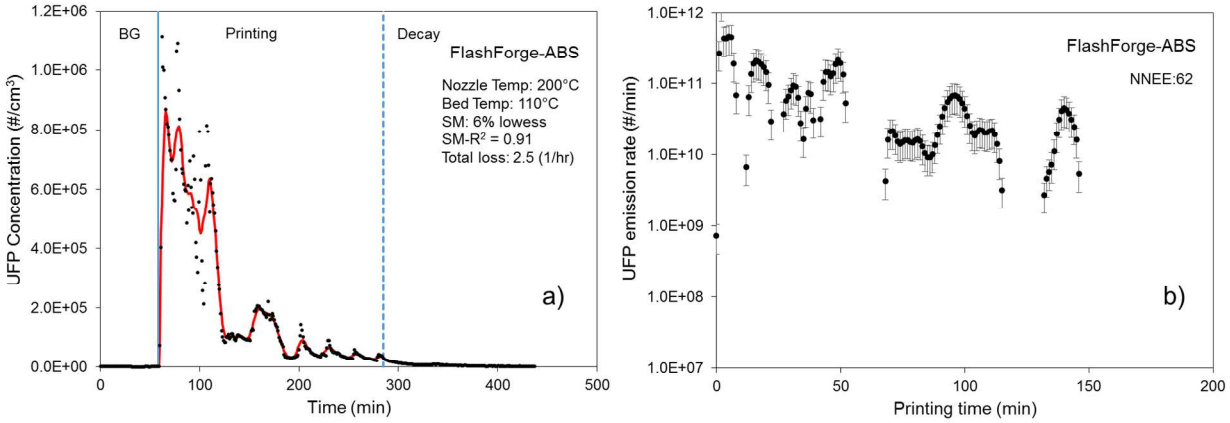

Figure S22: (a) Calibrated and smoothed UFP concentration inside the chamber and (b) Time varied UFP emission rate for FlashForge-ABS

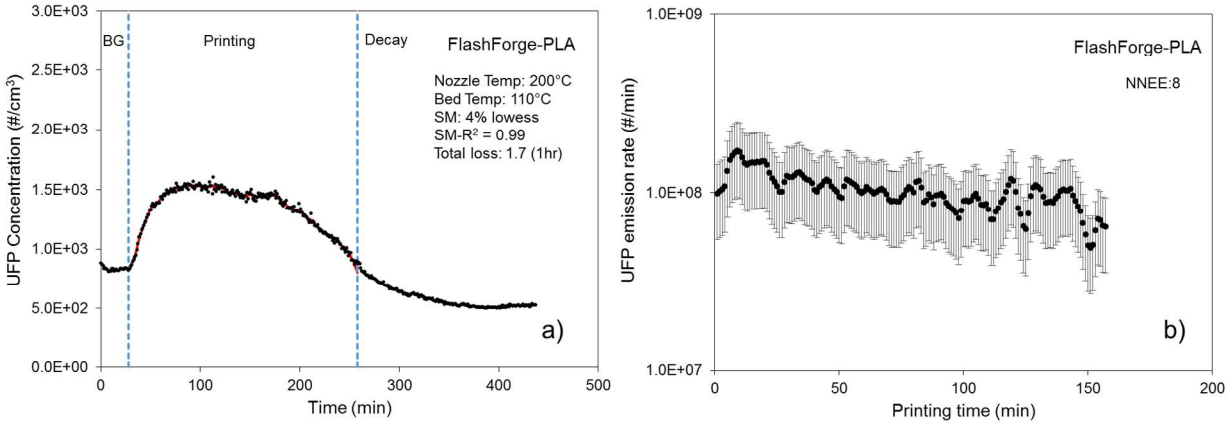

Figure S23: (a) Calibrated and smoothed UFP concentration inside the chamber and (b) Time varied UFP emission rate for FlashForge-PLA

10. VOC sampling summary

Table S2: The top 10 individual VOCs with the highest measured concentrations during printing and estimated steady-state emission rates.

	Rank	Compound name	Printing Conc. (µg/m^3)	Qual. (%)	BG Conc. (µg/m^3)	Emission rate (µg/min)
FlashForge-ABS	1	Styrene	461.0	97	0.0	33.5
	2	Propylene Glycol	158.5	64	201.5	-3.1
	3	Hexanal	135.4	90	109.2	1.9
	4	Octanal	61.1	86	55.1	0.4
	5	Nonanal	46.4	83	31.0	1.1
	6	1-Pentanol	44.1	72	48.0	-0.3
	7	Bicyclo[3.1.1]hept-2-ene, 2,6,6-tri	40.5	91	37.7	0.2
	8	Acetic acid	38.5	90	43.2	-0.3
	9	Toluene	37.8	93	89.4	-3.7
	10	Ethylbenzene	35.1	81	6.0	2.1
FlashForge-PLA	1	1,4-Dioxane-2,5-dione, 3,6-dimethyl	89.0	90	0.0	5.0
	2	Isopropyl Palmitate	79.6	93	95.6	-0.9
	3	Hexanal	39.7	90	50.4	-0.6
	4	12-Crown-4	35.1	38	0.0	2.0
	5	Nonanal	31.6	83	52.2	-1.1
	6	Octanal	30.0	86	36.8	-0.4
	7	Tetrachloroethylene	27.5	99	56.3	-1.6
	8	Benzene, 1,3-dimethyl-	24.4	95	32.5	-0.4
	9	1R-.alpha.-Pinene	21.3	95	26.8	-0.3
	10	Propylene Glycol	18.7	80	35.3	-0.9
XYZ-ABS	1	Styrene	243.2	97	0.0	11.5
	2	(S)-(+)-1,2-Propanediol (Propylene Glycol)	186.2	64	32.4	7.3
	3	Hexanal	72.9	90	55.2	0.8
	4	Glycerin	37.7	83	0.0	1.8
	5	Octanal	34.2	93	26.9	0.3
	6	1-Pentanol	31.5	72	0.0	1.5
	7	1R-.alpha.-Pinene	26.6	93	12.9	0.6
	8	Acetophenone	23.1	97	0.0	1.1
	9	Nonanal	22.3	72	22.1	0.0
	10	Decane	18.0	90	15.0	0.1
Dremel-PLA	1	Hexanal	67.4	72	88.2	-1.4
	2	1,4-Dioxane-2,5-dione, 3,6-dimethyl	53.8	90	0.0	3.7
	3	Toluene	52.9	97	87.6	-2.4
	4	Chloromethyl methyl sulfide	36.2	33	0.0	2.5
	5	Octanal	33.2	87	37.0	-0.3
	6	1-Propanol, 2-ethoxy-	29.9	42	0.0	2.1
	7	Nonanal	27.8	93	0.0	1.9
	8	2-Heptanone, 3-methyl-	26.3	9	37.0	-0.7
	9	1R-.alpha.-Pinene	25.3	96	28.7	-0.2
	10	Ethanol, 2-(2-butoxyethoxy)-	23.3	90	0.0	1.6

Table S2 continued. The top 10 individual VOCs with the highest measured concentrations during printing and estimated steady-state emission rates.

	Rank	Compound name	Printing Conc. (µg/m^3)	Qual. (%)	BG Conc. (µg/m^3)	Emission rate (µg/min)
Dremel-PLA (dupl.)	1	Hexanal	112.2	52	51.9	3.8
	2	1,4-Dioxane-2,5-dione, 3,6-dimethyl	65.6	90	21.3	2.8
	3	12-Crown-4	62.3	38	0.0	3.9
	4	Acetic acid	54.2	90	11.4	2.7
	5	Octanal	42.1	83	31.5	0.7
	6	Toluene	42.0	94	30.8	0.7
	7	Ethanol, 2-(2-butoxyethoxy)-	33.9	90	3.6	1.9
	8	1R-.alpha.-Pinene	30.9	95	32.5	-0.1
	9	Chloromethyl methyl sulfide	30.1	33	21.3	0.6
	10	Nonanal	29.4	83	23.9	0.3
LulzBot-HIPS	1	Styrene	242.3	97	13.6	19.6
	2	2-Butanone	134.8	50	131.8	0.3
	3	Toluene	109.6	94	149.9	-3.5
	4	Ethylbenzene	62.5	94	5.1	4.9
	5	Hexanal	57.7	90	35.8	1.9
	6	Octanal	43.4	91	27.1	1.4
	7	Decane	38.0	76	21.5	1.4
	8	Trimethylphosphine	36.5	33	19.5	1.5
	9	p-Xylene	30.6	95	16.0	1.2
	10	Bicyclo[3.1.1]hept-2-ene	30.1	90	23.0	0.6
LulzBot-HIPS (dupl.)	1	Styrene	212.6	97	9.6	20.7
	2	2-Butanone	81.6	50	96.6	-1.5
	3	Hexanal	55.4	90	42.8	1.3
	4	Toluene	54.5	97	65.5	-1.1
	5	Ethylbenzene	53.8	94	4.5	5.0
	6	Decane	44.7	87	31.6	1.3
	7	Acetic acid	42.9	90	13.4	3.0
	8	Octanal	39.1	91	26.6	1.3
	9	Bicyclo[3.1.1]hept-2-ene, 2,6,6-tri	30.6	91	20.8	1.0
	10	Nonanal	28.6	64	19.2	1.0
LulzBot-PLA	1	Hexanal	89.8	90	81.7	0.4
	2	1,4-Dioxane-2,5-dione, 3,6-dimethyl	79.4	90	0.0	4.4
	3	Toluene	46.9	94	46.0	0.0
	4	Octanal	45.0	94	49.5	-0.2
	5	Ethanol, 2-(2-butoxyethoxy)-	41.0	90	0.0	2.3
	6	Nonanal	38.1	86	38.2	0.0
	7	Styrene	35.4	97	12.3	1.3
	8	2-Butanone	32.4	43	64.8	-1.8
	9	Isopropyl Palmitate	30.8	96	28.0	0.2
	10	1R-.alpha.-Pinene	29.2	96	37.3	-0.4

Table S2 continued. The top 10 individual VOCs with the highest measured concentrations during printing and estimated steady-state emission rates.

	Rank	Compound name	Printing Conc. (µg/m^3)	Qual. (%)	BG Conc. (µg/m^3)	Emission rate (µg/min)
LulzBot-ABS	1	Styrene	912.8	97	8.7	54.2
	2	Hexanal	70.5	91	72.0	-0.1
	3	Acetophenone	61.5	97	0.0	3.7
	4	Ethylbenzene	59.9	87	3.4	3.4
	5	Benzenemethanol, .alpha.,.alpha.-di	44.8	72	0.0	2.7
	6	.alpha.-Pinene	42.2	64	24.0	1.1
	7	Octanal	41.4	95	39.8	0.1
	8	Toluene	40.4	94	26.4	0.8
	9	Nonanal	39.7	86	37.3	0.1
	10	1-Butanol	39.5	90	0.0	2.4
LulzBot-ABS (dupl.)	1	Styrene	919.3	97	7.4	42.7
	2	Caprolactam	272.4	94	144.9	6.0
	3	Acetophenone	70.2	97	2.8	3.2
	4	Isopropyl Palmitate	64.1	97	52.4	0.5
	5	Ethylbenzene	61.7	94	3.0	2.7
	6	Hexanal	52.5	90	67.3	-0.7
	7	Nonanal	52.1	72	33.7	0.9
	8	Octanal	46.2	90	37.1	0.4
	9	Benzenemethanol, .alpha.,.alpha.-di	44.5	80	0.0	2.1
	10	Bicyclo[3.1.1]hept-2-ene, 2,6,6-tri	44.5	89	29.6	0.7
LulzBot-ABS (cube)	1	Styrene	857.7	97	0.0	38.1
	2	Acetophenone	60.5	95	0.0	2.7
	3	Decane	58.7	94	0.0	2.6
	4	Ethylbenzene	57.3	94	24.4	1.5
	5	Isopropyl Palmitate	50.0	93	64.0	-0.6
	6	Hexanal	46.7	91	39.5	0.3
	7	Benzenemethanol, .alpha.,.alpha.-di	41.3	72	0.0	1.8
	8	Octanal	39.0	80	29.0	0.4
	9	Caprolactam	33.1	94	13.5	0.9
	10	Toluene	31.5	94	25.2	0.3
LulzBot-Nylon	1	Caprolactam	3078.3	95	35.1	182.6
	2	Hexanal	131.5	90	84.0	2.9
	3	Acetic acid	109.8	90	6.9	6.2
	4	Isopropyl Palmitate	51.1	93	21.7	1.8
	5	Octanal	50.4	83	52.4	-0.1
	6	Nonanal	50.4	83	38.3	0.7
	7	Pentanal	32.5	91	6.1	1.6
	8	1-Pentanol	32.2	59	0.0	1.9
	9	Benzyl Alcohol	30.5	93	25.8	0.3
	10	Propylene Glycol	29.2	72	29.2	0.0

Table S2 continued. The top 10 individual VOCs with the highest measured concentrations during printing and estimated steady-state emission rates.

	Rank	Compound name	Printing Conc. (µg/m^3)	Qual. (%)	BG Conc. (µg/m^3)	Emission rate (µg/min)
LulzBot-Laybrick	1	Caprolactam	1321.7	95	13.5	69.1
	2	Hexanal	110.2	91	103.1	0.4
	3	Acetic acid	61.4	90	16.8	2.4
	4	Octanal	60.0	80	52.4	0.4
	5	2-Hexenal, 2-ethyl-	58.6	93	0.0	3.1
	6	Isopropyl Palmitate	54.8	59	65.5	-0.6
	7	Nonanal	50.8	72	48.3	0.1
	8	1-Pentanol	47.1	64	39.6	0.4
	9	1R-.alpha.-Pinene	44.0	96	41.8	0.1
	10	Styrene	39.3	96	7.4	1.7
LulzBot-Laywood	1	Caprolactam	1128.6	95	33.0	45.4
	2	2-Hexenal, 2-ethyl-	96.9	86	0.0	4.0
	3	Hexanal	94.9	90	94.7	0.0
	4	Octanal	53.4	95	54.1	0.0
	5	Nonanal	46.8	64	60.9	-0.6
	6	Acetic acid	46.5	90	10.6	1.5
	7	1-Pentanol	35.5	78	36.6	0.0
	8	Isopropyl Palmitate	32.2	52	43.5	-0.5
	9	1R-.alpha.-Pinene	31.7	96	36.2	-0.2
	10	1,3,5,7-Cyclooctatetraene	31.2	97	10.1	0.9
LulzBot-TGlase	1	Caprolactam	72.8	95	30.0	1.5
	2	Hexanal	59.2	90	59.1	0.0
	3	Toluene	36.2	94	29.5	0.2
	4	Octanal	36.2	91	43.0	-0.2
	5	Nonanal	30.9	59	41.3	-0.4
	6	1R-.alpha.-Pinene	25.1	96	34.1	-0.3
	7	1-Pentanol	24.2	78	32.3	-0.3
	8	Styrene	22.1	97	9.7	0.4
	9	R-(-)-1,2-propanediol (Propylene Glycol)	22.0	80	5.4	0.6
	10	Isopropyl Palmitate	21.0	97	19.8	0.0
LulzBot-Polycarbonate	1	Propylene Glycol	141.6	64	257.5	-3.7
	2	Caprolactam	82.9	95	37.3	1.5
	3	Toluene	78.6	94	89.6	-0.3
	4	Hexanal	68.4	90	69.9	0.0
	5	Isopropyl Palmitate	58.6	93	63.1	-0.1
	6	Octanal	53.3	96	60.0	-0.2
	7	1R-.alpha.-Pinene	47.4	95	55.4	-0.3
	8	1-Pentanol	43.7	64	45.4	-0.1
	9	Styrene	42.6	97	21.1	0.7
	10	Nonanal	42.5	83	54.0	-0.4

Table S2 continued. The top 10 individual VOCs with the highest measured concentrations during printing and estimated steady-state emission rates.

	Rank	Compound name	Printing Conc. (µg/m^3)	Qual. (%)	BG Conc. (µg/m^3)	Emission rate (µg/min)
LulzBot-Polycarbonate (dupl.)	1	Isopropyl Palmitate	77.1	93	138.9	-3.0
	2	Decanal	64.6	87	0.0	3.2
	3	Hexanal	51.0	90	21.6	1.4
	4	Nonanal	49.1	83	29.4	1.0
	5	Octanal	49.0	83	22.2	1.3
	6	Tetrachloroethylene	47.5	99	113.9	-3.3
	7	Phenol	40.1	96	0.0	2.0
	8	Caprolactam	34.5	93	5.5	1.4
	9	1-Pentanol	31.1	43	0.0	1.5
	10	1R-.alpha.-Pinene	30.3	96	15.4	0.7
LulzBot-PCTPE	1	Caprolactam	4940.0	95	30.1	167.9
	2	Isopropyl Palmitate	72.2	58	41.0	1.1
	3	Hydrazinecarbothioamide	38.2	9	7.9	1.0
	4	Nonanal	37.5	83	19.8	0.6
	5	Styrene	23.2	97	5.7	0.6
	6	Silane, trimethyl(1-methylethoxy)-	20.6	59	0.0	0.7
	7	2-Hexene, 3,5,5-trimethyl-	20.5	43	3.8	0.6
	8	Octanal	18.0	91	10.0	0.3
	9	Hexanal	16.7	86	10.6	0.2
	10	1R-.alpha.-Pinene	15.4	96	11.9	0.1
MakerBot-w/-enclosure	1	Styrene	2478.7	97	0.0	113.0
	2	Acetophenone	164.4	95	0.0	7.5
	3	Isopropyl Palmitate	139.6	93	0.0	6.4
	4	Tetrachloroethylene	130.1	99	8.5	5.5
	5	Decane	127.8	94	0.0	5.8
	6	dl-2-Phenyl-1,2-propanediol	120.6	64	0.0	5.5
	7	Ethylbenzene	119.3	94	0.0	5.4
	8	Cyclotrisiloxane, hexamethyl-	117.0	83	0.0	5.3
	9	Benzeneethanamine, N-[(pentafl	89.0	32	0.0	4.1
	10	1-Butanol	87.7	78	0.0	4.0
MakerBot-w/o-enclosure	1	Styrene	1632.7	97	10.8	96.3
	2	Isopropyl Palmitate	207.3	96	48.4	9.4
	3	Nonane, 2,2,4,4,6,8,8-heptamet	122.8	83	0.0	7.3
	4	Acetophenone	118.3	95	3.9	6.8
	5	Chloromethyl methyl sulfide	89.5	33	0.0	5.3
	6	Benzenemethanol, .alpha.,.alph	81.3	64	0.0	4.8
	7	Nonanal	80.7	72	62.1	1.1
	8	Ethylbenzene	78.4	94	7.6	4.2
	9	Cyclotrisiloxane, hexamethyl-	75.8	87	13.0	3.7
	10	Benzeneethanamine, N-[(pentafl	59.9	37	0.0	3.6

Table S2 continued. The top 10 individual VOCs with the highest measured concentrations during printing and estimated steady-state emission rates.

	Rank	Compound name	Printing Conc. (µg/m^3)	Qual. (%)	BG Conc. (µg/m^3)	Emission rate (µg/min)
LulzBot without filament with applying on bed*	1	(S)-(+)-1,2-Propanediol	408.5	93	210.9	N/A‡
	2	Glycerin	199.4	87	0.0	N/A
	3	Hexanal	98.1	90	65.8	N/A
	4	Benzene, 1,3-dimethyl-	85.4	83	97.7	N/A
	5	Acetic acid	62.9	83	34.6	N/A
	6	Octanal	51.6	99	34.6	N/A
	7	Isopropyl Palmitate	39.8	96	59.2	N/A
	8	1-Pentanol	37.1	93	29.9	N/A
	9	Nonanal	35.5	43	30.0	N/A
	10	Heptanal	32.8	96	0.0	N/A

* We operated the 3D printer without any filament to characterize the individual VOC compounds emitted from the glue applied on the 3D printer bed, as glue was used in several normal printing tests to ensure that the printed piece adhered to the platform.

‡ We did not estimate emission rates because we could not confirm whether or not VOC concentrations reached to steady state levels when the printer was operated without filament (the duration of printing was short: about 45 mins).

Table S3: Top 10 individual VOCs with the highest measured concentrations outside the chamber

	Rank	Outside the chamber			Rank	Outside the chamber	
		Compound name	Conc. (µg/m^3)			Compound name	Conc. (µg/m^3)
LulzBot-ABS	1	Decane	0.02	LulzBot-ABS (dupl.)	1	Furfural	0.02
	2	Phenylethanolamine	0.02		2	Benzaldehyde	0.01
	3	Ethanol, 2-(2-ethoxyethoxy)-	0.01		3	Nonanal	0.01
	4	Nonane	0.01		4	n-Hexadecanoic acid	0.01
	5	Furfural	0.01		5	Tetrasiloxane, 1,1,3,3,5,5,7,7-octa	0.01
	6	Acetophenone	0.01		6	1-Propanol, 3-phenoxy-	0.01
	7	Undecane	0.01		7	Decane	0.01
	8	Decanal	0.01		8	Butanoic acid, 3-methylbutyl ester	0.01
	9	2-Butanone	0.01		9	Benzene, 1,2,3-trimethyl-	0.01
	10	Nonanal	0.01		10	Octanal	0.01
MakerBot-w/-enclosure	1	Isopropyl Palmitate	0.02	MakerBot-w/o-enclosure	1	Benzene, 1,3-dimethyl-	0.02
	2	Benzene, 1,3-dimethyl-	0.02		2	Isopropyl Palmitate	0.02
	3	Nonane, 2,2,4,4,6,8,8-heptamethyl-	0.02		3	Acetophenone	0.02
	4	Acetophenone	0.01		4	Nonanal	0.01
	5	Chloromethyl methyl sulfide	0.01		5	Benzene, 1,2,4-trimethyl-	0.01
	6	Nonanal	0.01		6	Octanal	0.01
	7	Decane	0.01		7	Tetrachloroethylene	0.01
	8	Octanal	0.01		8	Hexanal	0.01
	9	Hexanal	0.01		9	Benzene, 1,3,5-trimethyl-	0.01
	10	Toluene	0.01		10	Benzyl Alcohol	0.01

11. Validating the discretized UFP emission rate solution

In a few scenarios, UFP concentrations reach an approximately steady state level towards the end of printing period. We estimated the UFP emission rate during these time periods using a simple number balance equation as shown Equation S24.

$$\frac{E_{UFP,ss}}{VL_{UFP}} = C_{UFP,in,ss} - \frac{P_{UFP}\lambda C_{UFP,out}}{L_{UFP}} \quad \text{(S24)}$$

$C_{UFP,in,ss}$= UFP steady state concentration inside the chamber during the selected time period (#/cm^3)

$E_{UFP,ss}$= UFP steady state emission rate during the selected time period (#/min)

As previously mentioned, $\frac{P_{UFP}\lambda C_{UFP,out}}{L_{UFP}}$ is equal to average measured background concentration ($\bar{C}_{UFP,bg}$) and the total UFP loss rate (L_{UFP}) can be estimated from the final decay period after printing was stopped using a log-linear regression solution. We validated our method for estimating UFP emission rates by comparing the results from Equation S24 to average estimated UFP emission rates from discretized solution method (Equation S7 in Section 5). Five combinations of 3D printer and filament were selected for this comparison including LulzBot-ABS, LulzBot-PCTPE, LulzBot-TGlase, MakerBot-ABS with enclosure, and FlashForge-PLA. The summary of steady state time periods, estimated steady state UFP emission rates ($E_{UFP,ss}$), and the average estimated UFP emission rates using the discretized solution method ($\bar{E}_{UFP,ss}$) are listed in Table S4.

Table S4: Estimated UFP emission during steady state time periods using the simple mass balance model and the discretized solution method

Printer	*Filament*	*Time period (minutes after start printing)*	L_{UFP} *(1/min)*	$\bar{C}_{UFP,bg}$ *(#/cm^3)*	$C_{UFP,in,ss}$ *(#/cm^3)*	$E_{UFP,ss}$ *(#/min)*	$\bar{E}_{UFP,ss}$ *(#/min)*	*Difference (%)*
LulzBot	ABS	80-115	0.0354	1,166	722,395	9.19×10^{10}	9.69×10^{10}	5.5
	PCTPE	85-170	0.0281	429	222,012	2.24×10^{10}	2.33×10^{10}	3.7
	TGlase	140-180	0.029	931	56,401	5.79×10^{9}	5.71×10^{9}	1.4
MakerBot w/ enclosure	ABS	75-100	0.0333	1,214	535,999	6.41×10^{10}	5.99×10^{10}	6.6
FlashForge	PLA	60-140	0.028	523	1,487	9.72×10^{7}	9.38×10^{7}	3.6

The difference between estimated UFP emission rates using the steady state mass balance model and the discretized solution method remains under 7% for the 5 chosen 3D printer and filament combinations. Giving that the uncertainty around the estimated UFP emission rate is ~45%, the results demonstrate that there is no meaningful difference between UFP emission estimations from these two methods, which shows that the dynamic solution method used herein is reasonable.

12. Additional references

(1) Won, D.; Corsi, R. L.; Rynes, M. Sorptive Interactions between VOCs and Indoor Materials. *Indoor Air* **2001**, *11* (4), 246–256.

(2) Cox, S. S.; Little, J. C.; Hodgson, A. T. Predicting the Emission Rate of Volatile Organic Compounds from Vinyl Flooring. *Environ. Sci. Technol.* **2002**, *36* (4), 709–714.

(3) Hinds, W. C. *Aerosol technology: properties, behavior, and measurement of airborne particles*; John Wiley & Sons, 2012.

(4) Stephens, B.; Azimi, P.; Orch, Z. El; Ramos, T. Ultrafine particle emissions from desktop 3D printers. *Atmos. Environ.* **2013**, *79*, 334–339.

Predicting concentrations of ultrafine particles and volatile organic compounds resulting from desktop 3D printer operation and the impact of potential control strategies

Author Listing:

Parham Azimi[1], Torkan Fazli[1], and Brent Stephens[1*]
[1]Department of Civil, Architectural and Environmental Engineering, Illinois Institute of Technology, Chicago, IL USA

Address correspondence to:

Dr. Brent Stephens
Department of Civil, Architectural and Environmental Engineering
Illinois Institute of Technology
Alumni Memorial Hall Room 228
3201 South Dearborn Street
Chicago, IL 60616
Email: brent@iit.edu
Web address: http://built-envi.com

Keywords:

indoor air quality; air pollution; air emissions; exposure assessment; buildings; environmental health

Summary

Recent studies have shown that potentially hazardous volatile organic compounds (VOCs) and ultrafine particles (UFPs) are emitted from many desktop 3D printer and filament combinations. We use recently published measurements of UFP and speciated VOC emission rates from a number of desktop 3D printers and filaments to predict the magnitudes of human exposures to airborne pollutants that would be expected in multiple locations within a typical small office environment. We also model the impacts of several control strategies for reducing occupational exposures. Results demonstrate that UFP and VOC concentrations within close or moderate proximity (i.e., within 3 m and 3-18 m, respectively) to some desktop 3D printer and filament combinations with the highest emissions can exceed recommended exposure levels (RELs) for some VOCs and typical indoor concentrations for both UFPs and VOCs. Concentrations of caprolactam within close proximity to a printer using some nylon-based filaments are predicted to exceed both acute and chronic RELs set by the California Office of Environmental Health Hazard Assessment (OEHHA). UFP concentrations are predicted to reach as high as 80,000 #/cm^3 in close proximity to the highest emitting printer and filament combinations. The printer and filament combinations with the lowest UFP and VOC emission rates are not expected to yield concentrations at levels of concern. The most effective control strategies for reducing both UFP and VOC concentrations included installing a high-flow spot ventilation system and operating the printer in a sealed enclosure with high efficiency gas and particle filtration.

Introduction

Three-dimensional (3D) printers are rapidly gaining popularity for prototyping and manufacturing in a variety of industrial, educational, commercial, and residential settings. There are several additive manufacturing (AM) technologies used by 3D printers currently on the market (Afshar-Mohajer et al. 2015), although most relatively inexpensive desktop 3D printers utilize a technique called fused filament fabrication (FFF). In the FFF process, a 3D object is formed layer-by-layer as a thermoplastic filament is forced through a heated extrusion nozzle, melted, and deposited in thin layers onto a moving baseplate (Gross et al. 2014).

A few recent studies have shown that potentially hazardous gases and particles are emitted from many FFF 3D printers and filaments (Azimi et al. 2016; Kim et al. 2015; Steinle 2015; Stephens et al. 2013). Many printer and filament combinations have been shown to emit ultrafine particles (i.e., UFPs: particles smaller than 100 nm), while others have been shown to emit hazardous volatile organic compounds (VOCs) such as styrene and caprolactam (Azimi et al. 2016). Understanding the magnitude of these emissions has been critical, as exposure to thermal decomposition products from ABS and other thermoplastics are known to have toxic effects in animals and humans (Oberdorster et al. 2005; Schaper et al. 1994; Unwin et al. 2013; Zitting and Savolainen 1980). Moreover, exposure to UFPs from a variety of sources have been linked with a variety of adverse health impacts in humans (Oberdörster 2000; Peters et al. 1997).

In a recent screening analysis, we estimated that some of the highest emitting printer and filament combinations that have been tested to date could yield high concentrations of VOCs and UFPs that could be of concern for human health when operated in small office spaces (Azimi et al. 2016). However, we are not aware of any studies to date that have explored in detail the likely human exposures to both gas and particle emissions from desktop FFF 3D printers and filaments

in more realistic indoor environments. Therefore in this work, we use recently published measurements of emission rates of both UFPs and speciated VOCs from a wide variety of desktop FFF 3D printers and filaments to predict the magnitudes of human exposures to these same pollutants that would be expected in multiple spatial locations within a typical small office environment. We also use the worst case UFP and VOC emission scenarios to model the likely impacts of several potential control strategies for reducing exposures.

Methods

Characteristics of the modeled office environment

We used a multi-zone airflow and contaminant transport analysis modeling software, CONTAM 3.2 (NIST 2016), to predict concentrations resulting from gas and particle emissions from several combinations of desktop FFF 3D printers and filaments, assuming each printer is operated inside a one-story office building with a floor area of 511 m^2. The office building geometry and floor plan was taken from the Department of Energy (DOE) Commercial Reference Building data set (Ng et al. 2012). However, we modified some of the building characteristics in the CONTAM model to represent more realistic scenarios. Figure 1 shows the building floor plan divided into multiple zones and the maximum occupancy in each zone (Ng et al. 2012).

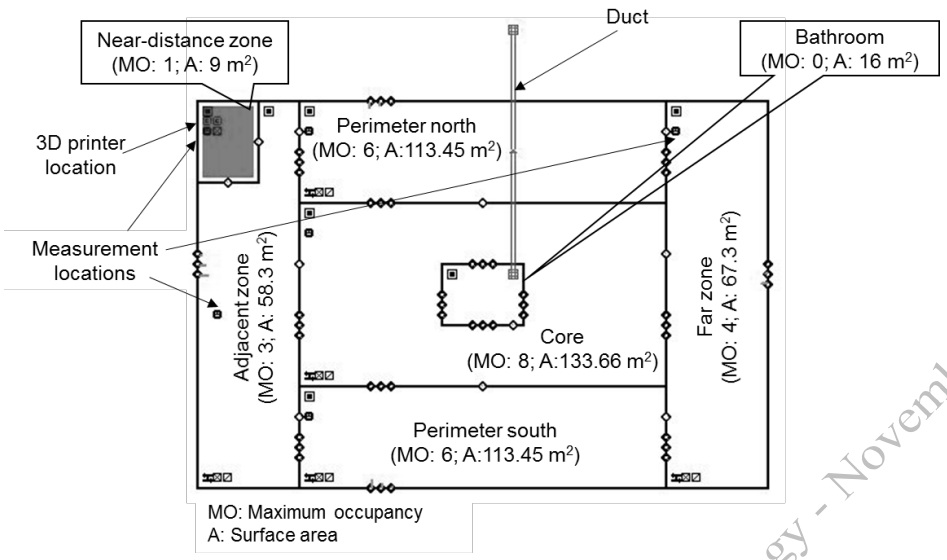

Figure 1. CONTAM model for the small office building (MO: maximum occupancy; A: floor area)

In Figure 1, each zone was assumed to be well-mixed with uniform temperature, relative humidity, and pollutant concentration. In all simulations, one desktop 3D printer was located in the small shaded zone in the top left corner of Figure 1. This zone does not have physical partitions like the other zones, but represents a 9 m^2 floor area space within the western perimeter zone in which the printer is contained. We refer to this zone as the "near-distance" zone, in which a person would be sitting within immediate proximity to an operating 3D printer (i.e., within ~3 m) for extending periods of time. We also refer to two other main zones in which occupants would be exposed to printer emissions only after the contaminants are transported from the printer location to those areas, including an immediately "adjacent zone" to the near-distance zone (within ~3-18 m) and a "far zone" that is on the far end of the building (between ~ 18 and ~33 m away).

Each zone (other than the bathroom and the "near-distance" zone) was modeled with its own air-handling unit (AHU) designed to recirculate indoor air and deliver outdoor air for

ventilation. The total supply and return airflow rates were the same for each AHU. We assumed that all five AHUs were designed to meet ASHRAE Standard 62.1-2010 minimum ventilation requirements based on both floor area and occupancy (ASHRAE 2010). One exhaust fan ducted to the exterior was also assumed to operate continuously in the bathroom at an airflow rate of 1.8 m^3/hr. The required outdoor air ventilation rate for each zone, $Q_{vent,i}$ (m^3/hr), was calculated using equation 1 (ASHRAE 2010).

$$Q_{vent,i} = A \times N_{occupants,i} + B \times A_{zone,i} \quad \text{Equation 1}$$

Where:

A = the required outdoor air ventilation per person for a small office (9 m^3/hr per person)

B = the required outdoor air ventilation per floor area (1.08 m^3/hr per m^2)

$N_{occupants,i}$ = the maximum number of occupants in zone i (-)

$A_{zone,i}$ = the floor area of zone i (m^2)

For the baseline simulation conditions, we also assumed that the AHUs met minimum HVAC filtration efficiency requirements in ASHRAE Standard 62.1-2010 with MERV 8 particle filters and no gas-phase filtration (ASHRAE 2012). We estimated the removal efficiency of MERV 8 filters for UFPs emitted from desktop 3D printers to be 43.5% by mapping the size-resolved removal efficiency of filters recently tested in Fazli and Stephens (2016) to the resulting size-resolved distribution of emitted particles from 3D printers in an office environment reported in Stephens et al. (2013) for particles less than 100 nm following a procedure described in Azimi et al. (2014).

We assumed default building occupancy and HVAC system runtime schedules from the NIST model, with the building occupied on weekdays from 7:00 am to 6:00 pm and the HVAC

system operating from 6:00 am to 10:00 pm on weekdays. In all cases, we assumed that a single desktop 3D printer operated continuously for 8 hours from 9:00 am to 5:00 pm, representing a relatively high, albeit not uncommon, duration of operation. We assumed that the building was located in Chicago, IL and used Typical Meteorological Year (TMY) 3 data for Chicago (NSRDB: 1991- 2005 Update: TMY3). Air infiltration through exterior walls was modeled using three characteristic openings in each wall representing various types of openings, including cracks and gaps in the walls, at the wall corners, and around large openings such as windows and doors. The effective leakage area was assumed to be 5.27 cm^2/m^2 at a reference pressure difference of 4 Pa for all three types of small openings (Emmerich and Persily 2011). All of the zones were connected to at least one other zone by large openings with cross sectional areas of 1 m^2, which served to simulate doorway openings. The zone boundaries for the "near-distance" 3D printing zone were modeled as walls with large openings the same size as their cross sectional areas (9 m^2).

Desktop 3D printer emission scenarios

Table 1 summarizes all of the recent measurements of particle and speciated VOC emission rates from desktop FFF 3D printers and filaments in the literature to date, including our recent study in which we measured both UFP and speciated VOC emissions tests for a total of 5 popular FFF 3D printers and 9 different filaments, including ABS, PLA, high impact polystyrene (HIPS), semitransparent nylon, laybrick (an imitation brick material of unknown chemical composition), laywood (an imitation wood material of unknown chemical composition), transparent polycarbonate, a semitransparent nylon-based plasticized copolyamide thermoplastic elastomer (PCTPE), and a transparent polyester resin filament called T-Glase (Azimi et al. 2016). The three primary VOCs include caprolactam emitted from nylon-based filaments,

styrene emitted from ABS and HIPS filaments, and lactide emitted from PLA filaments. For those pollutants that were consistently tested across all previous studies (i.e., UFPs from PLA and ABS), reported emission rates were generally within an order of magnitude of each other and thus the emission rates from Azimi et al. (2016) are considered reasonably representative of the other studies as well.

Table 1. Estimated particle and speciated VOCs from desktop 3D printers in existing literature

Reference	*Filament*	*Particle emission rate (#/min)*	*Primary emitted VOC*	*VOC emission rate (µg/min)*
Kim et al. (2015)	PLA*	4.6×10^{8}	Toluene	N/A
	ABS	1.6×10^{10}	Ethylbenzene	N/A
Steinle (2016)	PLA	2.1×10^{9}	Methyl methacrylate	6.5
	ABS	2.4×10^{8}	Styrene	5.8
Azimi et al. *(2016)*	PLA*	1.1×10^{8}	Lactide	4.4
	ABS*	6.1×10^{10}	Styrene	49.5
	HIPS	1.5×10^{10}	Caprolactam	19.6
	Nylon	2.4×10^{9}	Caprolactam	182.6
	PCTPE	2.8×10^{10}	Caprolactam	167.9
	Laybrick	6.9×10^{7}	Caprolactam	69.1
	Laywood	9.8×10^{7}	Caprolactam	45.4
	TGlase	3.1×10^{10}	Caprolactam	1.5
	Polycarbonate	6.2×10^{10}	Caprolactam	1.5

* Average of reported emissions in the referenced study

Given the breadth of the Azimi et al. (2016) study, we use the emission rates of UFPs and the primary speciated VOCs emitted from each of the 9 filaments to predict the time-varying concentrations of each pollutant that would likely be present in the previously defined near, adjacent, and far zones. We modeled the emitted pollutants "in addition" to what concentrations would have existed from other indoor sources. Thus, we assume that the concentrations of each pollutant in both outdoor and background indoor air are zero. In CONTAM, we assumed the diffusion coefficients of caprolactam and styrene in the office air are 0.065 and 0.071 cm^2/s (NJDEP 2015), respectively, and kept the UFP and lactide diffusion coefficients equal to

CONTAM defaults (0.2 cm^2/s). We also assumed default CONTAM values for the effective density and specific heat of UFP equal to 1 g/cm^3 and 1 kJ/kgK, respectively. Finally, the UFP decay rate was assumed 25×10^{-5} s^{-1}, equal to the median values measured in a recent study in UFP decay rates in residences (Wallace et al. 2013).

Evaluating exposure control strategies

We also modeled the impacts of several control strategies on resulting pollutant concentrations in the office space, including: (i) upgrading the central HVAC filtration throughout the office; (ii) operating portable stand-alone air cleaners within close proximity to the 3D printer; (iii) installing spot ventilation systems within close proximity to the 3D printer; and (iv) operating the 3D printer inside a prototype sealed enclosure with recirculating gas and particle filtration. For this analysis, we modeled only the highest emission rates for each of the primary emitted pollutants to model the likely impacts of control strategies on only the worst-case scenarios (i.e. emission rates of 6.1×10^{10} #/min for UFPs, 183 µg/min for caprolactam, 50 µg/min for styrene, and 4 µg/min for lactide).

Upgraded central HVAC system filtration

In the first exposure control scenario, we assumed that the HVAC filters installed in the central AHUs were upgraded to MERV 16 media impregnated with activated carbon to provide both gas and particle filtration. We estimated the UFP removal efficiency of the MERV 16 filter to be 97% using the same matching approach with data from Fazli and Stephens (2016) described earlier for MERV 8 filters. Because there is a lack of literature on the gas-phase removal efficiency of impregnated activated carbon filters for caprolactam, styrene, or lactide, we relied on estimates from Sidheswaran et al. (2012) who reported VOC removal efficiencies of

active carbon fiber filters for 6 speciated VOCs ranging between 60% and 80%. Therefore, we assumed that the removal efficiency of the HEPA filters with active carbon fibers for all of the emitted VOCs is equal to 70%.

Operating portable stand-alone air cleaners

Several previous studies have measured clean air delivery rates (CADRs) and/or single-pass removal efficiencies for UFPs from a number of commercial stand-alone air cleaners. Waring et al., (2008) reported a single-pass removal efficiency of ~60% for two HEPA air cleaners with average CADRs across all particle sizes of 188 and 324 m^3/hr, respectively. Other studies have reported CADRs for UFPs from other similar commercial air cleaner products ranging from ~100 to ~300 m^3/hr, with single-pass efficiencies typically ranging from ~45% to ~60% (Mølgaard et al. 2014; Sultan et al. 2011). Therefore, we modeled two distinct portable air cleaner scenarios with CADRs of 100 and 300 m^3/hr for UFPs. Assuming a single-pass efficiency of 60% for the HEPA filters, the airflow rates of the two air cleaners were calculated to be 167 m^3/hr and 500 m^3/hr, respectively. We assumed that the filters also contained impregnated carbon with 70% removal efficiency for each of the VOCs modeled herein (Sidheswaran et al. 2012), which yields CADRs for the modeled VOCs of 117 m^3/hr and 350 m^3/hr for the low- and high-efficiency air cleaner scenarios, respectively. Both air cleaners were modeled in CONTAM as an air handling system with equal supply and return air flows inside the "near-distance" zone and without any air exchange with outdoor air.

Spot ventilation systems

Next, we modeled the impacts of introducing spot ventilation in the "near-distance" zone within the immediate vicinity of the operating 3D printer. For lack of other data on exhaust systems that are designed specifically for 3D printer applications, we assumed that spot

ventilation systems performed similar to exhaust hoods installed in small commercial or residential kitchens. We assumed that the hoods were located approximately 1.5 m above the desktop 3D printer and exhausted directly to the outdoors. A few recent studies in test kitchens have reported widely varying nominal and measured airflow rates, as well as capture efficiencies for both gas and particle emissions from cooking, that are achievable by a number of kitchen exhaust fans (Delp and Singer 2012; Logue 2014; Singer et al. 2012). The nominal airflow rates in these studies ranged from 325 to 1300 m^3/hr (with measured airflow rates from 75 to 650 m^3/hr), and with low, moderate, and high pollutant capture efficiencies ranging from less than 50% to greater than 75%, generally scaling with airflow rates (Singer et al., 2012). Moreover, if we were to consider the 67.3 m^2 printing area in the office space as a "chemical storage room," ASHRAE Standard 62.1 would require a minimum exhaust airflow rate of 27 m^3/hr per m^2 of floor area (i.e., a total exhaust rate of 1817 m^3/hr) to meet minimum ventilation requirements (ASHRAE 2010).

Given these bounds of reasonable airflow rates and capture efficiencies (CEs), we modeled three distinct spot ventilation scenarios with the following characteristics: (1) low effectiveness with 90 m^3/hr (25 L/s) and 25% CE; (2) medium effectiveness with 360 m^3/hr (100 L/s) and 63% CE; and (3) high effectiveness with 1800 m^3/hr (500 L/s) 100% CE. To model the spot ventilation scenarios in CONTAM, we defined a hypothetical 1 m^2 space inside the "near-distance" zone with an exhaust fan ducted to the outdoor air. We divided the emission sources between the zones based on the CE of the spot ventilation scenario. For example, if the CE was 25%, 75% of the total emissions of the four main pollutants were assumed to flow into the "near-distance" zone where they could be transported to other spaces and result in exposure, while 25% of the total emissions remained only in the 1 m^2 "spot ventilation zone." We divided the HVAC

system supply airflow rates between the "near-distance" and "spot ventilation" zones in such a way that both zones have equal pollutant concentrations when the 3D printer operates and the spot ventilation airflow rate is zero.

Sealed enclosure with recirculating filtration

Finally, we modeled the impacts of operating the 3D printers inside a prototype sealed enclosure with recirculating gas and particle filtration to reduce emissions. For this analysis, a pilot experimental chamber study was conducted with two high emitting filament and printer combinations installed inside a prototype enclosure (Azimi, Zhao, and Stephens 2016). Average total VOC (i.e., TVOC) and UFP removal efficiencies of the enclosure were measured as ~90% and ~80%, respectively. For lack of other data, we assumed that the enclosure reduces the gas-phase emission rates equally (by 90%) for all speciated VOCs and all UFP emission rates equally (by 80%). The source emissions were simply reduced by 90% and 80% relative to the baseline scenario for gases and particles, respectively, in CONTAM.

Results and Discussion

Predicted concentrations of pollutants emitted from various 3D printer filaments

Figure 2 shows an example of modeled time-varying concentrations of UFPs and styrene in the three defined locations inside the small office environment during the weekdays of first week of January resulting from operating a single 3D printer with ABS filament (assuming the average ABS emission rate from data from Azimi et al. (2016) in table 1).

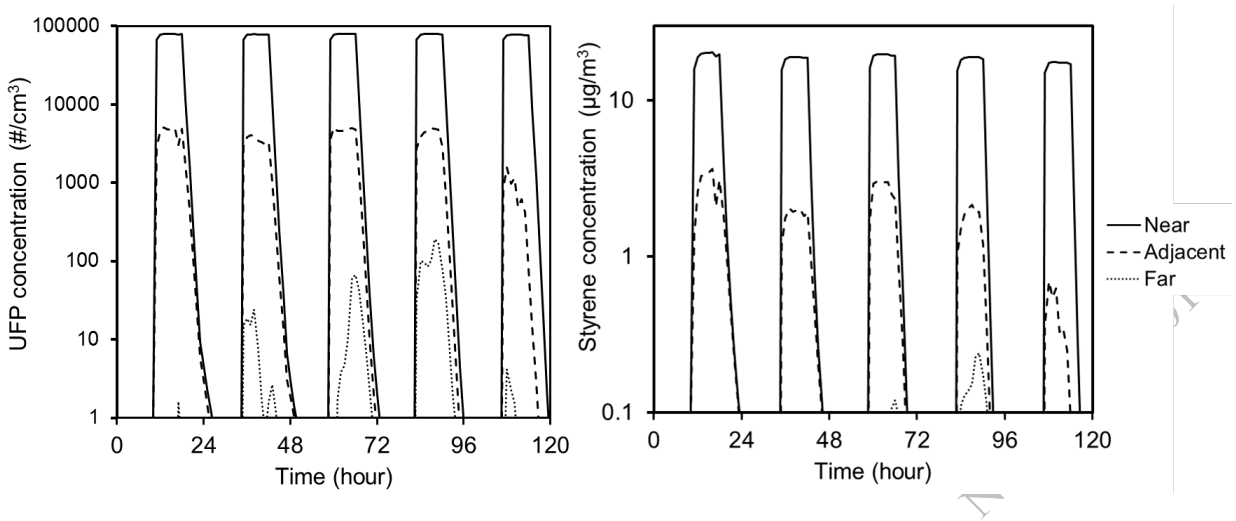

Figure 2. Typical hourly indoor concentration results from the CONTAM model with a single ABS printer operating in "near-distance", "adjacent", and "far" zones

The modeled time-varying concentration results demonstrate that the peak exposure to pollutants emitted by the 3D printer in the near-distance zone are typically more than 9 and 4 times higher than in the adjacent zone for UFPs and styrene, respectively, while a much smaller fraction of pollutants would actually reach the far-distance zone. The model results also reveal that the increase in both gas and particle concentrations in the near and adjacent zones occurs almost immediately after the printer begins operating, while concentrations peak much later in the far-distance zone. Modeled concentrations in the far zone are also more variable due to changes in air infiltration conditions. For example, the relative standard deviation of the predicted maximum 1-hour concentrations throughout the entire year is only 2% for UFPs and 15% for styrene in the near zone, slightly more variable in the adjacent zone (41% for UFPs and 58% for VOCs), and most variable for the far zone (114% for UFPs and 106% for VOCs). These profiles are repeated with reasonable consistency for all weekdays throughout the year.

Figures 3 and 4 summarize the predicted time-varying concentrations of UFPs and speciated VOCs in all three zones over the course of an entire year for each printer and filament

combination. Figure 3 shows concentrations predicted in the nearest zone and figure 4 shows concentrations predicted in both the adjacent and far zones. Results are presented as ranges of daily maximum 1-hour, 8-hour and 24-hour concentrations (i.e., there is a total of 260 data points representing 260 weekdays in each series), as some of these metrics can be used to compare directly to regulatory limits. The daily maximum 8-hour concentrations during each weekday are calculated by taking 8-hour averages of the predicted hourly concentrations and selecting the highest average 8-hour concentration period for each day. The daily 24-hour concentrations are simply the daily averages for each weekday over the course of the entire year.

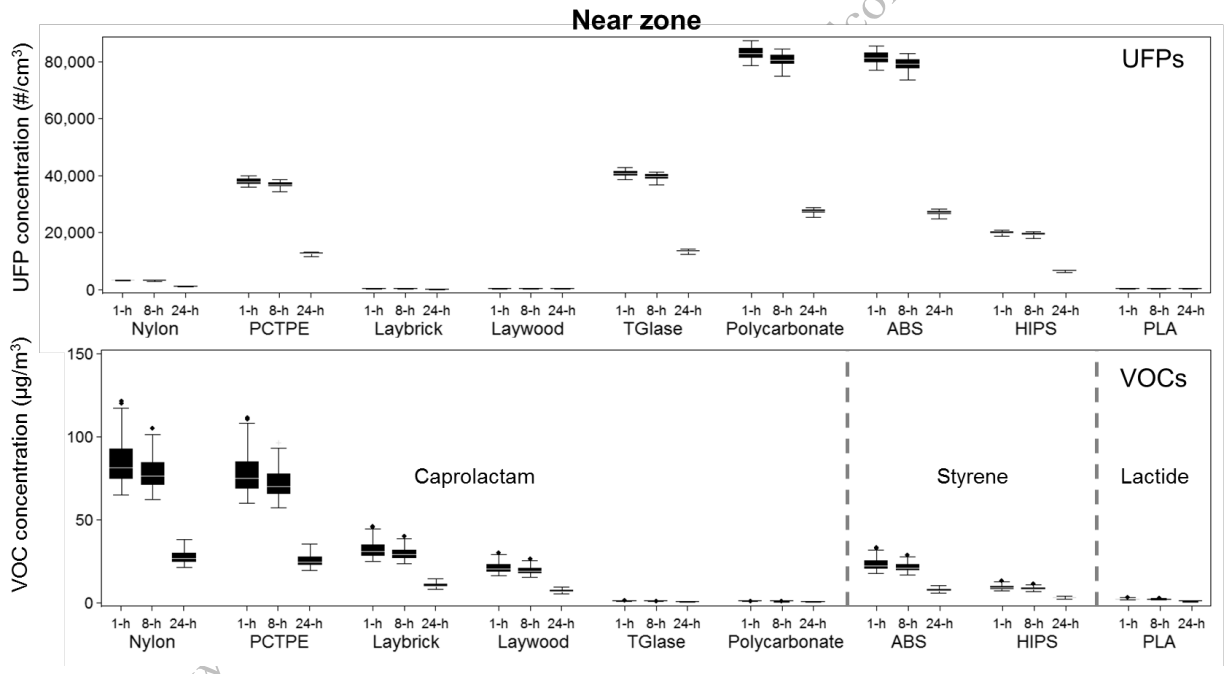

Figure 3. Ranges of predicted daily maximum 1-, 8-, and 24-hour concentrations of UFPs and speciated VOCs in the "near zone" for a typical year assuming a single desktop 3D printer with 9 different filaments operates continuously for 8 hours per day

The median values of daily maximum 1-hour UFP concentrations in the near zone ranged from just under 100 #/cm^3 for Laybrick, Laywood, and PLA filaments to nearly 80,000 #/cm^3 for ABS and Polycarbonate filaments. Median values of daily maximum 1-hour VOC concentrations

ranged from 0.7 to 80 μg/m^3 with caprolactam-emitting filaments (highest with Nylon and PCTPE), from 8 to 22 μg/m^3 with styrene-emitting filaments (ABS and HIPS), and were consistently under 2 μg/m^3 for lactide-emitting filaments. Since we assumed that the printer operates 8 hours per day, the maximum 1-hour and 8-hour daily concentrations are relatively similar, while the average 24-hour concentrations are substantially lower, with median values approximately 3% and 67% lower than the maximum 1-hour concentration.

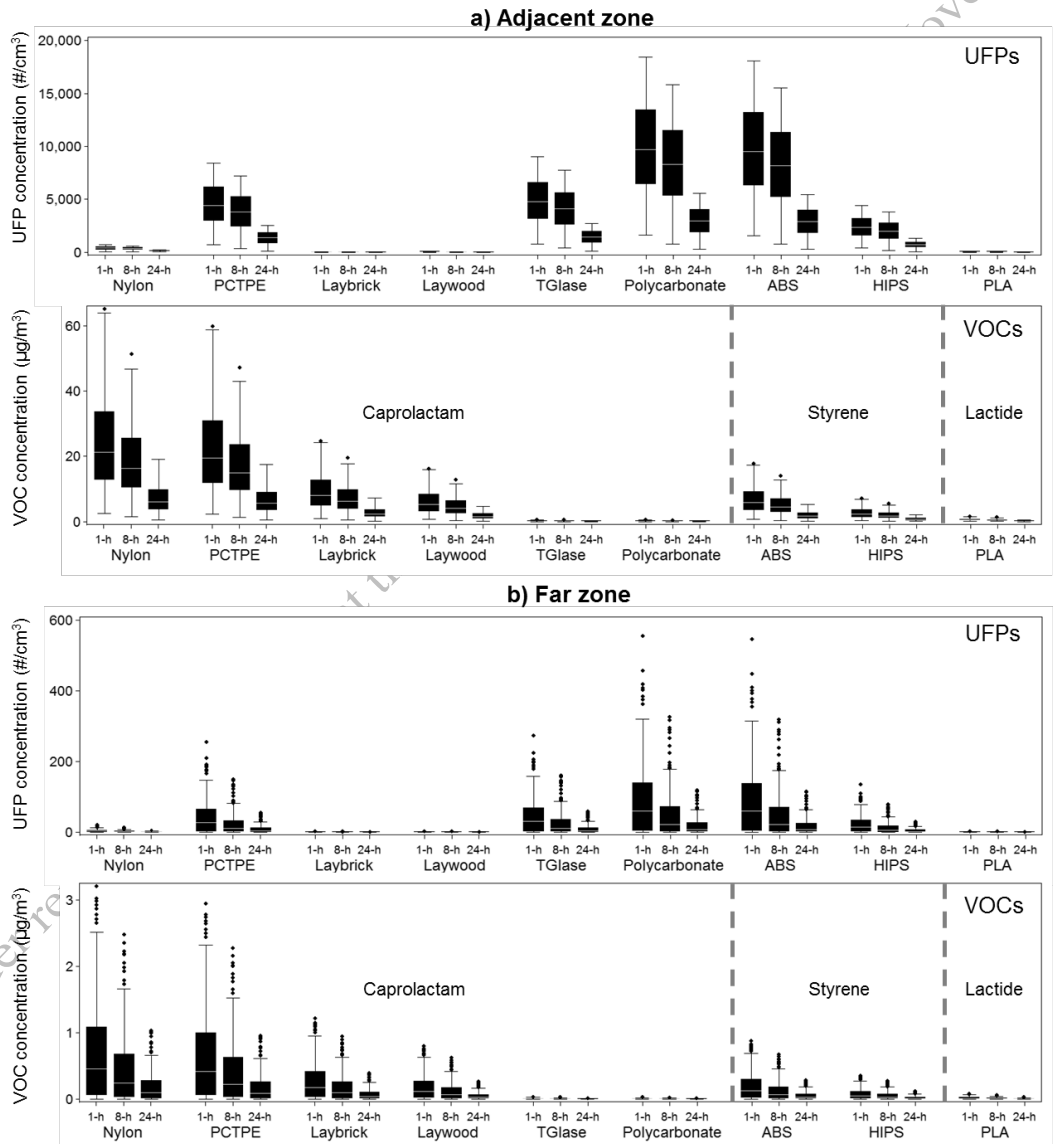

Figure 4. Ranges of predicted daily maximum 1-, 8-, and 24-hour concentrations of UFPs and speciated VOCs in the (a) "adjacent zone" and (b) "far zone" for a typical year assuming a single desktop 3D printer operates with 9 different filaments continuously for 8 hours per day

The median values of daily maximum 1-hour UFP concentrations in the adjacent zone ranged from less than 20 #/cm^3 for low-emitting filaments (e.g., Laybrick, Laywood, and PLA) to nearly 10,000 #/cm^3 for ABS and Polycarbonate filaments. The median values of daily maximum 1-hour VOC concentrations ranged from 0.2 to 20 μg/m^3 with caprolactam-emitting filaments, 2 to 6 μg/m^3 with styrene-emitting filaments, and were consistently lower than 1 μg/m^3 for lactide-emitting filaments. UFP and VOC concentration followed similar patterns in the far zone, albeit at much lower absolute concentrations. The median 1-hour, 8-hour, and 24-hour UFP concentrations in the far zone were only 60, 20 and 7 #/cm^3, respectively, when the 3D printer was modeled with polycarbonate and ABS filaments. The highest median 1-hour maximum concentrations of caprolactam, styrene, and lactide were only 0.5, 0.1, and 0.01 μg/m^3 when the 3D printer was modeled with nylon, ABS, and PLA filaments, respectively. Thus, UFP and VOC emissions from the lowest-emitting filaments had essentially no impact on concentrations in the far distance zone.

Implications for human health

Predicted concentrations in the near and adjacent zones have important implications for human health. For example, the California Office of Environmental Health Hazard Assessment (OEHHA) maintains acute (i.e., 1-hour average), 8-hour average, and chronic (i.e., continuous lifetime) reference exposure levels (RELs) of caprolactam of 50 μg/m^3, 7 μg/m^3, and 2.2 μg/m^3, respectively (OEHHA 2014). Moreover, acute exposure to high concentrations of caprolactam is known to be "irritating to the eyes and the respiratory tract" and "may cause effects on the central nervous system" (CDC 1994). Results from the simulations herein suggest that operating

a 3D printer with most of the nylon-based filaments (except TGlase and polycarbonate) would increase the concentration of caprolactam in both the adjacent and near zones to levels that would exceed both the 8-hour and chronic RELs set by OEHHA. Further, the predicted caprolactam concentration in the near zone during printing with nylon and PCTPE filaments would also exceed the acute REL. The predicted caprolactam concentrations in the far distance zone consistently remain under all RELs for all modeled nylon-based filaments.

Existing guidelines and recommendations for indoor styrene concentrations are limited to those set for industrial and workplace environments, including an 8-hour time-weighted-average (TWA) of 85 mg/m^3 and 426 mg/m^3 from the American Conference of Governmental Industrial Hygienists (ACGIH) and the Occupational Safety and Health Administration (OSHA) Standard # 29 CFR 1910.1000, respectively, and nearly 3000 mg/m^3 from the National Institute for Occupational Safety and Health (NIOSH). Further, the U.S. Environmental Protection Agency (EPA) maintains a Reference Concentration (RfC) for styrene of 1 mg/m^3 based on central nervous system effects in occupationally exposed workers (US EPA 2000). However, other health impacts of styrene exposure have also been shown in epidemiology studies at much lower concentrations than these reference levels. For example, styrene concentrations as low as a few μg/m^3 have been associated with elevated risk of pulmonary infections in infants (Diez et al. 2000). Our results demonstrate that the median styrene concentrations in the near distance zone can easily reach more than 10 times this value, and can be as much as three times higher than the highest measured styrene concentration of 7.5 μg/m^3 in typical commercial buildings in the U.S. EPA BASE study (Girman et al. 1999). Further, styrene is classified as a "possible human carcinogen" by the International Agency for Research on Cancer (IARC classification group 2B) (IARC 2002) and is "reasonably anticipated to be a human carcinogen" by the National

Toxicology Program (National Toxicology Program 2014). These levels suggest that although the predicted styrene concentrations in all zones from all printer and filament combinations used herein are all lower than defined exposure limits, resulting concentrations still may pose a health risk to occupants.

Although we are not aware of any regulatory limits for indoor UFP concentrations, increases in UFP concentrations of ~80,000 #/cm^3 in the near-distance zone and ~10,000 #/cm^3 in the adjacent zone resulting from printing with polycarbonate and ABS filaments, as well as increases of ~40,000 #/cm^3 in the near-distance zone and ~5,000 #/cm^3 in the adjacent zone with some other filaments, are substantial, particularly given what is known about the health effects associated with outdoor UFPs. For example, UFP concentrations of ~80,000 #/cm^3 have been reported within 100 m of highly trafficked roadways (Zhu et al. 2002), and some of the observed associations of adverse health effects with proximity to busy roadways are likely attributable in part to elevated UFPs (McConnell et al. 2010; Gauderman et al. 2007; Gauderman et al. 2005). Further, recent studies have shown that increases in outdoor UFP concentrations of ~10,000 #/cm^3 are associated with a ~3% increase risk in daily mortality (Stölzel et al. 2007) and increases in outdoor UFP concentrations of only ~1,000 #/cm^3 are associated with increased blood pressure in children (Pieters et al. 2015).

Comparing the modeled UFP concentrations to levels measured in other indoor environments, 80,000 #/cm^3 is about 50% higher than the highest time-averaged UFP indoor concentrations that have been observed in schools in previous investigations (Diapouli et al. 2007). Printing with other filaments such as PCTPE, TGlase, and HIPS would also increase the near zone UFP concentrations to between 2 and 5 times higher than indoor UFP concentrations typically observed in other buildings in the adjacent and near-distance zones, respectively.

Although much less is known about the adverse health effects of indoor-generated UFPs, recent studies of nanoparticles emitted from photocopiers and laser printers illustrate the potential hazard for human health. For example, ultrafine particles collected from a university copy center were recently shown to induce lung injury and inflammation in mice (Pirela et al. 2013) and upper airway inflammation and oxidative stress in healthy human volunteers (Khatri et al. 2013). These data suggest that controlling emissions and/or exposures from high emitting 3D printer and filament combinations is warranted in settings similar to the one modeled herein.

Impacts of control strategies on pollutant concentrations

Next, we chose the highest emitting printer and filament combinations for each pollutant and explored the impacts of various control strategies on the resulting concentrations in the same three locations within the modeled office environment. ABS, nylon, and PLA filaments were selected to represent the highest UFP and styrene, caprolactam, and lactide emissions, respectively. Figure 5 shows the predicted impacts of the various control strategies on maximum 1-hour UFP concentrations in the near, adjacent, and far distances with the 3D printer operating on the same schedule as all other simulations.

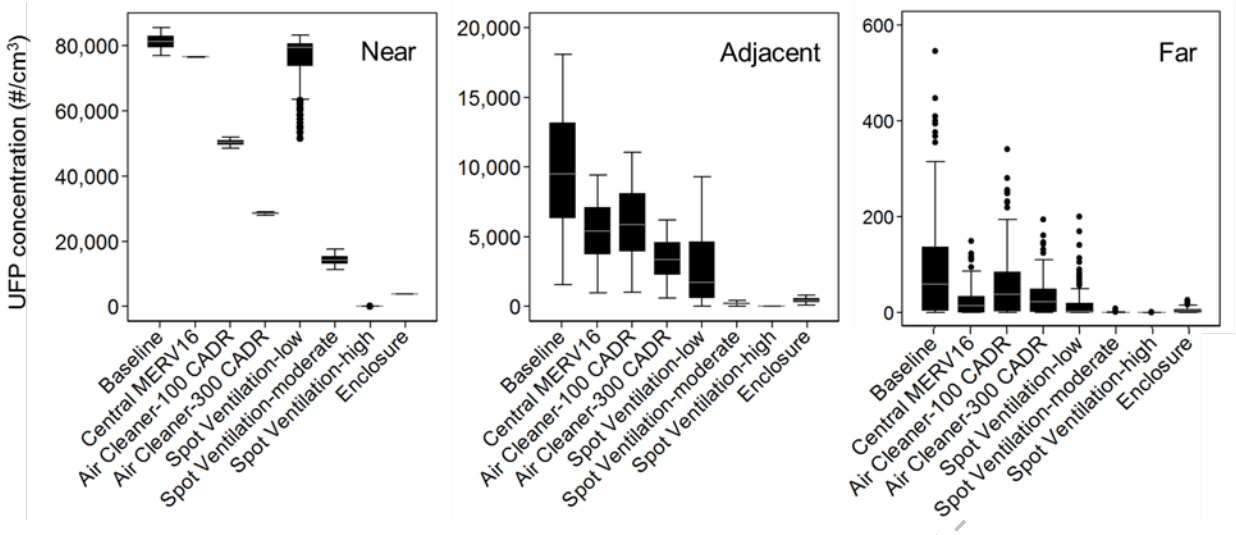

Figure 5. Modeled impacts of various control strategies on maximum 1-hour UFP concentrations in the near, adjacent, and far distances

Upgrading the central HVAC system filter to a MERV 16 with activated carbon and installing a low-flow (and low capture efficiency) spot ventilation system are predicted to yield the smallest reductions in daily maximum 1-hour UFP concentrations in the near zone. Conversely, installing a high-flow (and high capture efficiency) spot ventilation system has the greatest potential for reducing UFP concentrations in the near zone, followed by using the sealed enclosure with particle and gas filtration. Both are predicted to reduce median values of daily maximum 1-hour UFP concentrations from ~80,000 #/cm^3 to less than ~4000 #/cm^3. Both air cleaner scenarios have moderate impacts on UFP concentrations in the near zone. These results suggest that in order to reduce exposures in areas within immediate proximity to operating 3D printers, it is best to prioritize solutions that exhaust or control emissions directly at the source rather than attempting to lower UFP concentrations in the broader area with air cleaners and filtration.

Results are somewhat similar in the adjacent zone, albeit with some variability. Installing a low-CADR portable air cleaner and upgrading the central HVAC system filtration are

predicted to yield the smallest reductions in UFP concentrations in the adjacent zone, although the relative reductions in this zone are higher than those in the immediate vicinity of the printer. Both moderate- and high-flow spot ventilation systems, as well as the sealed enclosure, are predicted to yield the largest reductions in median values of daily maximum 1-hour UFP concentrations (all below 500 #/cm^3). And although the air cleaners and low-flow spot ventilation system have lower UFP removal effectiveness, they can still limit increases in UFP concentrations to less than 5,000 #/cm^3 in the adjacent zone. Similar relative concentration profiles are also observed for the far zone, but the baseline UFP concentrations are already quite low (~60 #/cm^3) and thus may not necessitate further control strategies.

Figure 6 shows the impacts of the same control strategies for reducing daily maximum 1-hour concentrations of individual VOCs, including (a) caprolactam, (b) styrene, and (c) lactide emitted from nylon, ABS, and PLA filaments, respectively.

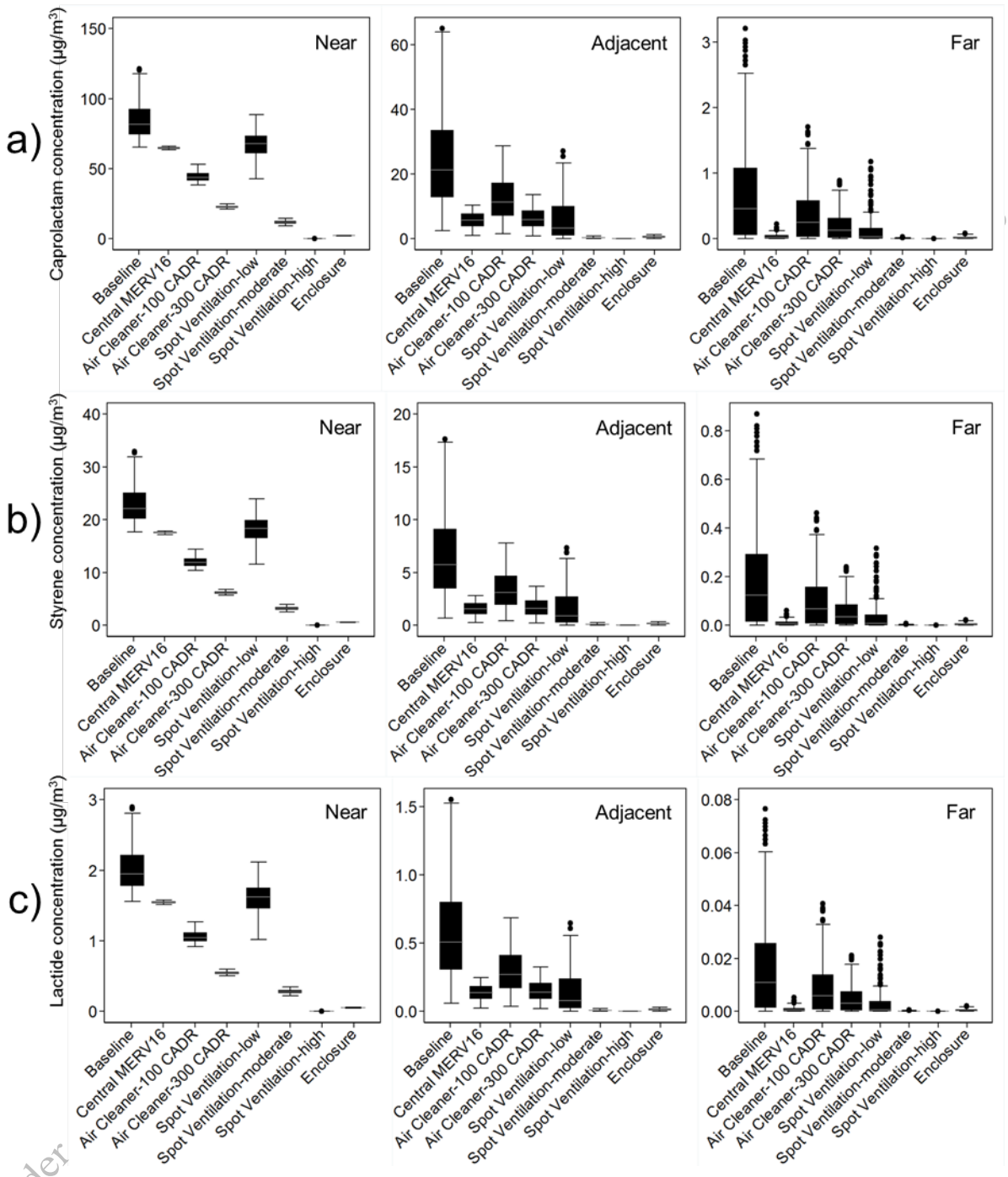

Figure 6. Modeled impacts of various control strategies on daily maximum 1-hour concentrations of (a) caprolactam, (b) styrene, and (c) lactide in the near, adjacent, and far zones

The relative reductions in daily maximum 1-hour concentrations with each control strategy are similar to those for UFP concentrations and are the same for all individual VOCs because most of the same assumptions for pollutant dynamics apply to each VOC. However,

absolute concentrations vary based on the strength of the emission source. In the near zone, upgrading central HVAC filtration and installing low-flow spot ventilation again have the smallest impacts on VOC concentrations, allowing most of the daily maximum 1-hour caprolactam concentrations from nylon-based filaments to still exceed the OEHHA acute REL of 50 $\mu g/m^3$. The remaining control strategies would all reduce the median daily maximum 1-hour caprolactam concentration below this level. Both the high-flow spot ventilation and the sealed enclosure with gas and particle filtration are predicted to reduce the median daily maximum 1-hour caprolactam concentration to less than 2 $\mu g/m^3$. Similarly, both moderate- and high-flow spot ventilation systems and the sealed enclosure are predicted to reduce the median daily maximum 1-hour styrene concentration to less than 7.5 $\mu g/m^3$ (i.e., the maximum level measured in U.S. commercial buildings in the BASE study).

Installing moderate- and high-flow spot ventilation systems and the sealed enclosure are predicted to yield the largest reductions in VOC concentrations in the adjacent zone, reducing daily maximum 1-hour caprolactam and styrene concentrations to less than 0.5 $\mu g/m^3$. The portable air cleaner scenarios yield smaller reductions in VOC concentrations in both the adjacent and far zones, but could still reduce peak caprolactam concentrations below the OEHHA acute REL for most days. All of the control strategies except for the low-CADR portable air cleaner are predicted to maintain the median daily maximum 1-hour styrene concentration in the adjacent zone below 2 $\mu g/m^3$. Median daily maximum 1-hour lactide concentrations remain below 2 $\mu g/m^3$ for all scenarios in all three zones, suggesting that lactide emissions from 3D printers using PLA filaments are likely not problematic for human exposure.

Pollutant removal effectiveness of the various control strategies

These same data were also used to calculate the effectiveness of each of the control strategies for reducing UFP and VOC concentrations in each zone using Equation 2. Removal effectiveness values are shown in Figure 7.

$$E_{control,i} = 1 - \frac{\bar{C}_i}{\bar{C}_{baseline,i}} \qquad \text{Equation 2}$$

Where:

$E_{control,i}$ = Effectiveness of a particular control strategy for removing UFPs/VOCs from a specific location (-)

$\bar{C}_i$ = Median concentration of UFPs/VOCs in a specific location predicted with the use of a particular control strategy (#/cm^3 or µg/m^3)

$\bar{C}_{baseline,i}$ = Median concentration of UFPs/VOCs in a specific location predicted without the use of any control strategies (#/cm^3 or µg/m^3)

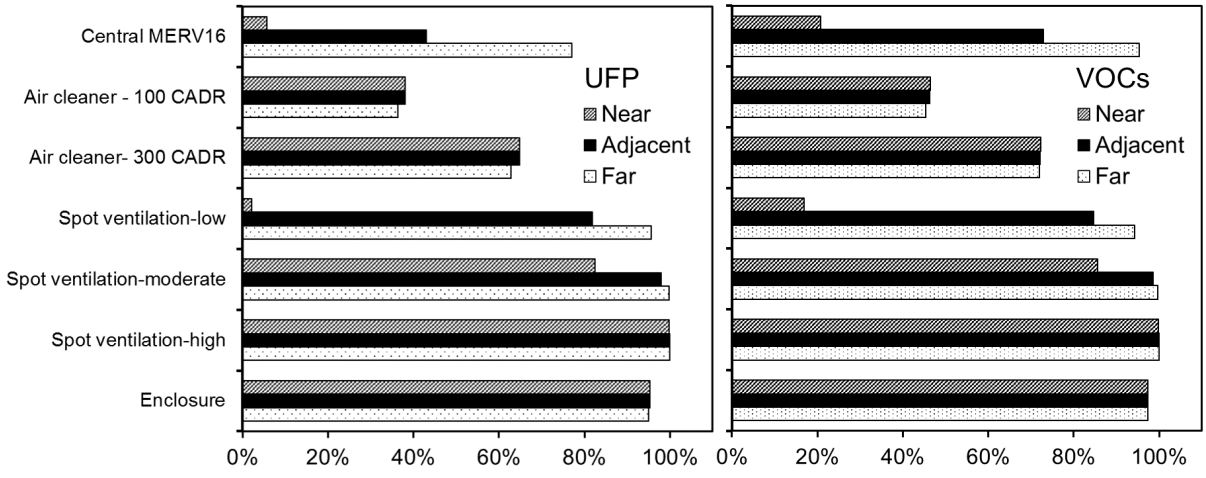

Figure 7. Removal effectiveness of each control strategy for reducing UFP and VOC concentrations in the near, adjacent, and far zones

Removal effectiveness values range from as little as 2% for the expected impact of a low-flow spot ventilation system on UFPs in the near zone to between 95% and 100% for the expected impact of a high-flow spot ventilation system or sealed and filtered enclosure on both UFPs and VOCs in all zones. Both portable air cleaner scenarios have similar UFP and VOC removal effectiveness for all zones: 38% for UFPs and 46% for VOCs with the low-CADR air cleaner, and 64% for UFPs and 72% for VOCs with the high-CADR air cleaner. The effectiveness of all other control strategies varied by zone. For example, the UFP and VOC removal effectiveness of upgraded central HVAC filtration is 6% and 21% in the near zone, 43% and 73% in the adjacent zone, and 77% and 95% in the far zone, respectively.

While these results provide insight into the likely impacts of realistic exposure control strategies on indoor concentrations of gas and particle emission products from desktop 3D printers, we should also note that some of these control strategies are more practical and cost-effective to apply than others. For example, high-flow rate spot ventilation systems that exhaust to the outdoors are likely cost prohibitive or impractical in many locations, and thus a sealed and filter enclosure may be a more appropriate solution in many environments. Further, operating a high-CADR stand-alone air cleaner with both gas and particle filtration can have a meaningful impact on both UFP and VOC concentrations in all zones, but could also come with a substantial energy penalty. We should also note that while the UFP and VOC emission rates from table 1 span a wide range of reasonable values, other printer and filament combinations will likely vary in both the magnitude of emissions and the types of individual VOCs emitted. Future work should also verify these findings with experimental data on both realistic exposures and the impact of control strategies in real environments.

Conclusions

Results from the simulations herein provide insight into the likely magnitude of human exposures to gas and particle emission products generated by desktop 3D printers and provide practical recommendations for exposure control strategies. Modeled concentrations in the three zones demonstrate that UFP and VOC concentrations within close or moderate proximity to some operating desktop 3D printers can exceed recommended exposure levels and may be cause for concern for both acute and chronic health effects. The results also suggest that the most effective control strategies for reducing both UFP and VOC concentrations in all zones from high emitters used in the modeled environment, in descending order of impact, include: (1) installing a high-flow spot ventilation system, (2) operating the printer in a sealed enclosure with high efficiency gas and particle filtration, (3) installing a moderate-flow spot ventilation system, and (4) operating a high-CADR stand-alone air cleaner with both gas and particle filtration within immediate proximity to the operating 3D printer. Upgrading central HVAC filtration, installing low-flow spot ventilation, and operating a low-CADR portable air cleaner are the least effective methods for reducing UFP and VOC concentrations resulting from 3D printer operation in this modeled environment. Results also demonstrate that some 3D printer and filament combinations with lower emissions (e.g., PLA filaments, which have both low UFP and VOC emissions) should be prioritized over higher emitting filaments to limit human exposures.

Acknowledgments

This research was funded by the Centers for Disease Control and Prevention through the National Institute for Occupational Safety and Health (Grant No. ROH010699). Its contents are solely the responsibility of the authors and do not necessarily represent the official views of the Centers for Disease Control and Prevention or the Department of Health and Human Services. The prototype sealed enclosure with recirculating gas and particle filtration was supplied by 3DPrintClean.

References

Afshar-Mohajer, Nima, Chang-Yu Wu, Thomas Ladun, Didier A. Rajon, and Yong Huang. 2015. "Characterization of Particulate Matters and Total VOC Emissions from a Binder Jetting 3D Printer." *Building and Environment* 93, Part 2 (November): 293–301. doi:10.1016/j.buildenv.2015.07.013.

ASHRAE. 2012. "Standard 52.2: Method of Testing General Ventilation Air-Cleaning Devices for Removal Efficiency by Particle Size." American Society of Heating, Refrigerating and Air-Conditioning Engineers.

ASHRAE, Standard. 2010. "Standard 62.1-2010." *Ventilation for Acceptable Indoor Air Quality, ASHRAE*.

Azimi, Parham, Dan Zhao, Claire Pouzet, Neil E. Crain, and Brent Stephens. 2016. "Emissions of Ultrafine Particles and Volatile Organic Compounds from Commercially Available Desktop Three-Dimensional Printers with Multiple Filaments." *Environmental Science & Technology*, January. doi:10.1021/acs.est.5b04983.

Azimi, Parham, Dan Zhao, and Brent Stephens. 2014. "Estimates of HVAC Filtration Efficiency for Fine and Ultrafine Particles of Outdoor Origin." *Atmospheric Environment* 98 (December): 337–46. doi:10.1016/j.atmosenv.2014.09.007.

———. 2016. "A Pilot Study of the Impact of a Prototype Sealed Enclosure with Recirculating Gas and Particle Filtration on Emissions from Desktop 3D Printers. Figshare." Built Environment Research Group: Illinois Institute of Technology. https://dx.doi.org/10.6084/m9.figshare.2369173.v1.

CDC. 1994. "The National Institute for Occupational Safety and Health (NIOSH) International Chemical Safety Cards (ICSC): Caprolactam." Centers for Disease Controls and Prevention. http://www.cdc.gov/niosh/ipcsneng/neng0118.html.

Delp, William W., and Brett C. Singer. 2012. "Performance Assessment of U.S. Residential Cooking Exhaust Hoods." *Environmental Science & Technology* 46 (11): 6167–73. doi:10.1021/es3001079.

Diapouli, E., A. Chaloulakou, and N. Spyrellis. 2007. “Levels of Ultrafine Particles in Different Microenvironments--Implications to Children Exposure.” *The Science of the Total Environment* 388 (1–3): 128–36. doi:10.1016/j.scitotenv.2007.07.063.

Diez, U., T. Kroessner, M. Rehwagen, M. Richter, H. Wetzig, R. Schulz, M. Borte, G. Metzner, P. Krumbiegel, and O. Herbarth. 2000. “Effects of Indoor Painting and Smoking on Airway Symptoms in Atopy Risk Children in the First Year of Life Results of the LARS-Study. Leipzig Allergy High-Risk Children Study.” *International Journal of Hygiene and Environmental Health* 203 (1): 23–28.

Emmerich, Steven J., and Andrew K. Persily. 2011. “US Commercial Building Airtightness Requirements and Measurements.” In *AIVC Conference*. http://www.aivc.org/sites/default/files/3b2.pdf.

Fazli, Torkan, and Brent Stephens. 2016. “Characterizing the in-Situ Size-Resolved Removal Efficiency of Residential and Light-Commercial HVAC Filters for Particle Sizes Between 0.01 and 10 Mm (OR-16-C025).” In .

Gauderman, W James, Edward Avol, Fred Lurmann, Nino Kuenzli, Frank Gilliland, John Peters, and Rob McConnell. 2005. “Childhood Asthma and Exposure to Traffic and Nitrogen Dioxide.” *Epidemiology* 16 (6): 737–43. doi:10.1097/01.ede.0000181308.51440.75.

Gauderman, W James, Hita Vora, Rob McConnell, Kiros Berhane, Frank Gilliland, Duncan Thomas, Fred Lurmann, Edward Avol, Nino Kunzli, and Michael Jerrett. 2007. “Effect of Exposure to Traffic on Lung Development from 10 to 18 Years of Age: A Cohort Study.” *The Lancet* 369 (9561): 571–77. doi:10.1016/S0140-6736(07)60037-3.

Girman, J.R., G.E. Hadwen, and L.E. Burton. 1999. “Individual Volatile Organic Compound Prevalence and Concentrations in 56 Buildings of the Building Assessment Survey and Evaluation (BASE) Study.” In *In the Proceedings of Indoor Air 1999*, 2:460–65.

Gross, Bethany C., Jayda L. Erkal, Sarah Y. Lockwood, Chengpeng Chen, and Dana M. Spence. 2014. “Evaluation of 3D Printing and Its Potential Impact on Biotechnology and the Chemical Sciences.” *Analytical Chemistry* 86 (7): 3240–53. doi:10.1021/ac403397r.

IARC. 2002. “IARC Monographs on the Evaluation of Carcinogenic Risks to Humans Volume 82.” International Agency for Research on Cancer. http://monographs.iarc.fr/ENG/Monographs/vol82/mono82-9.pdf.

Khatri, Madhu, Dhimiter Bello, Peter Gaines, John Martin, Anoop K Pal, Rebecca Gore, and Susan Woskie. 2013. “Nanoparticles from Photocopiers Induce Oxidative Stress and Upper Respiratory Tract Inflammation in Healthy Volunteers.” *Nanotoxicology* 7 (5): 1014–27. doi:10.3109/17435390.2012.691998.

Kim, Yuna, Chungsik Yoon, Seunghon Ham, Jihoon Park, Songha Kim, Ohhun Kwon, and Perng-Jy Tsai. 2015. “Emissions of Nanoparticles and Gaseous Material from 3D Printer Operation.” *Environmental Science & Technology* 49 (20): 12044–53. doi:10.1021/acs.est.5b02805.

Logue, Jennifer M. 2014. “Pollutant Exposures from Natural Gas Cooking Burners: A Simulation-Based Assessment for Southern California.” http://escholarship.org/uc/item/39s5x8qp.pdf.

McConnell, Rob, Talat Islam, Ketan Shankardass, Michael Jerrett, Fred Lurmann, Frank Gilliland, Jim Gauderman, et al. 2010. “Childhood Incident Asthma and Traffic-Related Air Pollution at Home and School.” *Environmental Health Perspectives* 118 (7): 1021–26. doi:10.1289/ehp.0901232.

Mølgaard, Bjarke, Antti Joonas Koivisto, Tareq Hussein, and Kaarle Hämeri. 2014. "A New Clean Air Delivery Rate Test Applied to Five Portable Indoor Air Cleaners." *Aerosol Science and Technology* 48 (4): 409–417.

National Toxicology Program. 2014. "Report on Carcinogens, Thirteenth Edition." Research Triangle Park, NC: U.S. Department of Health and Human Services.

Ng, Lisa C., Amy Musser, Andrew K. Persily, and Steven J. Emmerich. 2012. "Airflow and Indoor Air Quality Models of DOE Reference Commercial Buildings." *Gaithersburg, MD, National Institute of Standards and Technology* 163. http://www.ewp.rpi.edu/hartford/~ernesto/F2013/AWPPCE/Feedback/Bardin/Ng-NIST2012-AirQualityModeling-CONTAM.pdf.

NIST. 2016. "NIST Multizone Modeling Homepage." http://www.bfrl.nist.gov/IAQanalysis/index.htm.

NJDEP. 2015. "Guidance: Remediation Standards." May. http://www.nj.gov/dep/srp/guidance/rs/chemproperties.pdf.

"NSRDB: 1991- 2005 Update: TMY3." 2016. Accessed January 7. http://rredc.nrel.gov/solar/old_data/nsrdb/1991-2005/tmy3/.

Oberdörster, Günter. 2000. "Pulmonary Effects of Inhaled Ultrafine Particles." *International Archives of Occupational and Environmental Health* 74 (1): 1–8.

Oberdorster, Gunter, Eva Oberdorster, and Jan Oberdorster. 2005. "Nanotoxicology: An Emerging Discipline Evolving from Studies of Ultrafine Particles." *Environmental Health Perspectives* 113 (7): 823–39. doi:10.1289/ehp.7339.

OEHHA. 2014. "Table of All Acute, Chronic and 8 Hour Reference Exposure Levels." June. http://oehha.ca.gov/air/allrels.html.

Peters, Annette, H. Erich Wichmann, Thomas Tuch, Joachim Heinrich, and Joachim Heyder. 1997. "Respiratory Effects Are Associated with the Number of Ultrafine Particles." *American Journal of Respiratory and Critical Care Medicine* 155 (4): 1376–1383.

Pieters, Nicky, Gudrun Koppen, Martine Van Poppel, Sofie De Prins, Bianca Cox, Evi Dons, Vera Nelen, et al. 2015. "Blood Pressure and Same-Day Exposure to Air Pollution at School: Associations with Nano-Sized to Coarse PM in Children." *Environmental Health Perspectives*, March. doi:10.1289/ehp.1408121.

Pirela, Sandra, Ramon Molina, Christa Watson, Joel M. Cohen, Dhimiter Bello, Philip Demokritou, and Joseph Brain. 2013. "Effects of Copy Center Particles on the Lungs: A Toxicological Characterization Using a *Balb/c* Mouse Model." *Inhalation Toxicology* 25 (9): 498–508. doi:10.3109/08958378.2013.806614.

Schaper, Michelle M., Randolph D. Thompson, and Katherine A. Detwiler-Okabayashi. 1994. "Respiratory Responses of Mice Exposed to Thermal Decomposition Products from Polymers Heated at and Above Workplace Processing Temperatures." *American Industrial Hygiene Association Journal* 55 (10): 924–34. doi:10.1080/15428119491018420.

Sidheswaran, Meera A., Hugo Destaillats, Douglas P. Sullivan, Sebastian Cohn, and William J. Fisk. 2012. "Energy Efficient Indoor VOC Air Cleaning with Activated Carbon Fiber (ACF) Filters." *Building and Environment*, International Workshop on Ventilation, Comfort, and Health in Transport Vehicles, 47 (January): 357–67. doi:10.1016/j.buildenv.2011.07.002.

Singer, Brett C., William W. Delp, P. N. Price, and M. G. Apte. 2012. "Performance of Installed Cooking Exhaust Devices." *Indoor Air* 22 (3): 224–234.

Steinle, Patrick. 2015. "Characterization of Emissions from a Desktop 3D Printer and Indoor Air Measurements in Office Settings." *Journal of Occupational and Environmental Hygiene* 0 (ja): 1–36. doi:10.1080/15459624.2015.1091957.

Stephens, Brent, Parham Azimi, Zeineb El Orch, and Tiffanie Ramos. 2013. "Ultrafine Particle Emissions from Desktop 3D Printers." *Atmospheric Environment* 79 (November): 334–39. doi:10.1016/j.atmosenv.2013.06.050.

Stölzel, Matthias, Susanne Breitner, Josef Cyrys, Mike Pitz, Gabriele Wölke, Wolfgang Kreyling, Joachim Heinrich, H-Erich Wichmann, and Annette Peters. 2007. "Daily Mortality and Particulate Matter in Different Size Classes in Erfurt, Germany." *Journal of Exposure Science and Environmental Epidemiology* 17 (5): 458–67. doi:10.1038/sj.jes.7500538.

Sultan, Zuraimi M., Gregory J. Nilsson, and Robert J. Magee. 2011. "Removal of Ultrafine Particles in Indoor Air: Performance of Various Portable Air Cleaner Technologies." *HVAC&R Research* 17 (4): 513–525.

Unwin, John, Matthew R. Coldwell, Chris Keen, and John J. McAlinden. 2013. "Airborne Emissions of Carcinogens and Respiratory Sensitizers during Thermal Processing of Plastics." *Annals of Occupational Hygiene* 57 (3): 399–406. doi:10.1093/annhyg/mes078.

US EPA, OAR. 2000. "Styrene | Technology Transfer Network Air Toxics Web Site | US EPA." January. http://www3.epa.gov/airtoxics/hlthef/styrene.html#ref5.

Wallace, Lance, Warren Kindzierski, Jill Kearney, Morgan MacNeill, Marie-Ève Héroux, and Amanda J. Wheeler. 2013. "Fine and Ultrafine Particle Decay Rates in Multiple Homes." *Environmental Science & Technology* 47 (22): 12929–37. doi:10.1021/es402580t.

Waring, Michael S., Jeffrey A. Siegel, and Richard L. Corsi. 2008. "Ultrafine Particle Removal and Generation by Portable Air Cleaners." *Atmospheric Environment* 42 (20): 5003–14. doi:10.1016/j.atmosenv.2008.02.011.

Zhu, Yifang, William C Hinds, Seongheon Kim, Si Shen, and Constantinos Sioutas. 2002. "Study of Ultrafine Particles near a Major Highway with Heavy-Duty Diesel Traffic." *Atmospheric Environment* 36 (27): 4323–35. doi:10.1016/S1352-2310(02)00354-0.

Zitting, Antti, and Heikki Savolainen. 1980. "Effects of Single and Repeated Exposures to Thermo-Oxidative Degradation Products of Poly(acrylonitrile-Butadiene-Styrene) (ABS) on Rat Lung, Liver, Kidney, and Brain." *Archives of Toxicology* 46 (3–4): 295–304. doi:10.1007/BF00310447.

About the Authors

Parham Azimi and Torkan Fazli are Ph.D. Candidates and Brent Stephens is an Associate Professor in the Department of Civil, Architectural and Environmental Engineering at Illinois Institute of Technology in Chicago, IL, USA.